USCIPI REPORT #1060

Nonstationary Recursive Restoration of Images with Signal-Dependent Noise with Applications to Speckle Reduction

by

Darwin Ta-Wen Kuan

August 1982

Signal and Image Processing Institute
UNIVERSITY OF SOUTHERN CALIFORNIA
Department of Electrical Engineering-Systems
Powell Hall of Engineering
University Park/MC-0272
Los Angeles, CA 90089 U.S.A.

ACKNOWLEDGEMENTS

I would like to express my sincere appreciation to the chairman of my committee, Dr. Alexander A. Sawchuk, for his invaluable suggestions, guidance, and encouragement throughout the course of this research.

I would also like to thank the following individuals for their contributions to this work: Dr. Tim Strand for his many helpful discussions and suggestions and for serving as member of my committee; Dr. Alan Schumitzky for his guidance as member of my committee; Dr. Pierre Chavel for his many helpful suggestions and discussions as well as his sincere personal assistance during my visit at the Institut d'Optique, Orsay, France; and, Dr. Jerry Mendel for his support at the early stages of my graduate studies and for introducing me to the field of seismic data processing.

I would also like to thank the entire staff of the Image Processing Institute for their help and support in the preparation of this work.

Finally, I would like to thank my wife, Lilly, for her patience, sacrifice, and encouragement throughout my years of graduate studies at USC.

TABLE OF CONTENTS

LIST OF FIGURES

LIST OF TABLES

ABSTRACT

A two-dimension recursive image restoration filter is developed for images degraded by blur and a class of uncorrelated, signal-dependent noise. Unlike conventional image restoration techniques, the filter does not require any *a priori* information of the original image and adopts a nonstationary image model. All the parameters needed for the filter are estimated from the noisy image. The filter has a simple recursive structure, and is able to adapt itself to the nonstationary content of the image and to different types of signal-dependent noise.

The second major subject area of this dissertation is on speckle reduction techniques. Speckle noise inherently exists in all types of coherent imagery such as synthetic aperture radar imagery, acoustic imagery, and laser illuminated imagery. Past work on speckle reduction assumed that speckle noise is multiplicative and uncorrelated. We model the speckle according to the exact physical process of coherent image formation. The problem of how to generate discrete speckle images accurately without aliasing is discussed in detail. A local linear minimum mean square error speckle reduction filter is developed for intensity speckle images, where only the speckle intensity is observable. Unlike other existing approaches, this filter considers the second order statistics of speckle and uses a nonstationary image model. The two-dimensional recursive

implementation of this filter is also developed as a fast computation algorithm. In some applications, both the amplitude and phase of the speckle image are observable. In the past, the additional phase information is ignored in designing the speckle reduction filter. Here, we develop a nonlinear maximum a posteriori (MAP) filter for complex amplitude speckle images. The MAP equations can be expressed in terms of the filtered estimate and filtered covariance matrix of a nonstationary two-dimensional recursive filter and a cubic equation. Thus the MAP estimate can be solved iteratively by using the recursive filter as a fast computation algorithm and using the cubic equation as a constraint to optimize the estimate at each iteration.

Chapter 1

INTRODUCTION

1.1 Nonstationary Recursive Restoration of Images with Signal-Dependent Noise

The field of image restoration has been progressing rapidly in the last decade. Various image restoration and enhancement methods have been proposed for removing degradations due to blurring and noise [1-1,1-2]. The effectiveness of an image restoration algorithm depends on the validity of the image model, the criterion used to judge the quality of the restored image, and the statistical model for the noise process.

Early developments centered on nonrecursive processing in the discrete frequency domain [1-1,1-2] using the fast Fourier transform algorithm as a computational tool. While it is possible to perform image restoration within reasonable time, these approaches assumed a stationary image model and precluded local processing and real-time processing possibilities. Recent work of Woods *et al.* [1-3,1-4] extended the one-dimensional recursive Kalman filter to two-dimensions based on a stationary image model. The two-dimensional

recursive filter is implemented in the space domain with a reduced update approximation to reduce computation. This approach can easily process images with space-variant blur.

In a conventional stationary image model, all the statistical information in the image is carried by the constant mean and stationary covariance function. Hunt et al. [1-5] proposed a nonstationary mean Gaussian image model. In this model, an image is modeled as consisting of stationary fluctuations about a nonstationary ensemble mean. The ensemble mean has the gross structure that represents the context of the ensemble. This image model was later used by Trussell and Hunt [1-6], and Lo and Sawchuk [1-7] to perform maximum a posteriori (MAP) estimation of images degraded by film-grain noise and Poisson noise respectively. The algorithms are nonlinear in nature and a nonrecursive sectioning method is used to do local processing.

In this dissertation, we adopt a nonstationary mean and nonstationary variance (NMNV) image model that is an extension of Hunt's model. In this model, an image is decomposed into two components, a nonstationary mean and a nonstationary white residual process that can be characterized by its nonstationary variance. A 2-D recursive restoration filter for a class of uncorrelated signal-dependent noise [1-8] is derived based on this nonstationary image model and the linear minimum mean

square error (LMMSE) criterion. The filter uses a reduced update concept similar to Woods' to ease computation requirements, and is able to adapt itself to the nonstationary content of the image and to different types of signal-dependent noise. All the statistical parameters needed for the filter are estimated from the degraded image. Various ways of estimating these ensemble statistics from the noisy image are discussed and their performances are compared. Simulation results for additive noise, multiplicative noise, and Poisson noise are presented.

1.2 Speckle Reduction Techniques

Another important problem area that requires nonstationary image processing techniques is speckle reduction. This is a second major subject area of this dissertation. Speckle noise inherently exists in all types of coherent imagery such as synthetic aperture radar (SAR) imagery for remote sensing, acoustic imagery and laser illuminated imagery. Speckle is due to the random interference of the wavelets scattered by the microscopic fluctuations of the object surface within a resolution element [1-9]. Unlike multiplicative noise or Poisson noise, speckle noise is not only signal-dependent but also correlated. Although speckle statistics can be used to provide fine information on object structure and surface roughness, speckle is objectionable in all imaging situations because its high contrast and wide

frequency range dramatically reduce understandability and resolution when compared to incoherent imaging or to coherent imaging of non-scattering objects. Therefore, speckle reduction is of primary concern in coherent imaging systems.

Speckle reduction can be achieved by averaging multiple frames of uncorrelated speckle images of the same object on an intensity basis [1-9]. The signal-to-noise (SNR) ratio of the processed image is increased by a factor of $M^{1/2}$, where M is the number of frames. While this method is effective for speckle reduction when multiple frames of uncorrelated speckle images are available, it does not consider the image statistics and the correlation of speckle. Many authors [1-10,1-11,1-12] applying digital image processing techniques for speckle reduction assumed speckle noise is multiplicative and applied multiplicative noise filters to smooth the speckle noise. This multiplicative noise assumption, in general, is only a rough approximation for speckle noise.

In this dissertation, we model the speckle according to the exact physical process of coherent image formation. Thus, the model includes signal-dependent effects and accurately represents the higher order statistical properties of speckle that are important to the restoration procedure. The problem of how to accurately generate discrete speckle images without aliasing is also discussed [1-13].

In developing speckle reduction techniques, we restrict ourselves to the case called "fully developed" speckle [1-9]. In the optical case, where only the speckle intensity is observable, we develop a linear minimum mean square error (LMMSE) filter based on the NMNV image model. Unlike other approaches, this filter considers the second order statistics of speckle. Both low pass filtering and multiplicative noise filtering are special cases of this filter under some simplifying assumptions. The two-dimensional recursive implementation of this filter [1-14] is also developed as a fast computation algorithm.

In the SAR and ultrasonic domains, both the amplitude and phase of the speckle image are observable. It is shown that the additional phase information of the speckle image is useful for speckle reduction. A nonlinear maximum a posteriori (MAP) filter is developed for this case. The nonlinear MAP equation is solved using an iterative method, involving a nonstationary two-dimensional recursive filter and the solution of a cubic equation in each iteration. Simulation results are presented.

1.3 Organization and Contributions of the Dissertation

This dissertation consists of two interwoven parts. In the first part, a nonstationary 2-D recursive image restoration filter is developed for a class of uncorrelated signal-dependent noise. In the second part, we concentrate on discrete speckle modeling and speckle reduction techniques. The organization of the dissertation is shown in Fig. 1. In Chapter 2, stationary and nonstationary image models used for image restoration are examined. A nonstationary mean and nonstationary variance image model is introduced for future use. Different types of signal-dependent noise that are frequently encountered in image formation systems are discussed.

In Chapter 3, a speckle model is developed according to the exact physical process of coherent image formation. The statistical analysis of speckle for a general scattering surface is very complex and is still a subject of great interest. It is desirable to generate discrete speckle images with a digital computer for simulation studies of these statistics. The sampling theorem plays an important role in generating discrete speckle images accurately. In general, we need to oversample the object surface function by a factor of W to avoid aliasing effects. The minimum value of W is proportional to the variance of the surface roughness. Discrete speckle images generated by this method will be

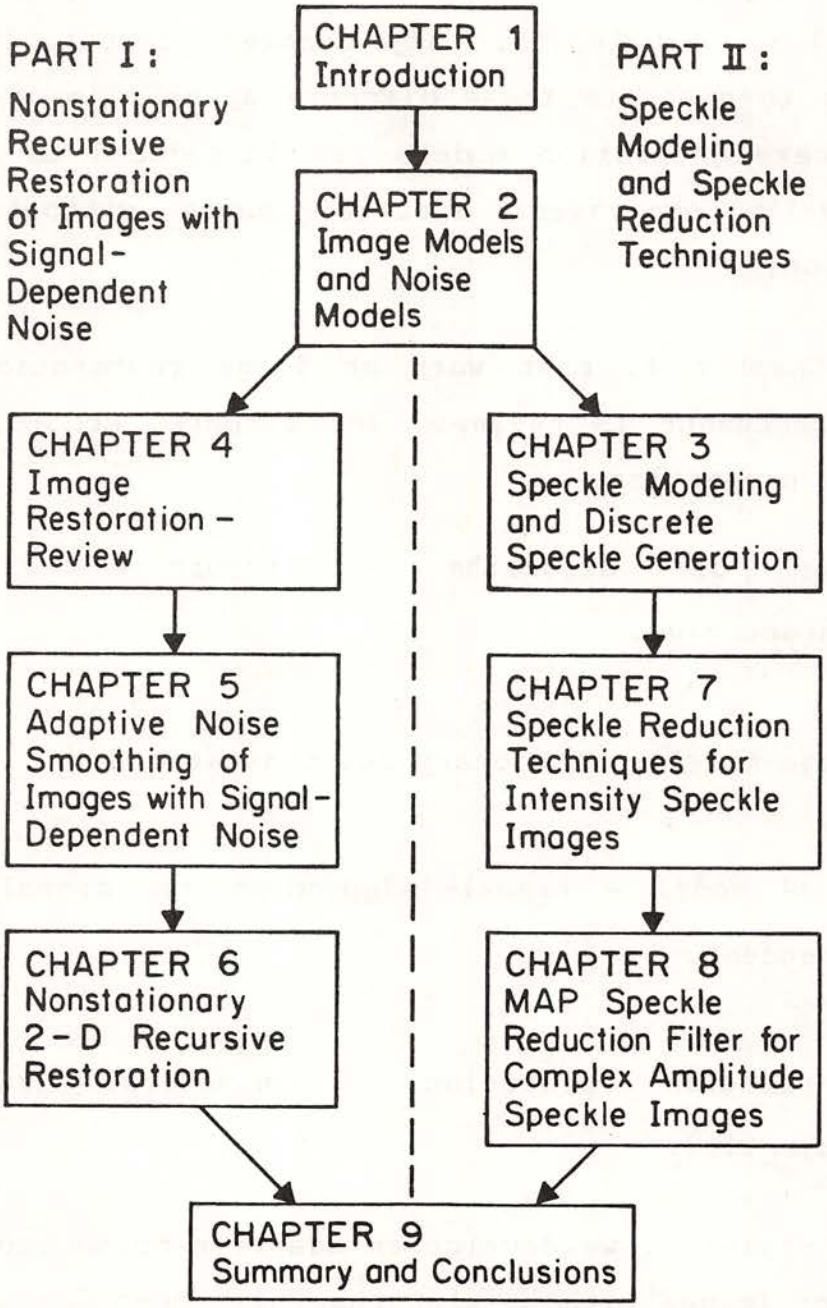

Figure 1.1 Organization of the dissertation

exactly the same as the speckle images produced by an equivalent optical system. For "fully developed" speckle, where the object surface is extremely rough compared with the optical wavelength, it becomes computationally demanding to generate these discrete speckle images. Two new discrete generation models are introduced to obtain statistically equivalent speckle images without much computation.

In Chapter 4, past work on image restoration and image enhancement is reviewed and compared according to following properties:

1. Type of algorithm - recursive vs. nonrecursive.

2. Image model - stationary vs. nonstationary.

3. Noise model - signal-independent vs. signal-dependent.

4. Restoration criterion - numerical vs. subjective.

In Chapter 5, we develop an adaptive noise smoothing filter for images without blur that have been degraded by a class of uncorrelated signal-dependent noise. The filter has a very simple structure (point processor), and

is able to adapt itself to the nonstationary content of the image and to different types of signal-dependent noise. All the statistical parameters needed for the filter are estimated from the degraded image. Various ways of estimating these ensemble statistics from the noisy image are discussed, and their performances are compared. Simulation results for additive noise, multiplicative noise, and Poisson noise are presented.

In Chapter 6, the adaptive noise smoothing filter is extended to image restoration where the image is degraded by blurring and noise. The filter is no longer a point processor, and a 2-D recursive implementation of the filter is considered. With the nonstationary mean and nonstationary variance image model, the state space model of the image can be easily implemented and is shown to be a shift operator. This simplifies the prediction step of the recursive filter considerably if we use indirect addressing techniques. The optimal filter requires excessive computation because of the high dimension of the state vector. A suboptimal filter similar to Woods' reduced update Kalman filter is used to reduce computation. Boundary problems can be easily resolved because of the image model assumed.

In Chapter 7, we consider speckle reduction techniques for the optical case where only the speckle intensity is observable. Various speckle reduction models are presented according to the speckle data format

available. If the recorded speckle image is undersampled such that the sampling interval is larger than the correlation length of the speckle, the speckle noise samples are statistically independent and multiplicative in nature. In this case, the adaptive noise smoothing filter developed in Chapter 5 can be used for speckle reduction. A one-point MAP filter that considers the negative exponential distribution of the speckle intensity is derived for this case. The one-point MAP estimate is shown to be the solution of a cubic equation. For the case that the speckle image is adequately sampled such that the correlation structure of the speckle is preserved, we derive a local linear minimum mean square-error (LLMMSE) filter that uses the correlation information of the speckle to further reduce the speckle noise. A nonstationary 2-D recursive implementation of this filter is developed as a fast computation algorithm. The MAP filter for the case of correlated samples is very complicated and the difficulties of deriving it are explained. For the case where multiple frames of independent speckle images are available, these speckle reduction techniques can be applied after the multiple frame averaging technique to further reduce the speckle noise.

In Chapter 8, we present a MAP filter for the digitally processed synthetic aperture radar (SAR) images where both the amplitude and phase of the speckle image are available. The MAP equations are nonlinear and can

only be solved by iterative methods. Fortunately, we are able to express the MAP equations in terms of the filtered estimate and filtered covariance matrix of the nonstationary 2-D recursive filter developed in Chapter 6. The resulting MAP equation is a cubic equation, and has the same form as the one-point MAP equation of the optical case with independent speckle samples. Thus the MAP equations can be easily solved iteratively by using the 2-D recursive filter as a fast computation algorithm and imposing a one-point MAP constraint (solution of a cubic equation) to optimize the estimate at each iteration. This is the first known use of amplitude and phase information in speckle reduction.

In the final chapter a summary of results is given along with the future research directions in image modeling, recursive restoration, and speckle reduction techniques.

Chapter 2

IMAGE MODELS AND NOISE MODELS

2.1 Introduction

The effectiveness and complexity of an image restoration algorithm depends heavily on the image model assumed. Image models are usually made implicit by the assumptions of the restoration schemes. For example, in order to apply a Wiener filter for image restoration, we implicitly assume that an image is a wide-sense stationary random field. In a conventional stationary image model, all the statistical information of the image is carried by a constant mean and a stationary correlation function. The statistical properties of an image are characterized globally rather than locally. The disadvantage of a stationary image model is that the restoration filter designed accordingly is insensitive to abrupt changes of the image and tends to smooth the edges. It is obvious that an image is best described by a nonstationary image model. However, stationary problems are much easier to solve than the nonstationary problems.

The nonstationary image models can be characterized into four different levels:

1. Stationary mean and nonstationary covariance image model

2. Nonstationary mean and stationary covariance image model

3. Both nonstationary mean and nonstationary covariance image model

4. Higher order nonstationary statistics image model.

In sections 2.3.1 and 2.3.2, we discuss some of the nonstationary image models used for image restoration. In section 2.3.3 we introduce a nonstationary mean and nonstationary variance image model that is a special case of the third level nonstationarity. The validity of this image model is examined for real images.

Most image restoration techniques model the noise process as additive, signal-independent white noise. It is well known, however, that many physical noise processes occurring in image formation systems are inherently signal-dependent. For example, the film-grain noise produced by a photographic emulsion during the process of image recording and reproduction and the photon noise in any image detected at low light levels. Restoration algorithms based on a signal-independent

noise model are expected not to have good performance in the signal-dependent noise environment. In section 2.4, we discuss various signal-dependent noise models and their statistical properties, including multiplicative noise, Poisson noise, and film-grain noise. In the final section, summary and conclusions are presented.

2.2 Image Formation and Discrete Image Representations

The fundamental linear model describing the image formation process is given by

$$g(x,y) = \int_{-\infty}^{+\infty}\int h(p,q;x,y)\, f(p,q)\, dpdq \qquad (2.1)$$

where $g(x,y)$ is the degraded image, $h(p,q;x,y)$ is the point spread function (PSF) of the image formation system, and $f(p,q)$ is the original object intensity. If the point spread function is space-invariant, we have the familiar two dimensional convolution expression

$$g(x,y) = \int_{-\infty}^{+\infty}\int h(x-p,y-q)\, f(p,q)\, dpdq. \qquad (2.2)$$

In order to represent a continuous image in a discrete space for digital processing, it is necessary to sample the continuous image according to the two-dimensional sampling theorem [2-1]. For a bandlimited image $g(x,y)$ with spatial frequency cutoffs of f_{xc} and f_{yc}, in the x and y directions respectively, the two-dimensional sampling theorem simply states that, in order to recover

the continuous image function from its samples, the sampling spacings in the x and y directions, Δx and Δy respectively, must satisfy the condition

$$\Delta x \leq 1/2f_{xc} \quad \text{and} \quad \Delta y \leq 1/2f_{yc}. \tag{2.3}$$

From Eq. (2.2), the resulting discrete samples can be expressed as

$$g(m\,\Delta x, n\,\Delta y) = \int_{-\infty}^{+\infty}\int h(m\,\Delta x - p, n\,\Delta y - q)\, f(p,q)\, dp dq. \tag{2.4}$$

This continuous-discrete formulation is a very practical description of the image formation system because the original object is usually continuous, while the recorded image is discrete because of detectors, sampling processes, and discrete display systems. However, the continuous object f(p,q) cannot be represented in a digital computer and, consequently, only discrete approximations are possible. If f(p,q) is also bandlimited and satisfies the condition in Eq. (2.3), Eq. (2.4) can be written as

$$g(m\Delta x, n\Delta y) = \sum_i \sum_j h(m\Delta x - i\Delta x, n\Delta y - j\Delta y)\, f(i\Delta x, j\Delta y). \tag{2.5}$$

There are two different discrete image representations for this discrete-discrete model, the spatial-variable representation and the lexicographic representation [2-2]. Without loss of generality, setting the sampling

spacings equal to 1, we have the spatial-variable representation

$$g(m,n)=\sum_i\sum_j h(m-i,n-j)f(i,j). \qquad (2.6)$$

In this representation, the two-dimensional relationship of the neighboring pixels are easily perceived. For recursive image processing algorithms, the locally recursive structure is usually pursued, and the spatial-variable representation is most suitable for these applications.

The lexicographic representation essentially raster scans the two-dimensional image samples and stacks them into a single vector. Considering the discrete image g(m,n) of size M by M for example, then its lexicographic representation is

$$\underline{g} = \begin{bmatrix} g(1,1) \\ g(1,2) \\ \vdots \\ g(1,M) \\ g(2,1) \\ \vdots \\ g(M,M) \end{bmatrix} \qquad (2.7)$$

i.e., the (i,j)th element of the M by M image is the [(i-1)*M+j]th element of the vector. Using this representation, the two-dimensional convolution in Eq. (2.6) can be written in matrix-vector form

$$\underline{g} = H\underline{f} \tag{2.8}$$

where $\underline{g}$ is an M^2*1 vector, $\underline{f}$ is an N^2*1 vector, and H is an M^2*N^2 point-spread matrix with certain block properties reflecting the effect of a raster scanning operator on both f(m,n) and g(m,n). With this transformation, we can simply use the matrix-vector notations as in Eq. (2.8) to formulate the two-dimensional image formation system as a one-dimensional problem. It is usually easier to formulate nonrecursive algorithms with the lexicographic representation. We will use both representations in the following chapters. The transformation between them is implicitly given in Eq. (2.7).

2.3 Nonstationary Image Models

In this section, we discuss various nonstationary image models used for image restoration.

2.3.1 Stationary Mean and Nonstationary Covariance Image Model

Lebedev and Mirkin [2-3] proposed a composite image model which assumes that an image is composed of many different stationary components. Each component has a distinct stationary correlation structure. An image model having five classes was chosen. Four of them were anisotropic, correlated in the directions 0^o, 45^o, 90^o, and 135^o. The last class had an isotropic structure. In

this model, the nonstationary content of an image at each point is described by a nonstationary correlation function that is a linear combination of five stationary components.

Ingle and Woods [2-4] applied a reduced update Kalman filter to image restoration by using this composite image model. The result is a bank of Kalman filters running in parallel, and each Kalman filter was designed according to the correlation function of one component. Instead of using the weighted sum of all the outputs of the Kalman filters, they used a decision scheme to choose the output of one filter at each point to reduce computation. This resulted in a "multiple model" recursive estimation technique. In this case, each point is assigned a stationary correlation function. The nonstationary content of an image is described by the spatial distribution of these five stationary models.

2.3.2 Nonstationary Mean and Stationary Covariance Image Model

Hunt et al. [2-5] proposed a nonstationary mean and stationary covariance Gaussian image model. They assumed that an image $\underline{f}$ can be decomposed into a nonstationary mean component $\underline{\bar{f}}$, and a stationary residual component $\underline{f}_0=\underline{f}-\underline{\bar{f}}$. The nonstationary mean describes the gross structure of an image and the residual component describes the detail variation of the image. They

described a "thought experiment" to support their model. Suppose that we have several thousand driver's license pictures showing head and shoulders of human subjects. If we compute the ensemble mean of these pictures, most likely we will have a nonstationary mean picture consisting of a fuzzy oval face, some dark spots for the eyes, mouth and the boundary of the shoulders. This is referred to as a context-dependent image ensemble. Most of the structural information of the context-dependent image ensemble is contained in the nonstationary mean vector $\underline{\bar{f}}$. For the ease of computation and mathematical tractability, the covariance function is assumed to be stationary and the joint probability density function (PDF) of $\underline{f}$ is assumed to be Gaussian, i.e.,

$$P(\underline{f}) = ((2\pi)^{N^2} |C_f|)^{-1/2} \exp[-1/2 (\underline{f}-\underline{\bar{f}})^T C_f^{-1} (\underline{f}-\underline{\bar{f}})]$$

where $|C_f|$ is the determinant of the covariance matrix C_f, and N is the size of the image. Hunt [2-6] derived a maximum *a posteriori* (MAP) estimate for a nonlinear image formation model based on this nonstationary mean image model. The MAP estimate is the solution of a set of nonlinear equations. Trussell and Hunt [2-7] used the sectioning method and the modified Picard iteration to reduce the computation efforts. They also made an assumption that $C_f = \sigma_f^2 I$ to simplify the computation.

2.3.3 Nonstationary Mean and Nonstationary Variance (NMNV) Image Model

In a conventional stationary image model, an image $\underline{f}$ is assumed to be a wide-sense stationary random field with constant mean vector and block Toeplitz covariance matrix. The joint probability density function is implicitly assumed to be multivariate Gaussian. All the statistical information of the image is carried by the covariance matrix. For a real world image as in Fig. 2.1(a), it is apparent from the picture that the image is not a stationary random field and the histogram (Fig. 2.1(b)) of the image is not Gaussian. Thus the conventional stationary image model is an oversimplified model assumed for computational purposes. The nonstationary mean Gaussian image model assumes that an image $\underline{f}$ can be decomposed into a nonstationary mean $\underline{\bar{f}}$ and a stationary residual $\underline{f}_0=\underline{f}-\underline{\bar{f}}$. If we approximate the nonstationary ensemble mean by a local mean estimate calculated over a 3*3 uniform window, and subtract the local mean from the original image, we have the residual image $\underline{f}_0$ that is shown for our example in Fig. 2.1(c). It is obvious from the picture that $\underline{f}_0$ is still a correlated nonstationary process. However, the shape of the histogram is more Gaussian (Fig. 2.1(d)). The stationary assumption about $\underline{f}_0$ is still for computational simplicity. ecause some of the structural information is now carried by the mean, it is reasonable to assume that the covariance structure may be simplified compared with

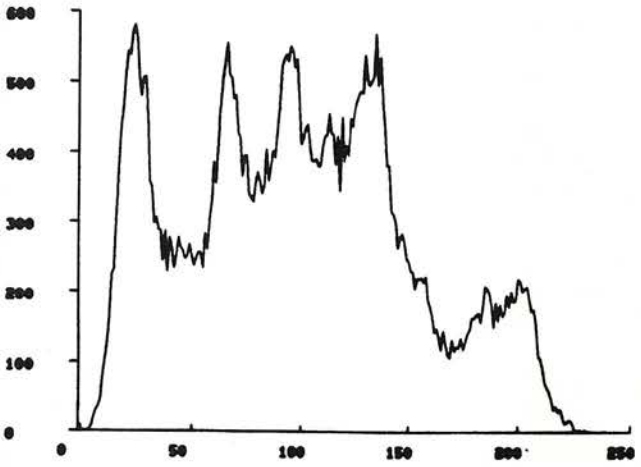

(a) Original image

(b) Histogram of (a)

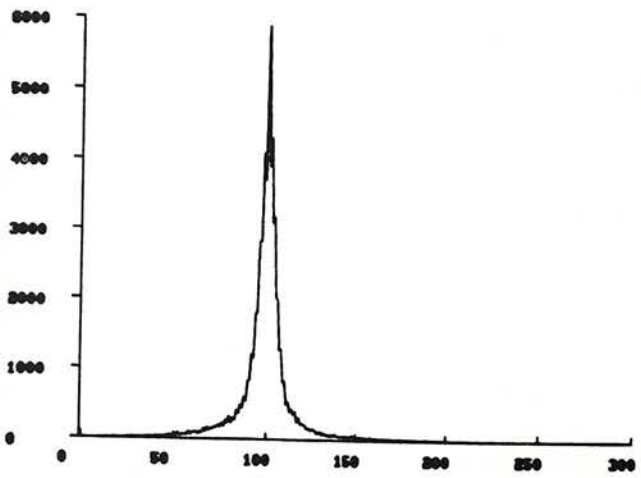

(c) Residual image of the original image and the local mean image

(d) Histogram of (c)

Figure 2.1 Nonstationary mean and stationary covariance image modeling

(a) Normalized residual image with unit variance

(b) Normalized unit variance residual image with an intelligent filter to calculate the local statistics

Figure 2.2 Nonstationary mean and nonstationary variance image modeling

the conventional stationary image model. Trussell and Hunt [2-7] assumed that the covariance matrix of $\underline{f}_0$ could be approximated by a diagonal matrix $\sigma_f^2 I$, where σ_f^2 is a scalar and I is the identity matrix. In this case, all the information is carried by the nonstationary mean. While letting the covariance matrix carry all the statistical information, as in a conventional stationary image model, is not satisfactory, neither is letting the nonstationary mean carry all the information. Therefore, it is heuristically reasonable to include more structure in the identity covariance matrix of the nonstationary mean Gaussian image model.

In order to consider the nonstationarity of the image and not to complicate the computation too much, we assume that $\underline{f}_0$ is a nonstationary white process. i.e., $\underline{f}_0$ is independent and is characterized by its nonstationary variance. This nonstationary mean and nonstationary variance (NMNV) image model has been used implicitly in some extent in the sectioned MAP method. There it was assumed that the nonstationary image can be divided into many sections and each section has the covariance matrix $C^{(i)} I$, where $C^{(i)}$ is a scalar that varies from section to section. The section size is chosen according to the length of the point spread function and the extent of stationarity assumed. An overlap-save sectioning method is used to suppress the convolution wraparound effect at the section boundary. For the noise smoothing problem (no blur), the section size can be reduced to a single

point and this becomes a NMNV image model. However, for the image restoration problem, the minimum section size cannot be reduced to a single point.

We can substitute the local variance for the nonstationary variance, and normalize $\underline{f}_0$ in Fig. 2.1(c) to have unit variance, i.e.

$$f_0'(m,n) = \frac{f_0(m,n)}{\sqrt{v_f(m,n)}} \tag{2.9}$$

where $v_f(m,n)$ is the local variance of f_0 at position (m,n). The normalized unit variance residual image $\underline{f}_0'$ is shown in Fig. 2.2(a). Note that in the uniform intensity region, there is no correlation and $\underline{f}_0'$ looks like white noise. This verifies that the NMNV image model is valid in those regions. However, in the neighborhood of an edge, visible correlations still exist in the normalized residual image. If we want to include these correlations into the image model, we need to specify a nonstationary mean and nonstationary covariance image model. While this is the direction to go, the possible performance improvement of using this model is hindered by the complexity of the restoration filter and the model identification procedure.

There is another factor that contributes to the correlation of the residual image in Fig. 2.2(a). Note that we used the local mean to substitute for the ensemble mean in the procedure. When there is a sharp

edge in the image, the averaging window tends to blur the local mean estimate by using pixels on both sides of the edge. To avoid this we can use a intelligent filter that recognizes an edge and calculates the local mean only using those pixels on the one side of the edge. Fig. 2.2(b) is the normalized residual image where the local mean and local variance are calculated by such a filter. Note that the correlations around the edges are reduced, and the residual image is more like a white noise process.

From the discussion above, we know that the validity of the NMNV image model depends on the methods we use to estimate the local mean and variance. Therefore, the process of estimating local statistics can be thought of as a way to find an operation that transforms an image into a white noise process in order to facilitate the restoration procedure.

2.4 Noise Models

2.4.1 Signal-Independent Additive Noise Model

This model is commonly used in digital image restoration. The degradation model is given by

$$g(m,n) = h(m,n) \circledast f(m,n) + v(m,n) \qquad (2.10)$$

where $g(m,n)$ is the degraded image, $h(m,n)$ is the

blurring function, f(m,n) is the object intensity, v(m,n) is the signal-independent, additive white noise, and ⊛ is the two-dimensional convolution operator. If we use the lexicographic representation, Eq. (2.10) can be expressed as

$$\underline{g} = H\underline{f} + \underline{v}. \tag{2.11}$$

The block diagram of this noise model is illustrated in Fig. 2.3. The additive noise model is a good description of the thermal noise in image sensors.

2.4.2 Signal-Dependent Uncorrelated Noise Models

Many physical noises are inherently signal-dependent. In this section, we discuss a class of signal-dependent noise that is spatially uncorrelated. In particular, multiplicative noise, film-grain noise, and Poisson noise.

(A). Multiplicative noise model

The block diagram of a multiplicative noise model is illustrated in Fig. 2.4. The mathematical expression is given by

$$g(m,n) = [h(m,n) \circledast f(m,n)]\, v(m,n) \tag{2.12}$$

where v(m,n) is a signal-independent white noise with

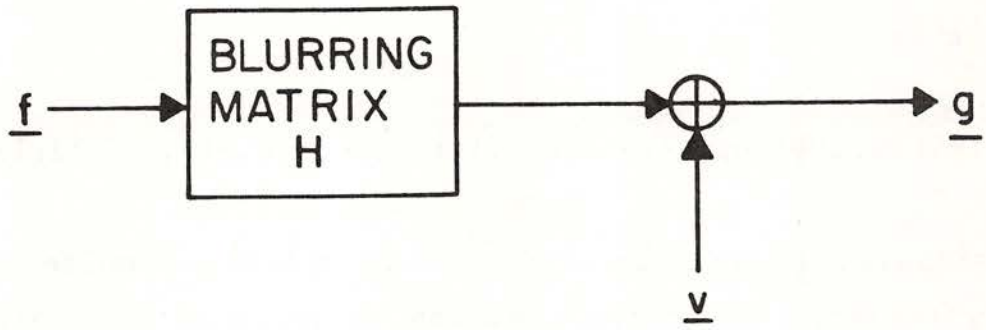

Figure 2.3 Block diagram of image degraded by blur and additive noise

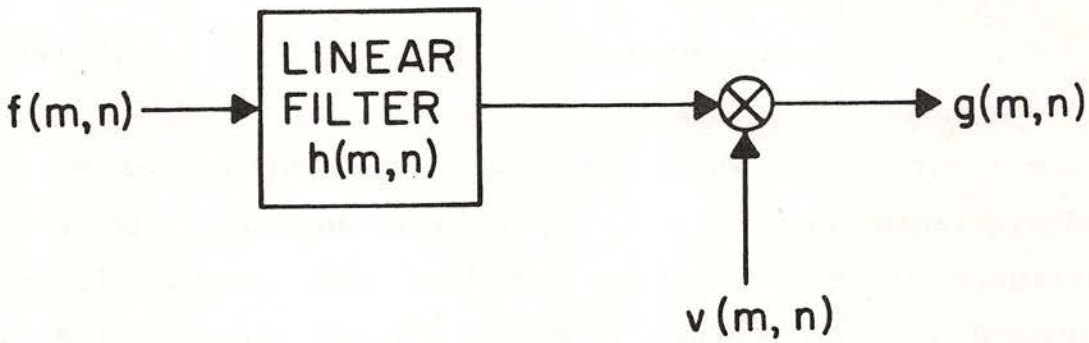

Figure 2.4 Block diagram of image degraded by blur and multiplicative noise

mean $\bar{v}$ and variance σ_v^2 . The signal-dependent characteristic of this noise model becomes clear if we express Eq. (2.12) in terms of a signal part and a noise part, that is

$$g(m,n)=\bar{v}h(m,n)\circledast f(m,n)+[v(m,n)-\bar{v}][h(m,n)\circledast f(m,n)]. \quad (2.13)$$

The signal-dependent nature of multiplicative noise is easily verified by noting that the variance of the noise part depends on the signal.

(B). Film-grain noise model

Film-grain noise describes the intrinsic noise produced by a photographic emulsion during the process of image recording and reproduction. Huang [2-8] modeled the film-grain noise as

$$g(m,n)=d(h(m,n)\circledast f(m,n)) + cd(h(m,n)\circledast f(m,n))^{1/3}v(m,n) \quad (2.14)$$

where v(m,n) is a white Gaussian noise, with mean zero and variance one, c is a scalar, and d(.) is the nonlinear D-logE function. Naderi and Sawchuk [2-9] proposed a more accurate film-grain model which includes additional complex optical and chemical effects. Huang's model is similar to the additive form of the multiplicative noise model and is signal-dependent uncorrelated noise. Naderi-Sawchuk's model contains a

blurring function after the noise degradation and thus produces signal-dependent and correlated noise. This case will be discussed in the next section.

(C). Poisson noise model

Because of the quantum nature of light, photon noise imposes a fundamental limitation on detected images. The emission of photons is described by a Poisson point process with the average rate of emission proportional to the incident intensity [2-10]. We use the following notation to describe a Poisson random number generator with a constant proportionality factor λ

$$g(m,n) = \text{Poisson}_{\lambda}(f(m,n)). \tag{2.15}$$

The probabilistic description of Poisson noise is given by

$$P(g(m,n)\,|\,f(m,n)) = \frac{(\lambda f(m,n))^{g(m,n)} e^{-\lambda f(m,n)}}{g(m,n)!}. \tag{2.16}$$

The conditional mean and variance of g(m,n) for a given f(m,n) are

$$E[g(m,n)\,|\,f(m,n)] = \lambda f(m,n) \tag{2.17}$$

$$\text{Var}[g(m,n)\,|\,f(m,n)] = \lambda f(m,n). \tag{2.18}$$

The signal-dependent nature of Poisson noise is demonstrated by the dependence of its variance on the signal. The uncorrelated property of Poisson noise is based on the assumption of independent photon counters. Poisson noise occurs in medical imaging, astronomical imaging and low light level television systems. Fig. 2.5 is the block diagram of images degraded by blur and Poisson noise.

2.4.3 Signal-Dependent Correlated Noise Models

Speckle [2-11] noise inherently exists in all types of coherent imagery. Many speckle reduction techniques assume that speckle noise is multiplicative and uncorrelated. This is only a rough approximation. In fact, speckle is not only signal-dependent but also correlated. The correlation function of speckle is of fundamental importance for speckle reduction.

The detail of speckle modeling and its statistical properties will be discussed in Chapter 3. Briefly speaking, speckle is the result of phase noise (multiplicative noise degradation in the complex amplitude domain of the object) which then proceeds through a linear filter and an intensity detector. The exchange of the sequence of degradations, first multiplicative noise then blur, makes speckle noise correlated and much more difficult to process when compared with signal-dependent uncorrelated noise.

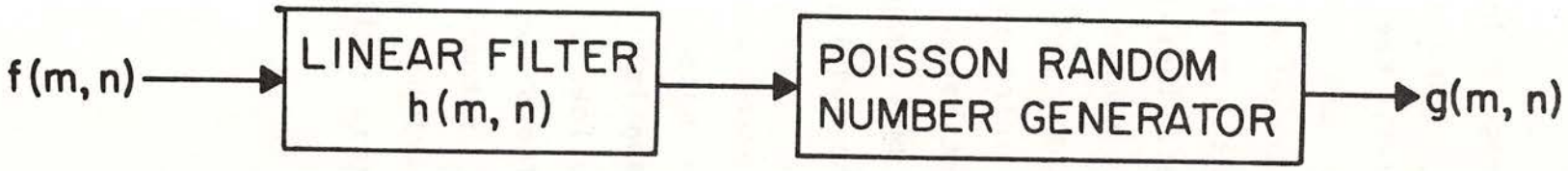

Figure 2.5 Block diagram of image degraded by blur and Poisson noise

2.5 Conclusions

A truly nonstationary image model which includes a nonstationary mean and a nonstationary covariance function is desirable. However, the complexity of the resulting restoration filter and the difficulties of estimating the image model parameters from the degraded image may overshadow the possible performance improvement of using such an image model. Therefore, a NMNV image model is introduced. The nonstationary mean describes the gross structure of the image and the nonstationary variance contains the edge information. These model parameters can be easily estimated from the degraded image. The validity of the NMNV image model depends on the method used to estimate the model parameters.

Many physical noise processes are inherently signal-dependent. We separate these noise processes into two classes according to the spatial correlation of the noise. This classification allows a unified approach to the design of restoration filters for a class of signal-dependent noise processes, rather than deriving a different filter for each individual case. The NMNV image model is most convenient for this application.

Chapter 3

SPECKLE MODELING AND DISCRETE SPECKLE IMAGE GENERATION

3.1 Introduction

The invention of the laser revealed a strange phenomenon known as "speckle". The origin of speckle is now well understood [3-1,3-2]. Speckle is due to the random interference of the wavelets scattered by the microscopic fluctuations of the object surface contained in one resolution element when illuminated with highly coherent light. Due to our lack of knowledge of the detailed structure of the object surface, speckle is best described by its statistical properties. The general statistical analysis of speckle is very complicated and is still the subject of active research, especially in the application of speckle measurements to obtain surface roughness properties [3-3]. In order to obtain useful expressions of the statistics of speckle, we will make some assumptions about the object surface.

A major difficulty in speckle modeling arises in the modeling of the scattering surface. Goodman [3-1] used a discrete model for so called "fully developed" speckle that occurs when the phenomenon can be described by a

complex circular Gaussian random process. In his model, the object surface is assumed to be a collection of a large number of independent scatterers, and the random phases introduced by the surface structure are uniformly distributed in the interval $[0,2\pi]$. The statistics of fully developed speckle can be easily calculated using these assumptions, and give results in agreement with the experimental measurements where the object surface is very rough compared with the optical wavelength. Pedersen [3-4] used a more sophisticated surface model that assumes that the object surface is a continuous Gaussian random field and at the same time takes into account spatial correlations of the surface height fluctuations. This is a more physically realistic surface model, but the calculation of speckle statistics is much more difficult because it requires the autocorrelation function of the object surface which is not available in most applications.

Discrete speckle image can be generated according to its true physical model with a digital computer for simulation studies. Previous work by Guenther et al. [3-5] generates discrete speckle images according to the first order probability density function of "fully developed" speckle. The discrete speckle image generated by this method is a simplification of the true physical process of speckle image formation and is lack of the second order statistical properties of speckle. Fujii et al. [3-6] generated discrete speckle images

deterministically according to the true physical model of speckle to study the surface roughness properties. However, they ignored the importance of the sampling theorem and the resulting discrete speckle images will not be the same as those produced by an equivalent optical system because of the aliasing effect.

In this chapter, we discuss the statistical properties of general speckle. It is shown that explicit expressions for general speckle statistics are difficult to obtain. These statistics may be studied by using discrete speckle images generated by a digital computer. The problem of generating discrete speckle images accurately to avoid aliasing effects is addressed. The sampling theorem plays an important role in this analysis. Generally speaking, we need to oversample the object surface function by a factor that is proportional to the variance of the surface roughness. For the case of "fully developed" speckle where the object surface is extremely rough compared with the optical wavelength, the statistics of speckle can be easily derived. However, the sampling rate required for accurately generating discrete "fully developed" speckle images is very high and imposes a computation problem because of the large number of samples required in the simulation. Instead of generating a discrete sampled version of a continuous speckle image with so much computation time, we introduce a new discrete model to generate statistically equivalent speckle images. Various methods for effectively generating these discrete speckle images are discussed.

3.2 Mathematical Model of Speckle

Consider the coherent imaging system illustrated in Fig. 3.1. A transparency of complex amplitude transmittance $\underline{t}(x,y)$ is illuminated by a unit-amplitude coherent beam. Here, $\underline{t}(x,y)$ can be represented as

$$\underline{t}(x,y) = f^{1/2}(x,y)\exp(j\phi(x,y)) \tag{3.1}$$

where $f^{1/2}(x,y)$ is the amplitude of the object transmittance, and $\phi(x,y)$ is the phase due to the roughness of the transparency surface. The complex amplitude field at the image plane is given by

$$\underline{b}(x,y) = \int_{-\infty}^{\infty}\int f^{1/2}(p,q)\exp(j\phi(p,q))h(x-p,y-q)\,dpdq \tag{3.2}$$

where $h(x,y)$ is the coherent point spread function [3-7] of the system and is related to the pupil function $P(r,s)$ in the pupil plane by

$$h(x,y) = \int_{-\infty}^{\infty}\int \frac{1}{\lambda^2 f_0^2} P(r,s)\exp[j\frac{2\pi}{\lambda f_0}(rx+sy)]\,drds$$

where f_o is the lens focal length, and λ is the wavelength. The pupil function $P(r,s)$ has the property that

$$P(r,s) = \begin{cases} 1 & \text{for } (r,s) \text{ inside the pupil} \\ 0 & \text{otherwise.} \end{cases}$$

If the pupil function is symmetric with respect to the

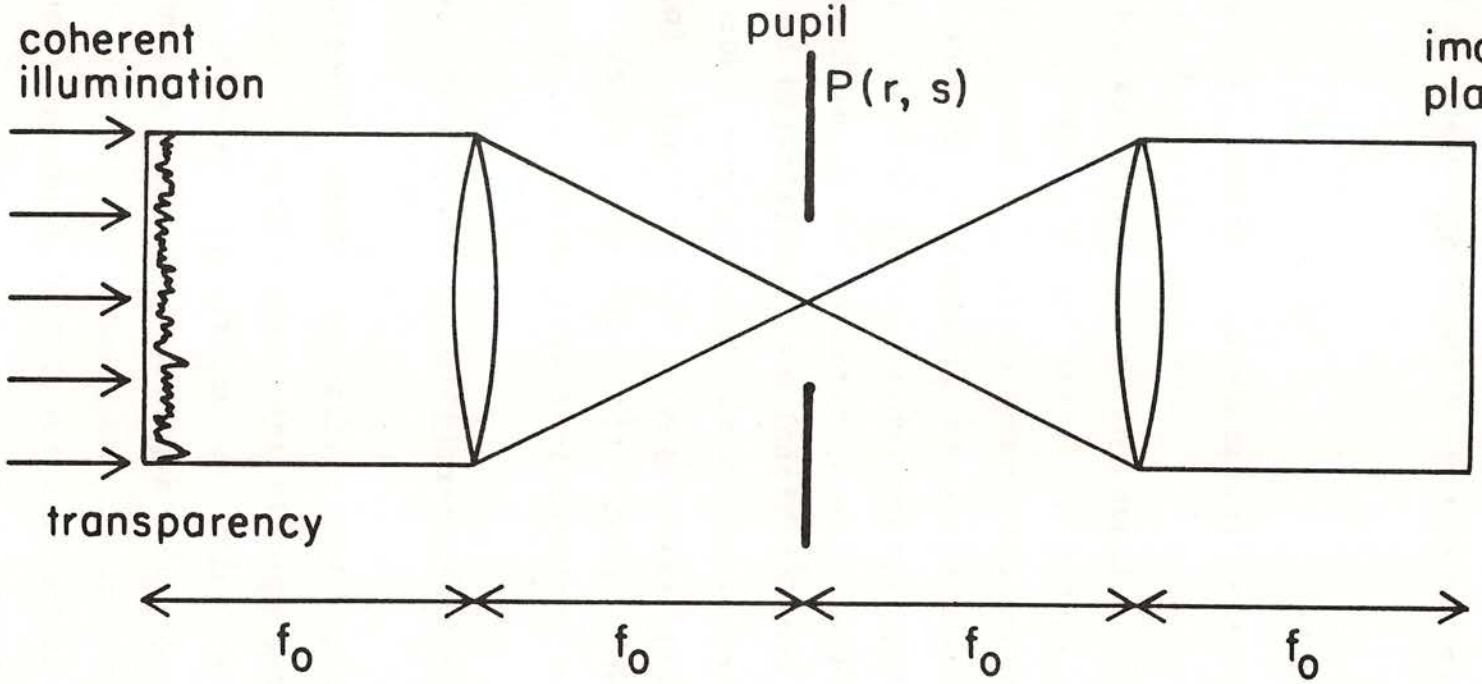

Figure 3.1 Coherent imaging system

origin, then $h(x,y)$ is a real function. This is assumed to be the case in the following discussion.

The speckle intensity in the image plane is given by

$$g(x,y) = |\underline{b}(x,y)|^2. \tag{3.3}$$

Note that if the transparency surface is perfectly smooth, i.e., $\phi(p,q)$ is constant, then $\underline{b}(x,y)$ is the desired coherent image of the object except for a constant phase factor and there is no speckle. Otherwise, speckle occurs in the image plane. A block diagram of the speckle image model is illustrated in Fig. 3.2. In this model, the random phase noise arising from the roughness of the object surface first multiplies the signal. This product signal is then filtered by a linear system and is recorded in the image plane. Note that it is the quantity $\exp[j\phi(p,q)]$ rather than $\phi(p,q)$ that directly feeds into the speckle model. Because $\exp[j\phi(p,q)]$ is periodic in ϕ with period 2π, i.e.,

$$\exp[j(\phi(p,q)+2n\pi)]=\exp[j\phi(p,q)] \text{ for any integer } n,$$

it is possible that different phase functions will produce the same speckle intensity pattern. Usually only the speckle intensity is observable. However, in some applications, both the amplitude and phase of the speckle image are accessible. The task of speckle reduction techniques is to recover the signal from the observations degraded by speckle.

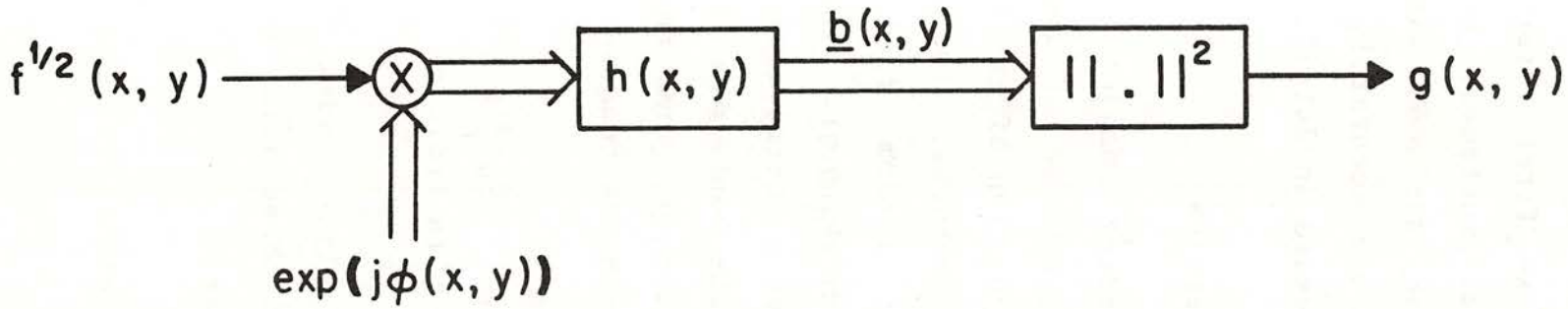

Figure 3.2 Block diagram of speckle model

3.3 General Speckle

In this section, we first formulate the statistics of speckle for general surfaces, then we derive some useful expressions for surfaces with Gaussian height fluctuations. A method for accurately generating discrete speckle images is discussed in detail.

3.3.1 Statistical Properties

Consider the coherent imaging system in Fig. 3.1. Let $\bar{d}$ be the mean thickness of the transparency and $d(p,q)$ be the height function of the transparency surface relative to its mean thickness. Assume that $d(p,q)$ is a wide-sense stationary random field with normalized autocorrelation function $\rho_d(p,q)$. The Fourier transform of $\rho_d(p,q)$ is the power spectral density function of the surface and indicates the bandwidth of $d(p,q)$. Let d_0 be the maximum value of $d(p,q)$, then the total phase delay caused by passing through the transparency is given by

$$\begin{aligned}\phi(p,q) &= \frac{2\pi}{\lambda}[n(\bar{d}+d(p,q))+(d_0-d(p,q))] \\ &= \frac{2\pi}{\lambda}(n\bar{d}+d_0)+\frac{2\pi}{\lambda}(n-1)d(p,q) \qquad (3.4)\end{aligned}$$

where n is the refractive index of the transparency material. The constant phase delay term in Eq. (3.4) can be neglected and we have

$$\phi(p,q)=\frac{2\pi}{\lambda}(n-1)d(p,q).$$

$\phi(p,q)$ is also a stationary random field because it is a scaled version of $d(p,q)$. The variance and normalized correlation function of $\phi(p,q)$ are

$$\sigma_\phi^2 = \left[\frac{2\pi}{\lambda}(n-1) \right]^2 \sigma_d^2$$

and

$$\rho_\phi(p,q) = \rho_d(p,q)$$

where σ_ϕ^2 and σ_d^2 are the variances of $\phi(p,q)$ and $d(p,q)$ respectively. If the transparency is not thick compared with the optical wavelength, the complex amplitude field across a plane immediately behind the transparency can be approximated as

$$f_\phi^{1/2}(p,q) = f^{1/2}(p,q) \exp(j\phi(p,q)),$$

and the complex field in the image plane is given by

$$\underline{b}(x,y) = \iint h(x-p, y-q)\, f^{1/2}(p,q) \exp(j\phi(p,q))\, dp\, dq.$$

Note that although $\phi(p,q)$ is closely related to the physical process of speckle image formation, $\exp(j\phi(p,q))$ is the quantity directly involved in the system.

We now turn to discuss the statistical properties of speckle. Since the intensity distribution $f(p,q)$ of the original object is unknown *a priori*, it can only be modeled as a random field. However, in deriving the

statistics of a speckle image, it is sometimes instructive to first look at $f(p,q)$ as a given function and calculate the conditional statistics, then treat $f(p,q)$ as a random field to obtain the overall statistics (unconditional statistics). In the following discussion, the conditional statistics will be specified explicitly.

A quantity of great interest is the conditional autocorrelation function of $\underline{b}(x,y)$ given $f(p,q)$, which has the form

$$\begin{aligned} R_b(x,y;x_1,y_1|f) &= E[\underline{b}(x,y)\underline{b}^*(x_1,y_1)|f] \\ &= \iiiint f^{1/2}(p,q)\, f^{1/2}(r,s)\, E\{\exp[j\phi(p,q)-j\phi(r,s)]\} \\ &\qquad h(x-p,y-q)\, h(x_1-r,y_1-s)\, dp\,dq\,dr\,ds \\ &= \iiiint f^{1/2}(p,q)\, f^{1/2}(r,s)\, R_{\exp(j\phi)}(p-r,q-s) \\ &\qquad h(x-p,y-q)\, h(x_1-r,y_1-s)\, dp\,dq\,dr\,ds. \end{aligned} \tag{3.5}$$

In order to calculate $R_b(x,y;x_1,y_1|f)$, we need to know the explicit form of $R_{\exp(j\phi)}(p-r,q-s)$ which is usually not available in most applications. In general, numerical integration has to be carried out for a given $R_{\exp(j\phi)}(p-r,q-s)$ to obtain the autocorrelation function of $\underline{b}(x,y)$. Other second order statistics can be calculated similarly with multiple integrations.

For the special case where $d(p,q)$ is a Gaussian random field, we can obtain explicit expressions for speckle statistics. The joint characteristic function of a zero-mean Gaussian distribution has the form

$$M(w_1,w_2) = E[\exp(jw_1\phi_1)\exp(jw_2\phi_2)]$$
$$=\exp[-1/2(w_1^2\ \sigma_\phi^2+w_2^2\ \sigma_\phi^2+2\rho_\phi\ w_1w_2)] \qquad (3.6)$$

where σ_ϕ^2 and ρ_ϕ are, respectively, the variance and correlation coefficient of two Gaussian random variables ϕ_1 and ϕ_2. The autocorrelation function of $\exp(j\phi(p,q))$ is given by

$$R_{\exp(j\phi)}(\Delta p,\Delta q)=E\{\exp[j(\phi(p,q)-\phi(p_1,q_1))]\}. \qquad (3.7)$$

From Eqs. (3.6) and (3.7), it is easy to see that

$$R_{\exp(j\phi)}(\Delta p,\Delta q) = M(1,-1)$$
$$= \exp[-\sigma_\phi^2(1-\rho_d(\Delta p,\Delta q))]. \qquad (3.8)$$

The autocorrelation function has a bias term $\exp(-\sigma_\phi^2)$ which indicates that $\exp(j\phi(p,q))$ has a nonzero mean. The mean of $\exp(j\phi(p,q))$ can be shown to be

$$E[\exp(j\phi(p,q))] = \exp(-\sigma_\phi^2/2).$$

The covariance function of $\exp(j\phi)$ has the form

$$C_{\exp(j\phi)}(\Delta p,\Delta q) = R_{\exp(j\phi)}(\Delta p,\Delta q)-\exp(-\sigma_\phi^2)$$
$$= \exp(-\sigma_\phi^2)[\exp(\sigma_\phi^2\rho_\phi(\Delta p,\Delta q))-1]. \qquad (3.9)$$

The normalized covariance function of $\exp(j\phi(p,q))$ is given by

$$\rho_{\exp(j\phi)}(\Delta p,\Delta q) = \frac{\exp[\sigma_\phi^2 \rho_\phi(\Delta p,\Delta q)] - 1}{\exp(\sigma_\phi^2) - 1}$$

In Fig. 3.4, $\rho_{\exp(j\phi)}(\Delta p,0)$ is plotted for different values of σ_ϕ^2 for the case when $\rho_\phi(\Delta p,0)$ has a triangular shape as in Fig. 3.3. It is easy to see that the effective width of $\rho_{\exp(j\phi)}(\Delta p,\Delta q)$ is much narrower than the width of $\rho_\phi(\Delta p,\Delta q)$ for large σ_ϕ^2. Therefore, the effective bandwidth of $\exp(j\phi(p,q))$ depends not only on the bandwidth of $\phi(p,q)$, but more importantly, on the variance of $\phi(p,q)$.

Let w_a and w_b be the widths defined by

$$\rho_\phi(w_a,0) = 1/e \text{ and } \rho_{\exp(j\phi)}(w_b,0) = 1/e$$

respectively. The ratio of w_a to w_b can be written as

$$W_r = \frac{1-e^{-1}}{1-\frac{1}{\sigma_\phi^2}\ln[\exp(\sigma_\phi^2-1)+1-e^{-1}]} \qquad (3.10)$$

In Fig. 3.5, W_r is plotted with respect to σ_ϕ^2. This curve is an approximate indication of the bandwidth ratio between $\exp(j\phi(p,q))$ and $\phi(p,q)$, and is of fundamental importance for accurately generating discrete speckle images. From Eq. (3.10), it is easy to see that W_r asymptotically approaches $(1-e^{-1})\sigma_\phi^2$ when σ_ϕ^2 becomes large.

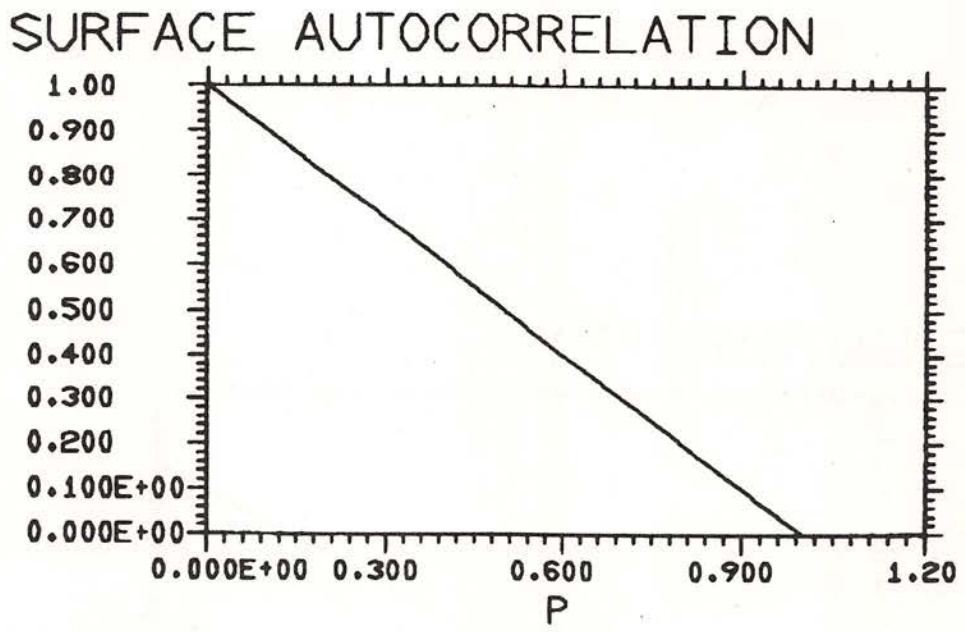

Figure 3.3 The autocorrelation function of $\phi(x,y)$

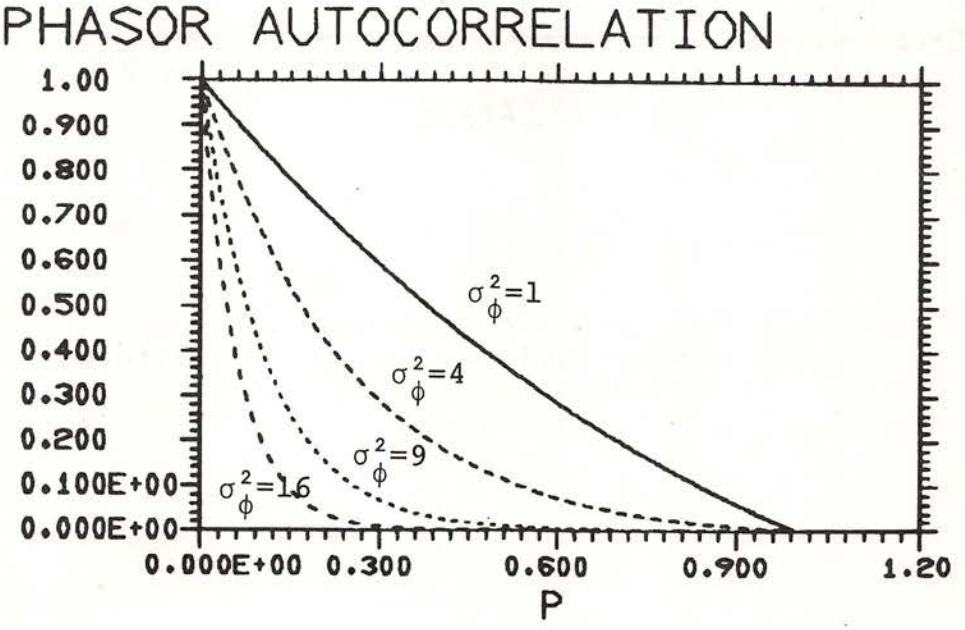

Figure 3.4 The autocorrelation function of $\exp(j\phi(x,y))$ for different σ_ϕ^2 values

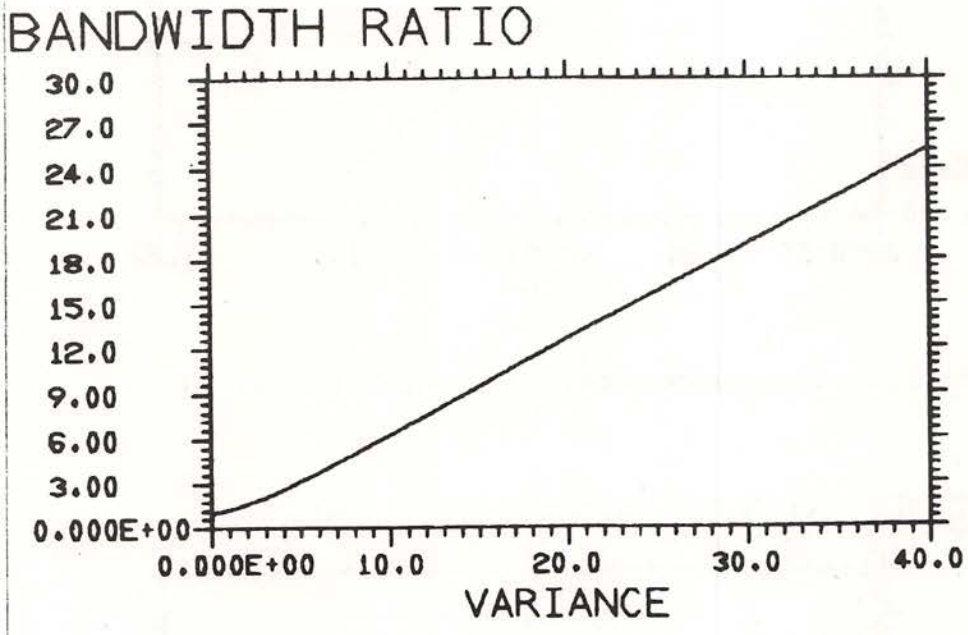

Figure 3.5 The relative bandwidth ratio of $\exp(j\phi(x,y))$ to $\phi(x,y)$ for different σ_ϕ^2 values

3.3.2 Discrete Speckle Image Generation

Since $\exp(j\phi(p,q))$ is a highly nonlinear function which expands the bandwidth of $\phi(p,q)$ significantly when the variance of $\phi(p,q)$ is large, we should be very careful about choosing the sampling frequency in order to avoid the aliasing effect. W_r shown in Fig. 3.5 is essentially the bandwidth ratio of $\exp(j\phi(p,q))$ to $\phi(p,q)$ when $\phi(p,q)$ is Gaussian. Consequently, if we want to represent $\underline{b}(x,y)$ accurately from the discrete samples of $f^{1/2}(p,q)$ and $\phi(p,q)$, the sampling frequency should be at least W_r times greater than the bandwidth of $\phi(p,q)$ according to the sampling theorem. This fact is usually ignored in the literature. An ambiguous statement is that "speckle will not occur if the imaging system can resolve the surface variation". As shown in the above discussion, the extent of speckle is determined by the effective bandwidth of $\exp(j\phi(p,q))$, which is much larger than the bandwidth of $\phi(p,q)$ for large σ_ϕ^2. Even though the imaging system may resolve $\phi(p,q)$, speckle will occur if σ_ϕ^2 is large. Fujii *et al.* [3-6] conducted a computer simulation study of speckle patterns for different surface profiles. They used the same sampling frequency for different σ_ϕ^2. If σ_ϕ^2 is large, the computer generated speckle patterns will be much different from those produced by an equivalent optical system because of the aliasing effect.

The discrete speckle image generation model for a

general surface case is illustrated in Fig. 3.6. The original object amplitude $f^{1/2}(x,y)$ and the object phase function $\phi(x,y)$ are sampled at a rate M times larger than the Nyquist frequency of ϕ in order to avoid the aliasing effect possibly arising from the nonlinear transformation $\exp(j\phi(p,q))$. Then the discrete samples $f^{1/2}(i,k)$ and $\exp(j\phi(i,k))$ are multiplied and the product is filtered by a low pass filter with passband W_L. The output of the filter is the discrete complex amplitude speckle $\underline{b}(m,n)$. The speckle intensity image $g(m,n)$ is obtained by taking the squared magnitude of $\underline{b}(m,n)$. At this stage, $g(m,n)$ is an oversampled image because its bandwidth is only $2W_L$ which is in general much smaller than the sampling frequency of the system.

Discrete speckle images can be easily generated according to the model given in Fig. 3.6. In order to observe the differences in speckle patterns clearly, we generate one-dimensional speckle intensity patterns for a general surface. We also assume that the object intensity is constant and $\phi(p,q)$ is a wide-sense stationary Gaussian process for simplicity. Instead of calculating the ratio M of the system sampling frequency beforehand, we interpolate the phase samples by a factor of 2 each time until the output discrete speckle intensity pattern does not change. This means that no aliasing occurs at this stage. In Fig. 3.7(a), we generated 128 independent Gaussian random variables as the discrete phase samples of a continuous Gaussian

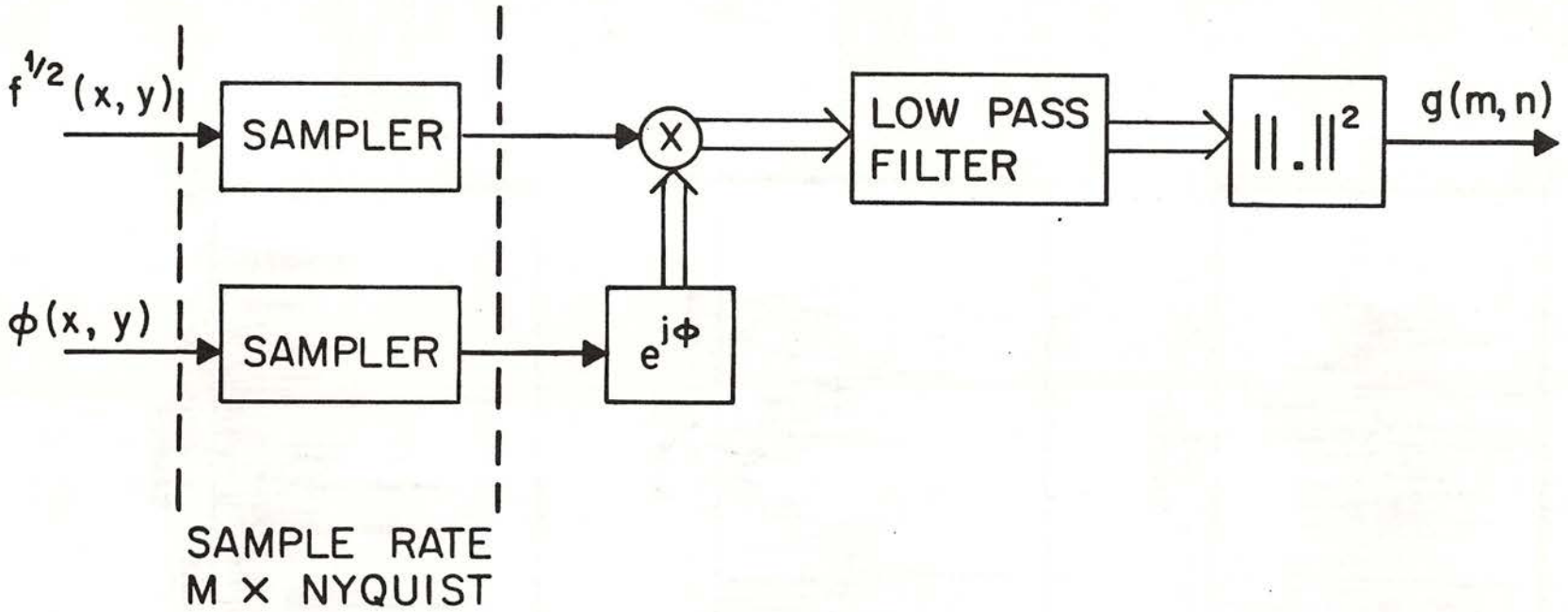

Figure 3.6 Discrete speckle generation model for general speckle

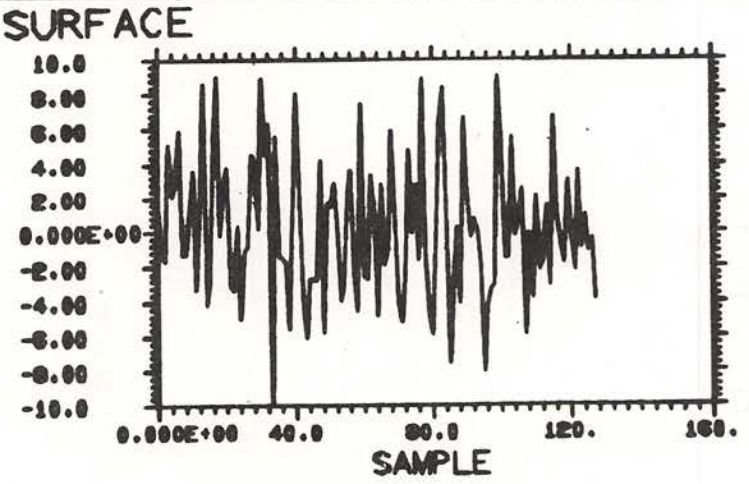

(a) Object surface phase function $\sigma_\phi = 4$

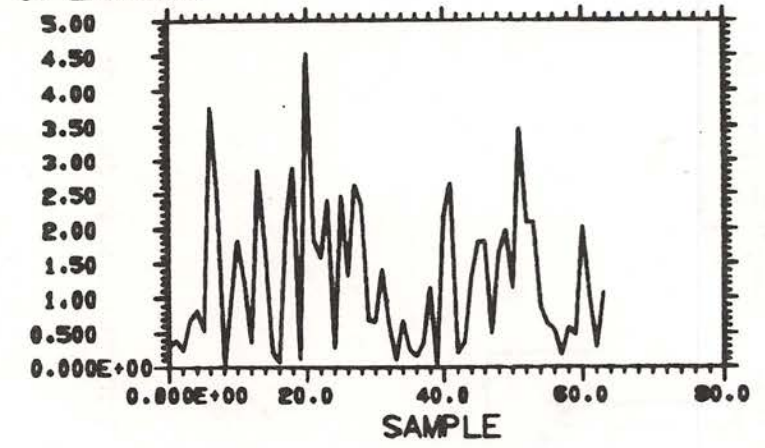

(b) Speckle pattern without phase interpolation

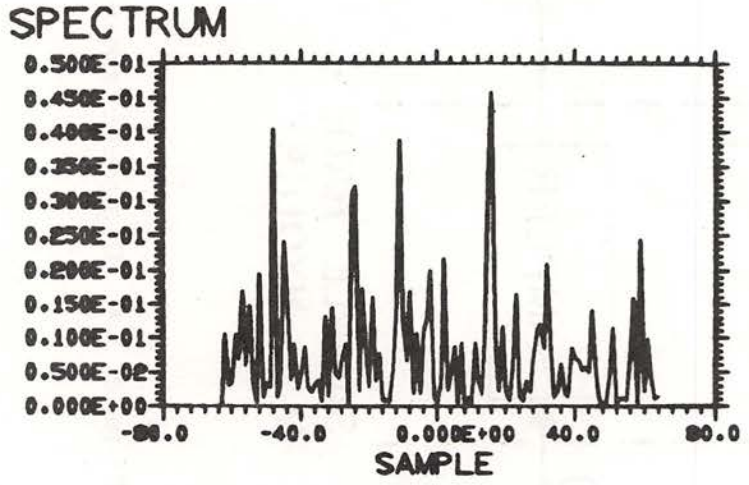

(c) Spectrum of $e^{j\phi}$ without phase interpolation

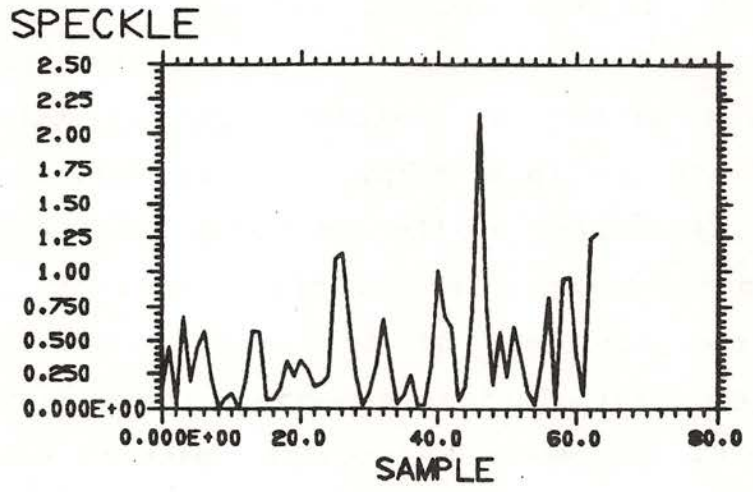

(d) Speckle pattern after 8 times phase interpolation

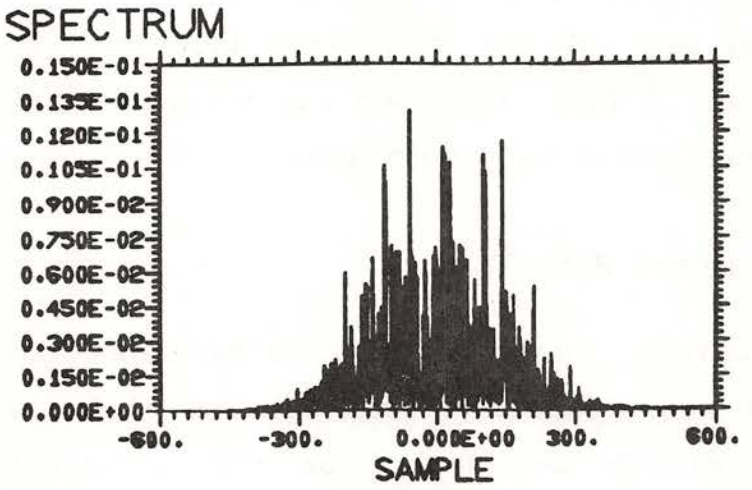

(e) Spectrum of $e^{j\phi}$ after 8 times phase interpolation

Figure 3.7 Example of discrete speckle generation for general speckle where $\sigma_{\phi}=4$

surface. The standard deviation of the phase samples is 4. Fig. 3.7(b) is the speckle pattern of a constant intensity object when the passband of the optical pupil is 32 samples wide. No interpolation of the phase samples is made at this step. It is sufficient to display only 64 samples of the speckle intensity pattern because the optical pupil is 32 samples wide. Fig. 3.7(c) is the squared magnitude of the Fourier transform of $\exp(j\phi)$. After interpolating the object phase samples by a factor of 8, the speckle intensity pattern converges and is shown in Fig. 3.7(d). Fig. 3.7(e) is the squared magnitude of the Fourier transform of $\exp(j\phi)$ after interpolation. Note that the speckle intensity patterns of Fig. 3.7(a) and (c) are entirely different. The flat spectrum in Fig. 3.7(c) indicates the severe aliasing for the case without phase interpolation.

3.4 Fully Developed Speckle

The explicit mathematical expressions of the statistics of speckle for general surface conditions are difficult to obtain and depend on the autocorrelation function of the object surface which is not available in most applications. If the object surface is extremely rough compared with the optical wavelength, from Fig. 3.5 we see that the effective bandwidth of $\exp(j\phi(p,q))$ is proportional to σ_ϕ^2 and is many times larger than the bandwidth of $\phi(p,q)$. In this case, $\exp(j\phi(p,q))$ can be considered as a white noise field for any practical

purpose when compared to the optical pupil. This is called "fully developed" speckle. The statistical properties of this fully developed speckle can be easily derived by using this "almost white" approximation, and are in agreement with the experimental measurements. These statistics are very important for developing speckle reduction techniques.

3.4.1 Statistical Properties

From Eq. (3.5) and the "almost white" assumption, the conditional autocorrelation function of $\underline{b}(x,y)$ for fully developed speckle can be written as

$$
\begin{aligned}
&R_b(x,y;x_1,y_1|f) \\
&= \iiiint f^{1/2}(p,q)\, f^{1/2}(r,s)\, R_{\exp(j\phi)}(p-r,q-s) \\
&\qquad h(x-p,y-q)\, h(x_1-r,y_1-s)\, dpdqdrds \\
&\cong \iint f(p,q)\, h(x-p,y-q)\, h(x_1-p,y_1-q) \\
&\qquad \left[\iint R_{\exp(j\phi)}(p-r,q-s)\, drds\right] dpdq \\
&= B \iint f(p,q)\, h(x-p,y-q)\, h(x_1-p,y_1-q)\, dpdq \qquad (3.11)
\end{aligned}
$$

where

$$
B = \iint_T R_{\exp(j\phi)}(p-r,q-s)\, drds,
$$

and region T is the extent of the object surface. The conditional mean of speckle intensity g(x,y) is given by

$$
\begin{aligned}
&E[g(x,y)|f] = R_b(x,y;x,y|f) \\
&= B \iint f(p,q)\, h^2(x-p,y-q)\, dpdq. \qquad (3.12)
\end{aligned}
$$

Note that the conditional mean of $g(x,y)$ is equal to the incoherent image of the system except for a scalar B. This suggests that we can have a good estimate of the incoherent image of the system by averaging over a large number of uncorrelated speckle intensity images of the same object. The scalar B is determined from the area of the autocorrelation function of $\exp(j\phi(p,q))$, and only affects the relative intensity level of speckle. From Eq. (3.8), we know that $R_{\exp(j\phi)}(p,q)$ has a bias term $\exp(-\sigma_\phi^2)$ if $\phi(p,q)$ is a zero-mean Gaussian variable. For fully developed speckle, $\sigma_\phi >> \pi$ so this bias term is very small and can be neglected. If σ_ϕ^2 is small and $\phi(p,q)$ has large bandwidth, i.e., $R_{\exp(j\phi)}(p,q)$ is still very narrow compared with $h(p,q)$ but has a bias term $\exp(-\sigma_\phi^2)$ that can not be neglected, Eq. (3.11) then becomes

$$
\begin{aligned}
&R_b(x,y;x_1,y_1|f) \\
&= \iiiint f^{1/2}(p,q)\, f^{1/2}(r,s)\, R_{\exp(j\phi)}(p-r,q-s) \\
&\qquad h(x-p,y-q)\, h(x_1-r,y_1-s)\, dpdqdrds \\
&= \iiiint f^{1/2}(p,q)\, f^{1/2}(r,s)\, h(x-p,y-q)\, h(x_1-p,y_1-q) \\
&\quad [\exp(-\sigma_\phi^2) + (R_{\exp(j\phi)}(p-r,q-s) - \exp(-\sigma_\phi^2))]\, dpdqdrds \\
&= \exp(-\sigma_\phi^2) \left[\iint f^{1/2}(p,q)\, h(x-p,y-q)\, dpdq\right] \\
&\quad \left[\iint f^{1/2}(r,s)\, h(x_1-r,y_1-s)\, drds\right] \\
&\quad + B_1 \iint f(p,q)\, h(x-p,y-q)\, h(x_1-p,y_1-q)\, dpdq \qquad (3.13)
\end{aligned}
$$

where

$$B_1 = \iint [R_{\exp(j\phi)}(p-r,q-s) - \exp(-\sigma_\phi^2)]\,dr\,ds.$$

Here, B_1 can be taken out of the integral since the autocorrelation function of $\exp(j\phi)$ is very narrow compared with h. Note that $\iint f^{1/2}(p,q)\,h(x-p,y-q)\,dp\,dq$ in Eq. (3.13) is the coherent image of $f^{1/2}(p,q)$. The conditional mean of g(x,y) now becomes

$$E[g(x,y)\,|\,f] = \exp(-\sigma_\phi^2)\left[\iint f^{1/2}(p,q)\,h(x-p,y-q)\,dp\,dq\right]^2 + B_1 \iint f(p,q)\,h^2(x-p,y-q)\,dp\,dq \qquad (3.14)$$

which is a weighted sum of the coherent image intensity and the incoherent image intensity of f(p,q). The coherent image part is the result of the smooth object surface that contributes to the in phase component of the object in the image plane. Therefore, a large bandwidth of $\exp(j\phi(x,y))$ is not sufficient to specify fully developed speckle. We also require that $\exp(j\phi(x,y))$ has zero mean. It is interesting to see that the autocorrelation function of $\underline{b}(x,y)$ for fully developed speckle only depends on the original object intensity and the coherent point spread function. The knowledge of the autocorrelation function of $\exp(j\phi(p,q))$ is not required and only serves as a scaling factor in the expression.

Goodman [3-1] used a discrete model for fully developed speckle and assumed that the object surface can be modeled as a collection of a large number of independent scatterers. The statistics derived based on

this simplified discrete surface model are the discrete representations of the statistics derived by using the "almost white" approximation. Since our goal is to use digital methods for speckle reduction, we will derive all the statistics needed in discrete form by using Goodman's speckle model.

Without loss of generality, assuming that the object surface is a collection of evenly spaced independent scatterers. Let h(m,n) be the coherent point spread function of the system, we have

$$\underline{b}(m,n)=\sum_i\sum_k f^{1/2}(i,k)\exp(j\phi(i,k))h(m-i,n-k) \qquad (3.15)$$

where $f^{1/2}(i,k)$ is the sampled object transmittance function, and $\phi(i,k)$ is the phase sample. The speckle intensity is given by

$$g(m,n)=|\underline{b}(m,n)|^2. \qquad (3.16)$$

We now restate the "fully developed" speckle assumptions of Goodman's model.

1. f(i,k) and $\phi(i,k)$ are statistically independent and $\phi(i,k)$ is independent of all other random phases. (i.e., the signal and the phase noise are statistically independent, and the phase noise is a white noise sequence.)

2. $\phi(i,k)$ is uniformly distributed in the interval $(0,2\pi]$. (i.e., the object surface is extremely rough compared with a wavelength, and the phase excursions of many times 2π radians are equivalent to a uniform distribution on the primary interval.)

3. The spacing between these independent phasors is very small compared with the coherent point spread function such that $\underline{b}(m,n)$ is a linear combination of a great many independent scatterers.

Assumption (2) is the result of rough object surface, and assumption (3) is the consequence of considering the sampling theorem for accurately generating a discrete speckle image in the rough surface case. These assumptions are in agreement with the principles of accurately generating discrete speckle images for general surface conditions. Assumption (1) may seem too strong for fully developed speckle. As shown in the previous discussion, the approximation we need to calculate the statistics of fully developed speckle is that $\exp(j\phi(x,y))$ is "almost white", without requiring that $\phi(x,y)$ is "almost white". However, here $\phi(i,k)$ is the phase value of the physical object surface in the primary interval $(0,2\pi]$ and it has a much larger bandwidth than the surface function. Therefore, assumption (1) is also in agreement with previous results.

From assumptions (1) and (3), the phasors $\exp(j\phi(i,k))$ are independent and the extent of $h(m,n)$ is broad compared with the sampling interval. These imply that $\underline{b}(m,n)$ is a superposition of a large number of independent random phasors. According to the central limit theorem, the complex random field $\underline{b}(m,n)$ asymptotically approaches a Gaussian random field as the number of phasors tends to infinity. Therefore, for fully developed speckle, $\underline{b}(m,n)$ can be approximated very well with a complex Gaussian random field. The conditional autocorrelation function of $\underline{b}(m,n)$ given $f(i,k)$ is given by

$$R_b(m,n;m_1,n_1|f) = E[\underline{b}(m,n)\underline{b}^*(m_1,n_1)|f]$$

$$= E\{\sum_i\sum_k\sum_r\sum_s f^{1/2}(i,k)\, f^{1/2}(r,s)\, h(m-i,n-k)\, h(m_1-r,n_1-s)\exp[j\phi(i,k)-j\phi(r,s)]|f\}$$

$$= \sum_i\sum_k h(m-i,n-k)\, h(m_1-i,n_1-k)\, f(i,k) \qquad (3.17)$$

where we have used the fact that

$$E[\exp(j\phi(i,k)-j\phi(r,s))] = \begin{cases} 1 & \text{if } (i,k)=(r,s) \\ 0 & \text{otherwise.} \end{cases}$$

It is easy to see that Eq. (3.17) is the normalized discrete representation of Eq. (3.11). The unconditional autocorrelation function of $\underline{b}(m,n)$ is

$$R_b(m,n;m_1,n_1) = E[R_b(m,n;m_1,n_1|f)]$$

$$= \sum_i\sum_k h(m-i,n-k)\, h(m_1-i,n_1-k)\, \bar{f}(i,k) \qquad (3.18)$$

where $\bar{f}(i,k)$ is the ensemble mean of $f(i,k)$.

The conditional mean of the speckle intensity is given by

$$E[g(m,n)|f] = R_b(m,n;m,n|f)$$
$$=\sum_i\sum_k h^2(m-i,n-k)f(i,k). \tag{3.19}$$

We now turn to calculate the first order probability density function of the speckle intensity. The mean of the real and imaginary parts of the complex amplitude speckle are

$$E[\underline{b}^r(m,n)]=E[\sum_i\sum_k f^{1/2}(i,k)h(m-i,n-k)\cos\phi(i,k)]$$
$$=\sum_i\sum_k E[f^{1/2}(i,k)]E[\cos\phi(i,k)]h(m-i,n-k)$$
$$= 0 \tag{3.20}$$

and

$$E[\underline{b}^i(m,n)]=E[\sum_i\sum_k f^{1/2}(i,k)h(m-i,n-k)\sin\phi(i,k)]$$
$$=\sum_i\sum_k E[f^{1/2}(i,k)]E[\sin\phi(i,k)]h(m-i,n-k)$$
$$= 0 \tag{3.21}$$

where we have used assumption (2) to calculate $E[\cos\phi(i,k)]$ and $E[\sin\phi(i,k)]$. The variance of the real and imaginary parts of $\underline{b}(m,n)$ are given by

$$\mathrm{Var}[\, b^r(m,n)\,]$$
$$=E[\sum_i\sum_k\sum_r\sum_s f^{1/2}(r,s)f^{1/2}(i,k)h(m-r,n-s)h(m-i,n-k)$$
$$\cos\phi(r,s)\cos\phi(i,k)]$$
$$=1/2\sum_i\sum_k E[f(i,k)]h^2(m-i,n-k), \tag{3.22}$$

$$\mathrm{Var}[b^i(m,n)] = 1/2 \sum_i \sum_k E[f(i,k)]h^2(m-i,n-k) \qquad (3.23)$$

and

$$E[b^r(m,n)b^i(m,n)]$$

$$= E[\sum_i \sum_k \sum_r \sum_s f^{1/2}(r,s) f^{1/2}(i,k) h(m-r,n-s)h(m-i,n-k)$$
$$\cos\phi(r,s)\sin\phi(i,k)]$$

$$= 0 \qquad (3.24)$$

where we have used the following equalities

$$E[\cos\phi(r,s)\cos\phi(i,k)] = E[\sin\phi(r,s)\sin\phi(i,k)]$$

$$= \begin{cases} 1/2 & \text{for } (r,s)=(i,k) \\ 0 & \text{otherwise,} \end{cases}$$

and

$$E[\cos\phi(r,s)\sin\phi(i,k)] = 0 \quad \text{for all } (i,k),(r,s). \qquad (3.25)$$

From these statistics and the complex Gaussian approximation of $\underline{b}(m,n)$, we can write down the joint probability density function of the real and imaginary parts of $\underline{b}(m,n)$,

$$P(b^r(m,n), b^i(m,n))$$

$$= \frac{1}{2\pi\sigma^2(m,n)} \exp\left\{ - \frac{[b^r(m,n)]^2 + [b^i(m,n)]^2}{2\sigma^2(m,n)} \right\} \qquad (3.26)$$

where

$$\sigma^2(m,n) = 1/2 \sum_i \sum_k E[f(i,k)]h^2(m-i,n-k). \qquad (3.27)$$

This is a circular complex Gaussian probability density

function. It is worthwhile to mention that the real and imaginary parts of the complex amplitude speckle are uncorrelated. Because they are also jointly Gaussian, they are statistically independent.

In some applications, only the intensity of the speckle image can be measured. To obtain the probability density function of $g(m,n)$, we express $\underline{b}(m,n)$ in polar coordinates

$$\underline{b}(m,n) = g^{1/2}(m,n)\, e^{j\theta(m,n)} \tag{3.28}$$

where $\theta(m,n)$ is in the primary interval $(0,2\pi]$. Applying the standard technique for the transformation of random variables, we have the joint probability density function

$$P(g(m,n),\theta(m,n)) = \begin{cases} (4\pi\sigma^2(m,n))^{-1} \exp(-g(m,n)/2\sigma^2(m,n)) & \text{for } g(m,n)\geq 0 \\ 0 & \text{otherwise.} \end{cases} \tag{3.29}$$

The marginal probability density functions are given by

$$P(g(m,n)) = \int_0^{2\pi} P(g(m,n),\theta(m,n))\, d\theta$$

$$= \begin{cases} (2\sigma^2(m,n))^{-1} \exp(-g(m,n)/2\sigma^2(m,n)) & \text{for } g(m,n)\geq 0 \\ 0 & \text{otherwise,} \end{cases} \tag{3.30}$$

which is a negative exponential density and

$$P(\theta(m,n)) = \int_0^{\infty} P(g(m,n),\theta(m,n))\, dg$$

$$= \begin{cases} (2\pi)^{-1} & \text{for } 0\leq\theta<2\pi \\ 0 & \text{otherwise,} \end{cases}$$

which is a uniform density.

Note that $P(g(m,n),\theta(m,n))=P(g(m,n))P(\theta(m,n))$. This means that the intensity and phase are statistically independent at any point (m,n). The signal-to-noise ratio at any point (m,n) is given by

$$SNR(m,n) = E[g(m,n)]/Var^{1/2}[g(m,n)] = 1 .$$

Another important characteristic of speckle is the speckle "size", or the correlation area of speckle. It is roughly the size of the incoherent point spread function of the system. This makes speckle a serious problem in coherent imaging systems because the speckle size is on the order of the resolution limit of the system. The conditional crosscorrelation function of f(m,n) and g(m,n) can be expressed as

$$\begin{aligned} R_{fg}(m,n;m_1,n_1|f) &= E[f(m,n)g(m_1,n_1)|f] \\ &= E\{f(m,n)\sum_i\sum_k\sum_r\sum_s h(m_1-i,n_1-k)h(m_1-r,n_1-s) \\ &\quad f^{1/2}(i,k)f^{1/2}(r,s)\exp[j\phi(i,k)-j\phi(r,s)]|f\} \\ &= f(m,n)\sum_i\sum_k h^2(m_1-i,n_1-k)f(i,k) . \end{aligned} \tag{3.31}$$

Taking an expectation over Eq. (3.31) with respect to f, we have the unconditional crosscorrelation function

$$\begin{aligned} & R_{fg}(m,n;m_1,n_1) \\ &= \sum_i\sum_k h^2(m_1-i,n_1-k)E[f(m,n)f(i,k)] \\ &= \sum_i\sum_k h^2(m_1-i,n_1-k)R_f(m,n;i,k) . \end{aligned} \tag{3.32}$$

The conditional autocorrelation function of g(m,n) is given by

$$R_g(m,n;m_1,n_1|f)$$
$$=E[\underline{b}(m,n)\underline{b}^*(m,n)\underline{b}(m_1,n_1)\underline{b}^*(m_1,n_1)|f]$$
$$=E[g(m,n)|f]E[g(m_1,n_1)|f]+|R_b(m,n;m_1,n_1|f)|^2 \qquad (3.33)$$

where we applied the following complex circular Gaussian moment theorem [3-2]:

Theorem: Let $\underline{u},\underline{v},\underline{s}$ and $\underline{t}$ be complex circular Gaussian random variables. Then

$$E[\underline{u}^*\underline{v}^*\underline{s}\underline{t}] = E[\underline{u}^*\underline{s}]E[\underline{v}^*\underline{t}]+E[\underline{u}^*\underline{t}]E[\underline{v}^*\underline{s}].$$

The conditional autocovariance function of g(m,n) has the form

$$C_g(m,n;m_1,n_1|f)=|R_b(m,n;m_1,n_1|f)|^2. \qquad (3.34)$$

The unconditional autocorrelation function of g(m,n) can be written as

$$R_g(m,n;m_1,n_1)=E[R_g(m,n;m_1,n_1|f)]$$
$$=\sum_i\sum_k\sum_r\sum_s R_f(i,k;r,s)h^2(m-i,n-k)h^2(m_1-r,n_1-s)+$$
$$\sum_i\sum_k\sum_r\sum_s R_f(i,k;r,s)h(m-i,n-k)h(m_1-i,n_1-k)$$
$$h(m-r,n-s)h(m_1-r,n_1-s). \qquad (3.35)$$

Similarly, the unconditional autocovariance function of g(m,n) can be written as

$$C_g(m,n;m_1,n_1)$$
$$=\sum_i\sum_k\sum_r\sum_s C_f(i,k;r,s)\,h^2(m-i,n-k)\,h^2(m_1-r,n_1-s)+$$
$$\sum_i\sum_k\sum_r\sum_s R_f(i,k;r,s)\,h(m-i,n-k)\,h(m_1-i,n_1-k)$$
$$h(m-r,n-s)\,h(m_1-r,n_1-s). \qquad (3.36)$$

These statistics are the basis for developing speckle reduction techniques.

3.4.2 Discrete Speckle Image Generation - Single Phase Model

To generate discrete speckle images accurately for fully developed speckle, the samplers in Fig. 3.6 need to be operated at a very high frequency in order to avoid the aliasing effect. This causes a serious computation problem because of the large number of samples required in the simulation. From the discussions in the last section, we know that Goodman's discrete model is statistically a good approximation for the case of rough surfaces. Instead of generating a "real" speckle image with so much computation time, we can generate a statistically equivalent speckle image based on this model, if our final goal is to analyze speckle images by their statistical properties. Another advantage of this approach is that we only need to characterize the object surface statistically rather than to specify it deterministically as in the general speckle generation model.

Fig. 3.8 illustrates the "single phase" model for generating statistically equivalent discrete fully developed speckle images. This generation model is the same as Goodman's discrete model. The random phase $\phi(i,k)$ is generated from a uniform random number generator in the interval $(0, 2\pi]$. $\phi(i,k)$ bears no relation to the physical object surface but has the same statistical assumptions. The sampler is operated at the same frequency as the random number generator. The product of $\exp(j\phi(i,k))$ and $f^{1/2}(i,k)$ goes through a low pass filter and a magnitude squared operator to obtain the speckle intensity image $g(m,n)$. Note that an implicit assumption in calculating the statistics of speckle for the very rough surface case is that $\underline{b}(m,n)$ has a complex circular Gaussian distribution. To satisfy this requirement, the sampling frequency of the "single phase" model should be large enough that the coherent point spread function covers many independent random phasors. Although the sampling requirement of the single phase model is more relaxed than that of the general speckle generation model, it is still computationally demanding.

3.4.3 Discrete Speckle Image Generation - Multiple Phase Model

The complex amplitude speckle $\underline{b}(m,n)$ generated from the single phase model can be expressed as

$$\underline{b}(m,n) = \sum_i \sum_k f^{1/2}(i,k) \exp(j\phi(i,k)) h(m-i,n-k) \qquad (3.37)$$

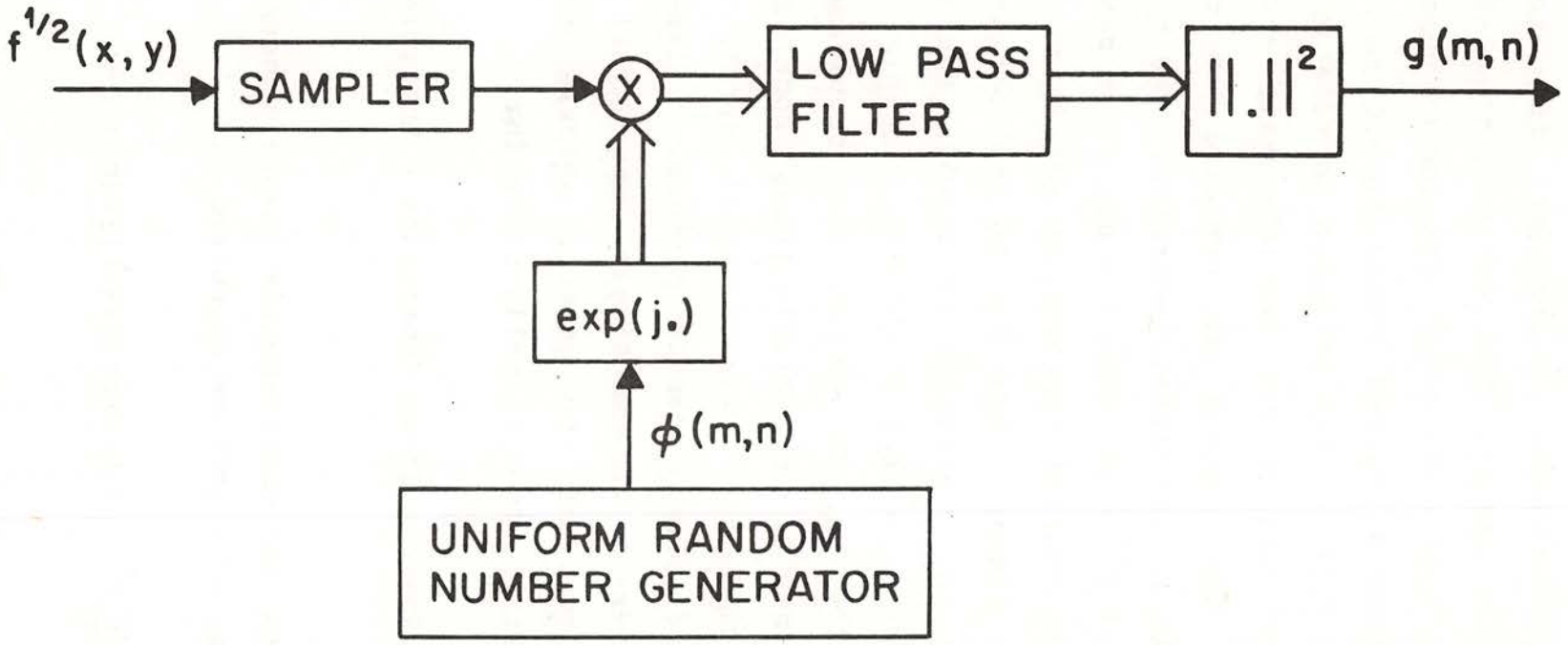

Figure 3.8 Single phase discrete speckle generation model for fully developed speckle

where the sampling frequency used in this model is usually several times larger than the bandwidth of the system and signal. Let us assume that the sampling frequency of the single phase model is r times larger than the maximum of the bandwidths of the incoherent imaging system and the signal in both x and y directions. It is reasonable to have the following approximations

$$f^{1/2}(ri+s,rk+t) \cong f^{1/2}(ri,rk)$$

and

$$h(ri+s,rk+t) \cong h(ri,rk) \quad \text{for } -(r-1)/2 \leq s,t \leq (r-1)/2$$

where r is assumed to be an odd integer. Using these approximations, the complex amplitude speckle at coordinate (rm,rn) in the single phase model can be expressed as

$$\underline{b}(rm,rn) \cong \sum_i \sum_k f^{1/2}(ri,rk) \left[\sum_{s=-p}^{p} \sum_{t=-p}^{p} \exp(j\phi(ri+s,rk+t))\right] h(rm-ri,rn-rk), \tag{3.38}$$

where $p=(r-1)/2$. Let

$$\underline{a}(ri,rk) = \sum_s \sum_t \exp(j\phi(ri+s,rk+t)),$$

then Eq. (3.38) can be written as

$$\underline{b}(rm,rn) \cong \sum_i \sum_k f^{1/2}(ri,rk)\,\underline{a}(ri,rk)\,h(r(m-i),r(n-k)).$$

Reducing the samples by a factor of r in both x and y directions, we have the "multiple phase" model

$$\underline{b}(m,n)=\sum_i \sum_k f^{1/2}(i,k)\,\underline{a}(i,k)\,h(m-i,n-k) \qquad (3.39)$$

where position (m,n) of the multiple phase model is the corresponding point (rm,rn) of the single phase model. Note that the sampling rate of this model is reduced by a factor of r in both x and y directions, and still guarantees that $\underline{b}(m,n)$ is close to a complex circular Gaussian random variable. The complex random variable $\underline{a}(i,k)$ in Eq. (3.39) asymptotically approaches a circular Gaussian random variable as the number of independent phasors tends to infinity. Instead of summing over a large number of independent phasors in the generation process, we can assume that $\underline{a}(i,k)$ is a complex circular Gaussian random variable and generate $\underline{a}(i,k)$ directly from a complex circular Gaussian random number generator. The block diagram of this discrete speckle generation model is illustrated in Fig. 3.9. This generation model not only reduces the sampling rate to the minimum value required for accurately representing the statistics of speckle, but also totally eliminates the dependence of the generation model on the object surface.

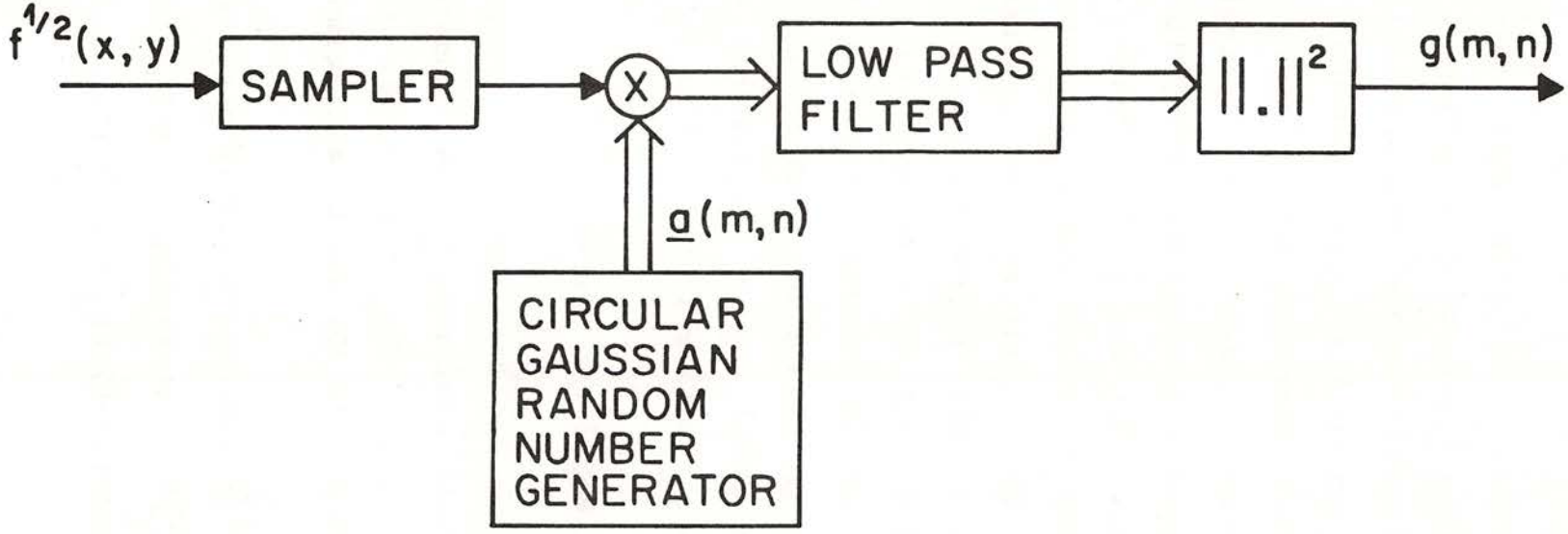

Figure 3.9 Multiple phase discrete speckle generation model for fully developed speckle

3.4.4 Simulation Results

In this section, we show some two-dimensional discrete speckle images generated according to the single phase and multiple phase models. The original girl image of size 256 is shown in Fig. 3.10(a). Figure 3.10(b) is the discrete speckle image of (a) by using the single phase speckle generation model. The optical pupil is assumed to be a square with length equal to 64 samples (1/4 of the image). The low pass filtering is carried out in the discrete frequency domain by using the fast Fourier transform. The speckle size is very large in this case and we can barely recognize the image. Figure 3.10(c) is generated from the same model except that the optical pupil size is 128 samples. Figure 3.10(d) is the discrete speckle image of (a) by using the multiple phase speckle generation model and a 128 samples wide pupil. As expected, the speckle size is reduced in (c) and (d).

3.5 Multiplicative Model for Speckle

Consider the special case where the bandwidth of the signal is very small compared to the bandwidth of the linear filter h(m,n). For this case, the speckle intensity g(m,n) in Eq. (3.37) can be approximated by

$$
\begin{aligned}
g(m,n) &= \left| \sum_i \sum_k f^{1/2}(i,k) \exp(j\phi(i,k)) h(m-i,n-k) \right|^2 \\
&\cong \left| f^{1/2}(m,n) \sum_i \sum_k h(m-i,n-k) \exp(j\phi(i,k)) \right|^2 \\
&= f(m,n) \left| \sum_i \sum_k h(m-i,n-k) \exp(j\phi(i,k)) \right|^2 . \qquad (3.40)
\end{aligned}
$$

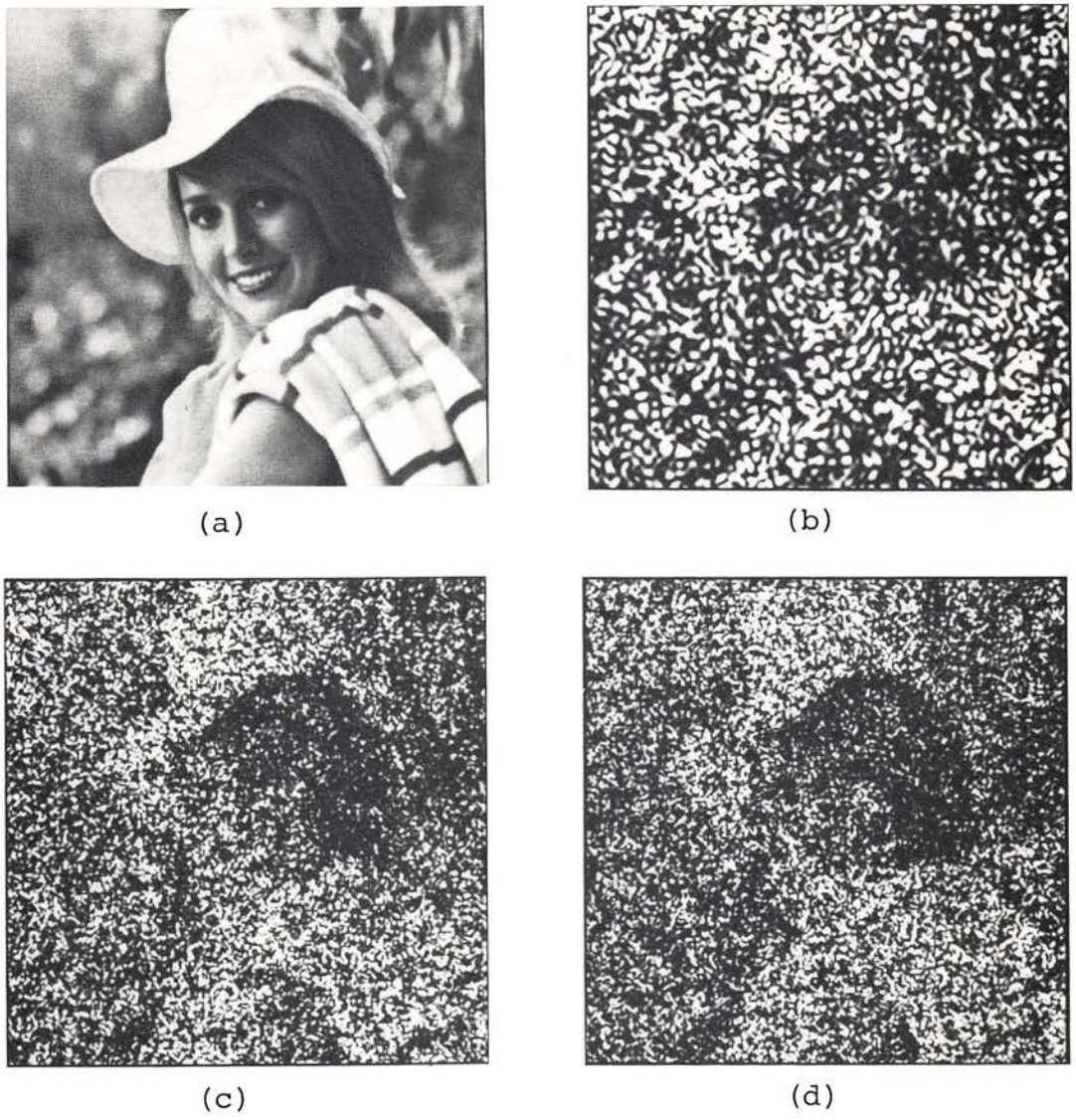

Figure 3.10 Examples of discrete speckle images

(a) Original image
(b) Speckle simulated using the single phase model - 1/2 bandwidth
(c) Speckle simulated using the single phase model - 1/4 bandwidth
(d) Speckle simulated using the multiple phase model - 1/4 bandwidth

Let

$$v(m,n) = \left| \sum_i \sum_k h(m-i,n-k) \exp(j\phi(i,k)) \right|^2, \qquad (3.41)$$

then we have the multiplicative model for fully developed speckle

$$g(m,n) = f(m,n)v(m,n) \qquad (3.42)$$

where $v(m,n)$ is signal-independent with a negative exponential distribution. Unlike the uncorrelated multiplicative noise model introduced in section 2.4.2, the multiplicative noise $v(m,n)$ in Eq. (3.42) is a correlated noise. The correlation properties of $v(m,n)$ are the same as those of the fully developed speckle derived in section 3.4.1 with the substitution of $f(m,n)$ by 1. Therefore, the power spectral density function of $v(m,n)$ is the same as the incoherent transfer function of the imaging system. Because we are only interested in the signal which has much smaller bandwidth than the noise spectrum, in principle, we can undersample the speckle intensity image $g(m,n)$ such that the sampling frequency is comparable to the bandwidth of $f(m,n)$. In this case, $v(m,n)$ becomes uncorrelated because the correlation length of the noise is much smaller than the sampling interval. The block diagram for this uncorrelated, multiplicative speckle model is shown in Fig. 3.12. Note that this model is also valid without assuming that the bandwidth of $f(m,n)$ is much smaller than the bandwidth of the system, as long as the sampling interval is larger than the correlation length of speckle. However, in this case we introduce aliasing in the object spectrum.

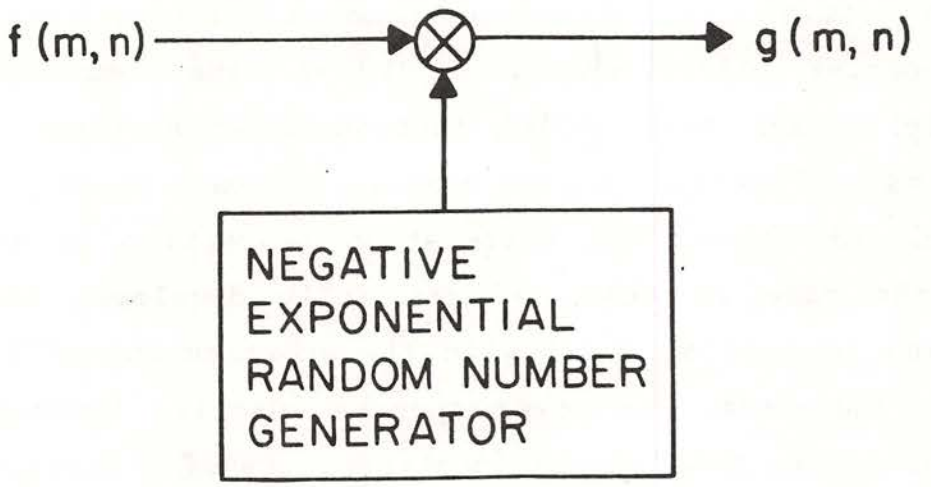

Figure 3.11 Multiplicative model of speckle

3.6 Summary and Conclusions

The statistical properties of general speckle are difficult to obtain analytically and require the autocorrelation function of the object surface. A special case of interest is "fully developed" speckle where the object surface is very rough compared with the optical wavelength. Under this condition, the statistical properties of speckle can be easily derived and only depend on the original object intensity and the coherent point spread function of the system. The autocorrelation function of the object surface does not appear in the expressions and only serves as a normalization factor.

Discrete speckle image generation is a good way to study the statistics of general speckle. Due to the bandwidth expansion caused by the nonlinear function $\exp(j\phi(p,q))$, we need to oversample the object phase function by a factor of W proportional to the variance of the object surface, in order to avoid the aliasing effect. This general speckle generation method becomes computationally demanding for fully developed speckle. A single phase generation model similar to Goodman's discrete speckle model is introduced to reduce computation efforts. Unlike the general speckle generation model, the object surface function is not required in the single phase model. Only some statistical assumptions about the random phase function are needed. However, the speckle images generated in this way are

only statistically equivalent to those speckle images produced by an equivalent optical system. A multiple phase generation model is introduced to further simplify the computation process. This model is not only computationally simple, but also eliminates the dependence of the generation model on the object surface.

Under the assumption that the signal bandwidth is very small compared with the bandwidth of the system, speckle can be approximated by a multiplicative noise model. This model is the result of some approximations to the true physical process of coherent image formation. In Chapters 7 and 8, we will discuss various speckle reduction techniques for different speckle models. A summary of all the discrete speckle generation models discussed in this chapter is given in Table 3.1.

Discrete Speckle Generation Model	Assumptions and Information Required for the Model	Sampling Frequency Requirement	Generation Diagram	Properties of the Discrete Speckle Image
General Speckle Generation Model	No assumption on the object surface. The surface phase function $\phi(x,y)$ is required for discrete speckle generation	Sampling frequency is determined from the bandwidth of $\exp(j\phi(x,y))$. Usually many times larger than that of $\phi(x,y)$. The sampling frequency roughly proportional to σ_ϕ^2.	Fig. 3-6	The discrete speckle generated by this model is the same as the speckle image generated from an equivalent optical system. These discrete speckle images can be used to study the statistical properties of general speckle.
Single Phase Model	Assume the object surface is very rough. $\phi(x,y)$ is not required in the generation process. Only some statistical assumptions are used to generate random phase samples $\phi(m,n)$	Several times larger than the maximum of the bandwidths of the object and the point spread function $h(x,y)$, in order to satisfy the circular complex Gaussian distribution assumption.	Fig. 3-8	Has the same statistical properties as fully developed speckle.
Multiple Phase Model	Assume that the object surface is very rough, and is an approximation of the single phase model. Random phase $\phi(m,n)$ is not required.	Larger than the maximum bandwidth of the object and the incoherent point spread function $h^2(x,y)$ in order to have the correct discrete speckle statistics.	Fig. 3-9	Has the same statistical properties as fully developed speckle. Eliminates the dependence of the generation model on the object surface phase.
Multiplicative Model	Assume the object surface is very rough, and the object bandwidth is much smaller than the bandwidth of $h(x,y)$.	The same as the bandwidth of the object intensity	Fig. 3-11	Speckle samples are independent. Only have the first order statistical properties of fully developed speckle.

Table 3.1 Summary of speckle generation models

Chapter 4

IMAGE RESTORATION - REVIEW

4.1 Introduction

The field of image processing has been expanding rapidly in the last decade. Various image restoration and enhancement methods have been proposed for removing degradations due to blurring and noise. The effectiveness of an image restoration algorithm depends on the validity of the image model, the criterion used to judge the quality of the restored image, and the statistical model for the noise process.

Early techniques concentrated on nonrecursive algorithms implemented in the discrete frequency domain. The necessary computations are carried out by the fast Fourier transform (FFT) techniques. The use of the FFT makes it possible to do image restoration within reasonable time. However, this approach cannot deal with images degraded by space-variant blur easily and assumes a stationary image model. More recent work has centered on two-dimensional recursive filtering techniques developed from the one dimensional Kalman filtering algorithm [4-1,4-2,4-3]. The main problems of two-

dimensional recursive filtering are both the difficulty in establishing a suitable 2-D recursive model and the high dimensionality of the resulting state vector. The advantages of 2-D recursive filters are that they can be implemented in the space domain and can handle the space-variant blur easily.

Progress in image modeling has been relatively slow. The conventional image model assumes that an image is a wide-sense stationary field. In recent years, Hunt [4-4] proposed a nonstationary mean Gaussian image model. In his nonstationary image model, an image is modeled as stationary fluctuations about a nonstationary ensemble mean which has the gross structure that represents the context of the ensemble. Lebedev and Mirkin [4-5] suggested a composite image model which assumes that an image is composed of many different stationary components.

In contrast to the signal-independent, additive noise model assumed in most image restoration algorithms, many physical noise processes are inherently signal-dependent. Naderi and Sawchuk [4-6] derived a nonstationary discrete Wiener filter for a signal-dependent film-grain noise model. In addition to the generality of the noise model, the filter is able to adapt itself to the signal-dependent noise. Lo and Sawchuk [4-7] developed a nonlinear MAP filter for images degraded by Poisson noise.

In designing the restoration filter, the characteristics of the receiver, which in many cases is the human visual system, are usually ignored. Anderson and Netravali [4-8] considered the properties of the human visual system and derived an anisotropic filter based on a subjective visibility function. The filter has better performance than the conventional stationary Wiener filter.

In order to compare these existing methods, we will discuss the image restoration algorithms according to the following properties:

Type of algorithm - recursive vs. nonrecursive.

Image model - stationary vs. nonstationary.

Noise model - signal-independent vs. signal-dependent.

Restoration criterion - numerical vs. subjective.

4.2 Type of Algorithm - Recursive vs. Nonrecursive

4.2.1 Nonrecursive Algorithms

Consider the linear space-invariant image formation model with additive, signal-independent observation noise. The lexicographic representation of this model is given by

$$\underline{g} = H\underline{f} + \underline{v} \tag{4.1}$$

where $\underline{g}$ is the N^2*1 degraded image vector

$\underline{f}$ is the N^2*1 original image vector

$\underline{v}$ is the N^2*1 noise vector

H is the N^2*N^2 blurring matrix with block Toeplitz structure.

If the extent of the blurring function is much narrower than the size of the image, the blurring matrix H can be approximated by a circulant matrix. With this circulant approximation and the use of FFT techniques, the computational process of image restoration can be simplified considerably. The typical nonrecursive algorithm is the discrete Wiener filter that was derived by Helstrom [4-9]. The discrete Wiener filter has the form

$$\hat{\underline{f}} = C_f H^T (HC_f H^T + C_v)^{-1} \underline{g} \qquad (4.2)$$

where C_f and C_v are the covariance matrices of $\underline{f}$ and $\underline{v}$ respectively. If we assume that the signal and noise are stationary fields, then we can use the circulant approximation and FFT techniques to compute the estimate. Even with FFT techniques, this still requires a substantial amount of calculation which currently precludes real time image processing. Note that if the image field is nonstationary or the blur is space-variant, we cannot use the FFT algorithm directly and there is no simplification of Eq. (4.2) for fast computation.

4.2.2 Recursive Algorithms

The power of Kalman filter in one dimensional signal processing is well recognized. The recursive Kalman filter has great computational advantages over nonrecursive methods, and is easy to implement with a digital computer for real time processing. Nahi and Assefi [4-1] converted the planar information of an image into a scan-ordered image and derived a Kalman filter to process the data line by line. Nahi [4-10] extended the procedure to include vector processing, where several lines were processed simultaneously. Silverman *et al.* [4-2,4-11] considered general motion blur and derived a recursive restoration filter on a line by line basis. All these scan-ordered recursive algorithms are basically one dimensional approaches. The scanning process converts two dimensional image data into a one dimensional ordering.

Woods and Radewan [4-3] extended the Kalman filtering techniques to two dimensions. They assumed that the ideal image is a stationary Markov field. After applying the 2-D spectral factorization routine [4-12] and using the spatial-variable representation, we have an (L*L) th order dynamic model for the original image,

$$f(m,n) = \sum\sum_{R^+} c(k,l)\, f(m-k,n-l) + u(m,n) \qquad (4.3)$$

where the region $R^+ = \{k \geq 0, l > 0\} \cup \{k < 0, l > 0\}$, $u(m,n)$ is a white noise field and $c(k,l)$ are the coefficients of the

model determined from the spectrum of the image field. Eq. (4.3) is known as the nonsymmetric half-plane (NSHP) model. To simplify the discussion, we assume there is no blur degradation. Then the observation equation has the form

$$g(m,n)=f(m,n)+v(m,n) \tag{4.4}$$

where $g(m,n)$ is the degraded image, $f(m,n)$ is the original object intensity, and $v(m,n)$ is a signal-independent white noise. Defining the state vector

$$\underline{x}(m,n)=[f(m,n),f(m,n-1),\ldots,f(m,1);f(m-1,N),\ldots,$$
$$f(m-1,1);f(m-L,N)\ldots,f(m-L,n-L)],$$

where N is the size of the image and L is the order of the image model, Eqs. (4.3) and (4.4) can be expressed as

$$\underline{x}(m,n+1) = A\underline{x}(m,n) + Bu(m,n) \tag{4.5}$$

$$g(m,n) = C\underline{x}(m,n) + v(m,n) \tag{4.6}$$

where A is the system propagation matrix determined by $c(k,l)$, and

$$B^T = C = [1,0,0,\ldots,0].$$

This is the state space model for estimating the image signal from noisy observations. Note that in Eqs. (4.5) and (4.6), the spatial index (m,n) indicates the

"present" position inside the image, and the matrix-vector formulation (state space representation) is the result of lexicographic ordering. It is straightforward to apply the Kalman filter equations [4-13] to this model. However, the dimension of the matrices is of order L*N. This causes a serious problem both for computation and memory requirement because N, the size of the image, is usually a large number. Woods and Radewan suggested a suboptimal reduced update Kalman filter that only updated those points of the state vector within a certain distance from the present point. This is a good approximation because pixels in an image have no predictable correlation beyond a certain distance. With this reduced update idea, there are only $O(L^2)$ points to be updated at each point. Further approximation can be made to reduce the update region of the filtered covariance matrix. With this reduced update Kalman filter, 2-D recursive processing becomes feasible.

Recursive filters can be easily extended to deal with space-variant blur, while nonrecursive methods can only be extended to include these variations at the expense of large computation time. Both the recursive and nonrecursive algorithms discussed here use a stationary image model and the MMSE criterion. In general, images are nonstationary and the human visual system is sensitive to a small amount of noise in a uniform intensity region, but is unable to perceive the same amount of noise in the surroundings of an edge. As a

result, these algorithms sacrifice resolution near edges and do too much noise smoothing.

4.3 Image Model - Stationary vs. Nonstationary

The effectiveness of an image restoration algorithm depends on the validity of the image model assumed. Image models are usually implicit in the assumptions of the restoration scheme. For example, in order to apply a Wiener filter to image restoration, we implicitly assume that an image is a wide-sense stationary random field with constant mean and space-invariant covariance function. As shown in Chapter 2, it is obvious that an image is best described by a nonstationary image model. However, stationary problems are much easier to solve than the nonstationary problems. The disadvantage of using a stationary image model is that the restoration filter accordingly designed is insensitive to abrupt changes of the image and tends to smooth the edges. For this reason, various restoration filters based on nonstationary image models were recently proposed (see section 2.3).

Lee [4-14] derived a local statistics algorithm for noise smoothing. He considered an additive noise model

$$g(m,n) = f(m,n) + v(m,n) \tag{4.7}$$

where $v(m,n)$ is a signal-independent, zero-mean, white

noise. In his algorithm, local statistics were estimated over a (2p+1)*(2q+1) window. The local mean and local variance of g(m,n) are defined as

$$\mu_g(m,n) = \frac{1}{(2p+1)(2q+1)} \sum_{i=m-p}^{i=m+p} \sum_{j=n-q}^{j=n+q} g(i,j) \qquad (4.8)$$

and

$$v_g(m,n) = \frac{1}{(2p+1)(2q+1)} \sum_{i} \sum_{j} (g(i,j)-\mu_g(m,n))^2 \qquad (4.9)$$

respectively. From Eq. (4.7), we have the following relations

$$E[f(m,n)] = E[g(m,n)] \qquad (4.10)$$

and

$$Var[f(m,n)] = Var[g(m,n)] - Var[v(m,n)] \qquad (4.11)$$

where Var[f(m,n)] is the ensemble variance of f(m,n). If we substitute the local statistics for the ensemble statistics in Eqs. (4.10) and (4.11) and apply weighted least square estimation techniques, we have the local statistics filter

$$\hat{f}(m,n) = \mu_f(m,n)+k(m,n)(g(m,n)-\mu_g(m,n)) \qquad (4.12)$$

where $\mu_f(m,n)$ is the local mean of f(m,n), and

$$k(m,n) = \frac{v_g(m,n)-Var[v(m,n)]}{v_g(m,n)} . \qquad (4.13)$$

The local statistics algorithm was later extended to include multiplicative noise. In fact, the algorithm implicitly used a nonstationary mean and nonstationary variance image model. For the additive noise case, the local statistics algorithm is the linear optimal filter in the minimum mean square error sense, and is equivalent to the sectioned MAP method [4-15] when the section size is only one point. However, for the multiplicative noise model, we will show in Chapter 5 that the local statistics algorithm is suboptimal.

4.4 Noise Model - Signal Independent vs. Signal Dependent

Most image restoration techniques model the noise process as additive, signal independent white noise. It is well known, however, that many physical noise processes occurring in image formation systems are inherently signal-dependent. For example, the film-grain noise produced by a photographic emulsion during the process of image recording and reproduction and the photon noise in any detected image at low light levels are signal-dependent. Restoration algorithms based on a signal-independent noise model are not expected to be very effective in the signal-dependent noise environment.

Walkup and Choens [4-16] derived a Wiener filter for signal-dependent film-grain noise. Kondo et al. [4-17] developed a Wiener filter for an additive, signal-modulated noise model and multiplicative noise model. The signal-modulated noise model considered is

$$g(x,y) = h(x,y) \circledast f(x,y) + [h(x,y) \circledast f(x,y)]v(x,y) \qquad (4.14)$$

where $\circledast$ denotes the 2-D convolution operator, and $v(x,y)$ is a signal-independent noise. The Wiener filter for this model has the form

$$W(w_x,w_y) = \frac{H^*(w_x,w_y)}{S_f(w_x,w_y)|H(w_x,w_y)|^2 + [S_f(w_x,w_y)|H(w_x,w_y)|^2] \circledast S_v(w_x,w_y)} \qquad (4.15)$$

where $S_f(w_x,w_y)$ and $S_v(w_x,w_y)$ are the power spectral density functions of the original object and the noise process respectively. $H(w_x,w_y)$ is the Fourier transform of $h(x,y)$ and * denotes the complex conjugate. The photon noise is inherent in any detected image, especially at low light levels. The emission of photons follows an inhomogeneous Poisson process with the rate parameters proportional to the original object intensities. Goodman and Belsher [4-18] derived a linear minimum mean square error filter for images degraded by photon noise. Note that these filters that consider the signal-dependent property of the noise process are implemented in the discrete frequency domain and assume a stationary image model.

Naderi and Sawchuk [4-6] developed a discrete Wiener filter for a more accurate film-grain noise model based on a nonstationary mean image model. The filter operated

adaptively according to the nonstationary mean of the image. Trussell and Hunt [4-15] considered the nonlinear D-logE characteristic curve of the recording film and derived a nonlinear MAP estimate for this nonlinear observation model. Lo and Sawchuk [4-7] developed a nonlinear MAP estimate for images degraded by Poisson noise. The MAP filter is optimal in the sense that it maximizes the a posteriori probability density function. However, the filter has highly nonlinear structure and iterative schemes have to be used to solve the nonlinear equations over sections of the image. These filters were implemented in the space domain by using nonrecursive algorithms.

As discussed in Chapter 3, speckle noise is a major obstacle in coherent imaging systems. Most of the methods for speckle noise reduction assume that the speckle noise is multiplicative. This is only a rough approximation for speckle under some restricted conditions. We will consider a more accurate model for speckle and derive optimal filters for speckle noise reduction in Chapters 7 and 8.

4.5 Restoration Criterion - Numerical vs. Subjective

There is no universal agreement on the criterion that should be used to judge the quality of a restored image. The minimum mean square error (MMSE) criterion adopted by many image restoration algorithms is based on

the numerical closeness of the restored image to the original image. The numerical criterion is well defined and easy to compare. The drawback of this approach is that the numerical closeness does not imply that the restored image "looks good" to a human observer. The human visual system is very complex and not well understood, however, research in vision shows that the MMSE criterion is not a suitable measure if it is used globally. Pearlman [4-19] derived an optimal filter based on a subjective distortion criterion which was derived from an eye-brain system model. Anderson and Netravali [4-8] introduced a subjective visibility function and used the "Backus-Gilbert" approach to make a balance between the resolution and noise smoothing. They first defined the "masking function" M(m,n) at point (m,n) as a measure of local spatial detail. The masking function had high values at picture elements around the edges. Subjective tests were performed to determine a "visibility function" which gave the relative visibility of unit noise for different spatial details. The visibility function was then plotted with respect to the masking function value, and the curve was found to decrease exponentially. This indicated that the human visual system is not very sensitive to the noise around the edges. Then they used the "Backus-Gilbert" approach to minimize the joint objective function J,

$$J = bV_v + (1-b)V_r \qquad (4.16)$$

where b is a "tuning" parameter to balance the resolution and the amount of noise smoothing, V_v and V_r are the measure functions for the noise term and resolution term respectively. A family of filters were derived for different values of b. At each pixel, the visibility function was used to tune the filter via the parameter b in order to suppress the same amount of subjective noise over the whole picture. They also considered an anisotropic filter which can recognize an edge and avoid averaging across it to preserve edge sharpness. Abramatic and Silverman [4-20] generalized the idea and related it to the classical Wiener techniques.

4.6 Conclusions

The standard Wiener filter for image restoration is a nonrecursive algorithm based on a stationary image model and minimum mean square error criterion. The poor quality of images restored using the Wiener filter is partly due to the minimum mean square error (MMSE) criterion that is not a good measure for visual quality, and more importantly also due to the stationary assumptions of the image model.

Recursive filtering not only has a computational advantage over nonrecursive filtering, but also emphasizes on local processing concept. Recent work on image restoration is trying to improve the standard Wiener filter by using a more sophisticated image model

and error criterion. Recursive implementation is usually desirable in order to do real-time processing. Therefore, various filters using nonstationary image models and recursive implementations are proposed. Another approach is to design a filter based on a subjective criterion such that the restored image will "look" better. However, these filters are usually very complex and only consider the additive, signal-independent noise. In the next two chapters, we will develop a nonstationary two-dimensional recursive image restoration filter which has a simple structure and works for signal-dependent noise.

Chapter 5

ADAPTIVE NOISE SMOOTHING FILTER FOR IMAGES WITH SIGNAL-DEPENDENT NOISE

5.1 Introduction

From the preceding review of existing image restoration techniques and the discussion of different statistical image models and noise models, we think the following features are desirable in designing an image restoration filter:

1. The filter should be recursive in nature and suitable for real-time processing

2. The filter should incorporate a nonstationary image model and adapt itself to the nonstationary content of an image

3. The filter should require minimal *a priori* information about the original image, but should be able to use this information if available

4. The filter should be easily modified to deal with different noise models, either signal-independent or signal-dependent noise

5. The filter should incorporate a subjective error criterion making use of human visual system properties.

Woods' 2-D reduced update Kalman filter [5-1] assumes a stationary image model and requires a priori information about the original image in order to construct the state space model. In practice, we generally only have the degraded image. A common procedure for obtaining this a priori information is to use the correlation properties of a statistically similar image. While this seems reasonable, the mean square error increases significantly due to the substitution. The reduced update Kalman filter was later modified for a "multiple image model" [5-2] to consider the nonstationary nature of the image. Here, obtaining the a priori information becomes a more serious problem. The resulting filter uses an identification-estimation procedure and requires excessive computation. The sectioning MAP method [5-3] uses a nonstationary mean Gaussian image model. The algorithm is nonrecursive and requires the joint probability density function (complete statistics) of the signal and noise. In general, the MAP estimate requires the solution of a set of nonlinear equations and is difficult to obtain. The sectioning

method is used to reduce computation and to do local processing. The MAP filter is optimal, but in some applications, it might be acceptable to trade off theoretical performance for ease of implementation. This becomes more appropriate when we consider the adaptive filtering techniques where the filter parameters have to be estimated from the noisy observations.

Another approach to an improved restoration filter was proposed by Anderson and Netravali [5-4]. Instead of using a nonstationary image model, they used a subjective error criterion including human visual system and derived a nonrecursive filter that adapts itself to make a compromise between the loss of resolution and noise smoothing. Abramatic and Silverman [5-5] generalized this procedure and related it to the classical Wiener filter.

The signal-dependent properties of many physical noise processes are usually ignored in the restoration procedure. In this chapter, we develop an adaptive noise smoothing filter for images degraded by a class of signal-dependent, uncorrelated noise by using the linear minimum mean square error (LMMSE) criterion and a nonstationary image model. The filter has very simple structure (point processor) and is able to adapt itself to the nonstationary content of the image and to different types of signal-dependent noise. All the statistical parameters required for the filter are

estimated from the degraded image, and no *a priori* information of the original image is needed. The methods used to estimate the ensemble statistics from the degraded image are critical to the quality of the results. Various ways of estimating these ensemble statistics are discussed and their performance is compared. The adaptive noise smoothing filter has a form similar to Abramatic's filter, and the relationship between the nonstationary image modeling approach and the nonlinear subjective filter approach becomes clear. Based on this connection, we show that the minimum mean square error criterion is not a bad criterion if it is used locally. The explicit structure of the adaptive noise smoothing filter for multiplicative noise, film-grain noise, and Poisson noise is derived for completeness. The comparison of the adaptive noise smoothing filter with Lee's local statistics algorithm [5-6] shows that the introduction of the nonstationary mean and nonstationary variance (NMNV) image model is not only valuable for systematically deriving the optimal estimator structure, but also very useful for the extension of the adaptive noise smoothing filter to image restoration when the images are degraded by both blurring and signal-dependent noise. This problem will be discussed in Chapter 6.

5.2 Local Linear Minimum Mean Square Error Filter for a Class of Signal-Dependent Noise

In this section, we will derive a linear minimum mean square error (LMMSE) filter for images degraded by a class of signal-dependent noise based on the NMNV image model introduced in section 2.3.2. In order to distinguish this filter from the conventional LMMSE filter that is derived based on a stationary image model, we shall call it a local linear minimum mean square error (LLMMSE) filter to emphasize that the minimum mean square error criterion is used locally rather than globally.

Consider the observation equation

$$\underline{g} = H\underline{f} + \underline{v} \tag{5.1}$$

where $\underline{g}$ is the degraded observation, $\underline{f}$ is the original signal, $\underline{v}$ is a zero mean noise that can be signal-independent or signal-dependent, and H is the blurring matrix. Define

$$E[\underline{f}]=\bar{\underline{f}} \text{ and } E[(\underline{f}-\bar{\underline{f}})(\underline{f}-\bar{\underline{f}})^T]=C_f \tag{5.2}$$

where $\bar{\underline{f}}$ and C_f are the mean and covariance matrix of $\underline{f}$ respectively. The minimum mean square error (MMSE) estimate of $\underline{f}$ given observation $\underline{g}$ is the conditional mean estimate

$$\hat{\underline{f}} = E[\underline{f}|\underline{g}]. \tag{5.3}$$

In general, the MMSE estimate is nonlinear and depends on the probability density functions of $\underline{f}$ and $\underline{v}$. The explicit form of the MMSE estimator is difficult to obtain for the general case. If we impose a linear constraint on the estimator structure, we have the local linear minimum mean square error (LLMMSE) estimator [5-7]

$$\hat{\underline{f}}_{LLMMSE} = \bar{\underline{f}} + C_{fg} C_g^{-1} (\underline{g} - \bar{\underline{g}}) \tag{5.4}$$

where C_{fg} is the crosscovariance matrix of $\underline{f}$ and $\underline{g}$, C_g and $\bar{\underline{g}}$ are the covariance matrix and mean of $\underline{g}$ respectively. Unlike the MMSE filter that requires the conditional mean, the LLMMSE filter only requires the second order statistics of the signal and noise. It is well known that Gaussian probability density function is characterized by its second order statistics, and consequently the LLMMSE estimate for Gaussian statistics is equal to the MMSE estimate. Another important property of the LLMMSE filter is that it is unbiased.

To have the explicit structure of the LLMMSE filter, we need to calculate the covariance matrices in Eq. (5.4). The cross-covariance matrix C_{fg} is given by

$$\begin{aligned} C_{fg} &= E[(\underline{f}-\bar{\underline{f}})(\underline{g}-\bar{\underline{g}})^T] \\ &= E\{(\underline{f}-\bar{\underline{f}})[H(\underline{f}-\bar{\underline{f}})+\underline{v}]^T\} \\ &= C_f H^T + E[(\underline{f}-\bar{\underline{f}})\underline{v}^T]. \end{aligned} \tag{5.5}$$

Similarly, the covariance matrix C_g can be calculated as

$$C_g = E[(\underline{g}-\bar{\underline{g}})(\underline{g}-\bar{\underline{g}})^T]$$

$$= E\{[H(\underline{f}-\bar{\underline{f}})+\underline{v}][H(\underline{f}-\bar{\underline{f}})+\underline{v}]^T\}$$

$$= HC_fH^T+C_v+HE[(\underline{f}-\bar{\underline{f}})\underline{v}^T]+E[\underline{v}(\underline{f}-\bar{\underline{f}})^T]H^T \quad (5.6)$$

where C_v is the covariance matrix of $\underline{v}$. If we assume that $E[(\underline{f}-\bar{\underline{f}})\underline{v}^T]=0$, then Eqs. (5.5) and (5.6) become

$$C_{fg} = C_fH^T \quad (5.7)$$

$$C_g = HC_fH^T+C_v. \quad (5.8)$$

This condition is generally satisfied by many physical noise processes.

Considering the special case of no blurring where H is an identity matrix, the cross-covariance matrix C_{fg} becomes a diagonal matrix because we use the NMNV image model and C_f is a diagonal matrix. The covariance matrix C_g is also diagonal if the noise process $\underline{v}$ is uncorrelated, i.e., C_v is diagonal. Therefore, under these conditions, it is not necessary to invert the covariance matrix C_g in Eq. (5.4) and the LLMMSE filter for this class of noise can be expressed by a set of scalar equations

$$\hat{f}_{LLMMSE}(m,n)=\bar{f}(m,n)+\frac{\sigma_f^2(m,n)}{\sigma_f^2(m,n)+\sigma_v^2(m,n)}(g(m,n)-\bar{g}(m,n)) \quad (5.9)$$

In summary, the following conditions are required to make the LLMMSE filter a point processor.

1. There is no blur degradation, i.e., H=I.

2. The degraded image g(m,n) can be expressed as

$$g(m,n) = f(m,n) + v(m,n) \tag{5.10}$$

where f(m,n) is the original image, and v(m,n) is the noise term which can be signal-dependent or signal-independent.

3. The noise term v(m,n) is uncorrelated, i.e.,

$E[v(m,n)v(m_1,n_1)]=0$ for $(m,n)\neq(m_1,n_1)$.

4. The conditional mean of v(m,n) given $\underline{f}$ denoted by $E[v(m,n)|\underline{f}]$ satisfies the condition that

$$E[v(m,n)|\underline{f}] = 0 \tag{5.11}$$

This is a sufficient condition for $E[(\underline{f}-\bar{\underline{f}})\underline{v}^T]=0$.

Note that Eq. (5.10) uses an additive form to describe the noise degradation. This does not imply that the noise has to be an "additive" noise in the usual sense. Any noise degradation can always be expressed in terms of the signal part and the noise part, although this may not be the most convenient way to represent it. The formulation in Eq. (5.10) with condition (4) imposes the constraint

$$E[g(m,n)|\underline{f}] = E[f(m,n)|\underline{f}] = f(m,n). \tag{5.12}$$

This by no means limits the generality of the noise

model. It simply assumes that the noisy observation $g(m,n)$ has been normalized such that it has the same intensity level as the original image, and that the noise term $v(m,n)$ has no bias. This condition is generally satisfied by many physical noise models. The uncorrelated, signal-dependent noise models discussed in section 2.4.2 such as multiplicative noise, film-grain noise, and Poisson noise all satisfy these three conditions. Instead of deriving a different filter for each individual case, we use a unified approach to design a noise smoothing filter for this class of signal-dependent noise.

In Eq. (5.9), if the a priori statistics of the image are known, then $\hat{f}_{LLMMSE}(m,n)$ is a function of $g(m,n)$ only, and each pixel can be processed separately at the same time. This parallel processing characteristic is very attractive and permits real-time image processing. Using the normalized assumption that $\bar{g}(m,n)=\bar{f}(m,n)$, we can rearrange Eq. (5.9) as

$$\hat{f}_{LLMMSE}(m,n)=(1-w(m,n))\bar{f}(m,n)+w(m,n)g(m,n) \qquad (5.13)$$

$$\text{where} \quad w(m,n) = \frac{\sigma_f^2(m,n)}{\sigma_f^2(m,n)+\sigma_v^2(m,n)} \quad .$$

It is easy to see that the LLMMSE estimate is a weighted sum of the ensemble mean $\bar{f}(m,n)$ and the normalized observation $g(m,n)$, where the weight is determined by the

signal variance and the noise variance. For a low signal-to-noise ratio (SNR), the LLMMSE filter puts more weight on the a priori mean $\bar{f}(m,n)$ because the observation is too noisy to make an accurate estimate of the original image. Conversely, for high SNR, the LLMMSE estimate puts more weight on the noisy observation and the result is to preserve the edge sharpness.

It is interesting to compare these properties of the LLMMSE filter with the results obtained by Anderson and Netravali [5-4], in which they derived a nonlinear restoration filter based on a subjective visibility function to make a balance between noise smoothing and resolution. The nonlinear filter tends to average out the random noise in the flat areas and preserve edge sharpness so that the same amount of subjective noise is suppressed in the whole image. The response of this nonlinear filter is similar to that of the LLMMSE filter. The nonlinear approach implicitly used a nonstationary image assumption to calculate the "masking function" value for suppressing the same amount of subjective noise over the whole image by using an exponentially decreasing visibility function, whereas the LLMMSE filter directly uses a nonstationary image model and tries to minimize the local mean square error. The net effect of these two approaches are similar because one is varying the noise variance according to the contextual information in the image, while the other imbeds the contextual information directly into a nonstationary image model. Therefore,

the local variance not only has its statistical meaning but also serves as a spatial "masking function", and the LLMMSE filter is similar to a subjective smoothing filter with a linearly decreasing visibility function. The seemingly different two approaches are now related and support the idea that the minimum mean square error criterion is a better measure for image restoration if it is used locally with a nonstationary image model.

5.3 Adaptive Noise Smoothing Filter

5.3.1 Principle

The LLMMSE filter shown in Eq. (5.9) requires the ensemble mean and variance of f(m,n). Usually these statistics are not available a priori and can only be estimated from the degraded image. If we assume that the ensemble statistics in Eq. (5.9) can be substituted by local statistics that are estimated from the degraded image, we have the adaptive noise smoothing filter

$$\hat{f}(m,n) = \mu_f(m,n) + \frac{v_f(m,n)}{v_f(m,n)+v_v(m,n)}(g(m,n)-\mu_g(m,n)) \quad (5.14)$$

where $\mu_f(m,n)$ and $\mu_g(m,n)$ are the local mean of f(m,n) and g(m,n) respectively, and $v_f(m,n)$ and $v_v(m,n)$ are the local variance of f(m,n) and v(m,n) respectively. It is interesting to see that the adaptive noise smoothing filter is a nonlinear filter even though it has the same linear form as the LLMMSE filter. The nonlinearity is introduced by the ratio of the local variances that are

estimated by nonlinear functions of the noisy observation g(m,n). The performance of the adaptive noise smoothing filter depends heavily on the method used to calculate the local statistics. We will discuss various methods for calculating these local statistics in the next section.

5.3.2 Computation of the Local Statistics

The underlying assumption of the adaptive noise smoothing filter is that an image is locally ergodic such that the ensemble statistics can be substituted locally by the local statistics. Therefore, it is critical to choose the method used for estimating local statistics. One way to obtain the local mean and local variance is to calculate over a uniform moving average window of size (2p+1)*(2q+1). We have

$$\mu_g(m,n) = \frac{1}{(2p+1)(2q+1)} \sum_{i=m-p}^{i=m+p} \sum_{j=n-q}^{j=n+q} g(i,j) \qquad (5.15)$$

and

$$v_g(m,n) = \frac{1}{(2p+1)(2q+1)} \sum_{i=m-p}^{i=m+p} \sum_{j=n-q}^{j=n+q} (g(i,j)-\mu_g(m,n))^2 \qquad (5.16)$$

where $\mu_g(m,n)$ and $v_g(m,n)$ are the local mean and local variance of g(m,n) respectively. These statistics are commonly known as the sample mean and sample variance. They are widely used in statistical analysis and are shown to be the maximum likelihood estimates of the

unknown mean and variance of a Gaussian probability density function [5-8], by assuming that the samples are from the same ensemble. The local statistics of f(m,n) can be calculated from the local statistics of g(m,n) by assuming the relationship between their ensemble statistics also holds for the local statistics. Therefore, the functional forms of these transformations depend on the particular noise structure. The local statistics of f(m,n) then feed into the filter to adapt the filter to the nonstationary content of the image and signal-dependent characteristics of the noise. For simplicity, let us consider the signal-independent, additive noise model. The local mean of f(m,n) is equal to the local mean of g(m,n) because the observation is normalized. It is straightforward to show that the local variance of f(m,n) is given by

$$v_f(m,n) = v_g(m,n) - \sigma_v^2(m,n). \tag{5.17}$$

With these quantities, the adaptive noise smoothing filter is complete. The block diagram of the adaptive noise smoothing filter is illustrated in Fig. 5.1.

The adaptive estimate is a balance between the local mean estimate $\mu_f(m,n)$ and the noisy observation g(m,n). The local variance $v_f(m,n)$ is an indication of our confidence on the local mean estimate. For the signal-independent, additive noise model, the adaptive noise smoothing filter with local statistics defined as in Eqs. (5.15) and (5.16) is the same as Lee's local

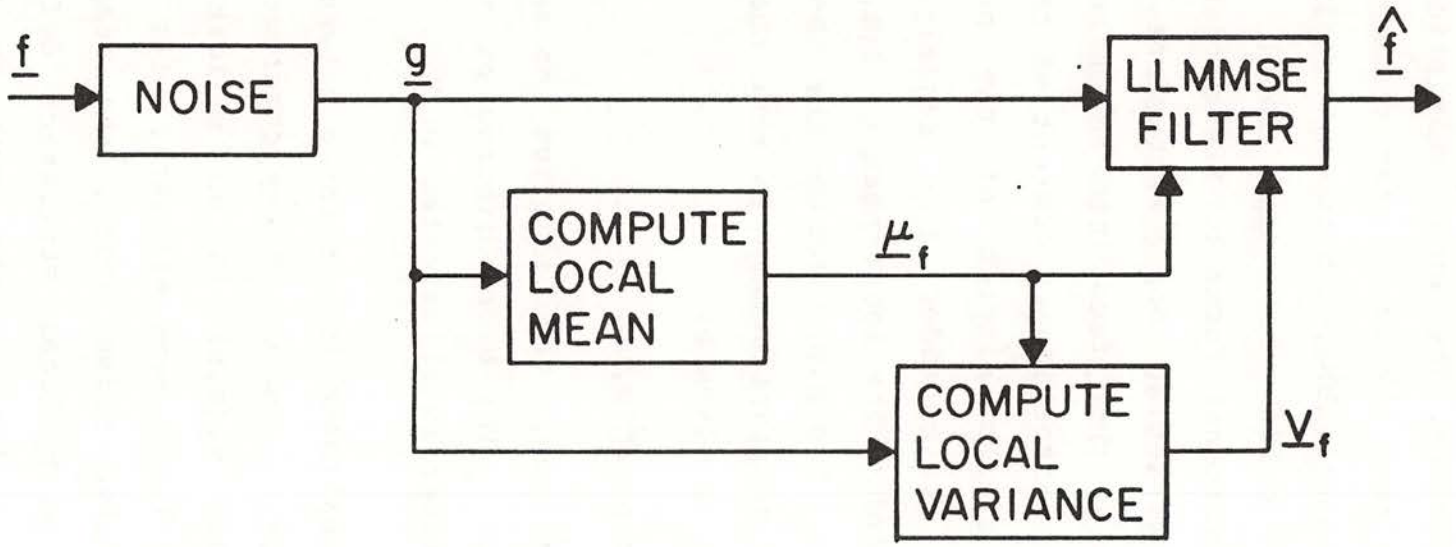

Figure 5.1 Adaptive noise smoothing filter structure

statistics algorithm [5-6]. However, unlike Lee's heuristic argument of using local mean and variance, we introduced a nonstationary image model, and with this image model, we can have a better understanding of the problem and the extension of this filter to signal-dependent noise and image restoration become obvious. For the multiplicative noise model and signal-dependent noise in general, we will show that Lee's approach is not optimal.

The local statistics calculated according to Eqs. (5.15) and (5.16) assume that the samples within the averaging window are from the same ensemble. This is not true if there is a sharp edge within the window. The value of the sample variance near the edge will be larger than the ensemble variance because we use samples in two entirely different ensembles to calculate the local variance. The sample mean will tend to smear out compared with the ensemble mean. To avoid these effects, we should have an intelligent filter that can find edges and use the correct neighborhood of a pixel for calculating the local statistics. Various approaches for using edge detectors have been proposed for designing an anisotropic restoration filter and calculating the local statistics [5-4,5-9]. A problem associated with these approaches is that edge detectors do not work well on a noisy image. Here, we introduce a simple functional form for estimating the local variance by including the nonstationarity of the image in the function.

The inaccurate sample mean seems to have less effect to the filter output than the inaccurate sample variance because the NMNV image model only uses the nonstationary mean to describe the gross structure of the image, while the nonstationary variance is used to characterize the edge information. In order to preserve the noise smoothing ability of the local mean, we still use the sample mean as our local mean estimate. The new local variance is defined as

$$v_g(m,n) = \frac{1}{(2p+1)(2q+1)} \sum_i \sum_j c(m-i,n-j) \, (g(i,j)-\mu_g(i,j))^2 \qquad (5.18)$$

where $c(m,n)$ is a weighting function. The sample variance estimate in Eq. (5.16) implicitly assumes that $g(i,j)$ is locally stationary such that $\mu_g(m,n)$ can be used as the local mean for all $g(i,j)$ within the averaging window. In our new local variance estimate, the locally stationary assumption is removed and the local mean $\mu_g(i,j)$ is allowed to vary for each $g(i,j)$ within the window. Therefore, this new local variance should perform well even near the edges. Other advantages of this estimate compared with the edge detection approach are that it is more robust, insensitive to noise, and easy to implement.

5.3.3 Simulation Results

The original girl image is shown in Fig. 5.2(A). Figure 5.2(B) is the original image degraded by a signal-independent, additive, white noise with variance 100. The degraded image is processed by the adaptive noise smoothing filter with the sample mean and sample variance calculated over a 5*5 window as the local statistics, and the smoothed image is shown in Fig. 5.2(C). In the uniform region, the estimate is close to the local mean estimate and the noise is smoothed by a large amount. Conversely, in the edge area, the restored image is close to the noisy observation and the edge sharpness is preserved. The mean square error (MSE) between the smoothed image and the original image is 36.7 per pixel. This value is very small compared with the MSE of 94.1 per pixel for the local mean estimate that is essentially a spatially invariant low pass filter. Figure 5.2(D) shows the adaptive noise smoothing estimate of the original image using Eq. (5.18) to calculate the local variance. This estimate seems to have better visual quality than Fig. 5.2(C). It looks smoother both at the step edges and ramp edges. The MSE of Fig. 5.2(D) is 34.6 per pixel which is a little smaller than that of the sample variance case, and indicates the performance improvement of using the new local variance estimate. The same sequence of simulation results for a low SNR case where the noise variance is equal to 400 are shown in Fig. 5.3.

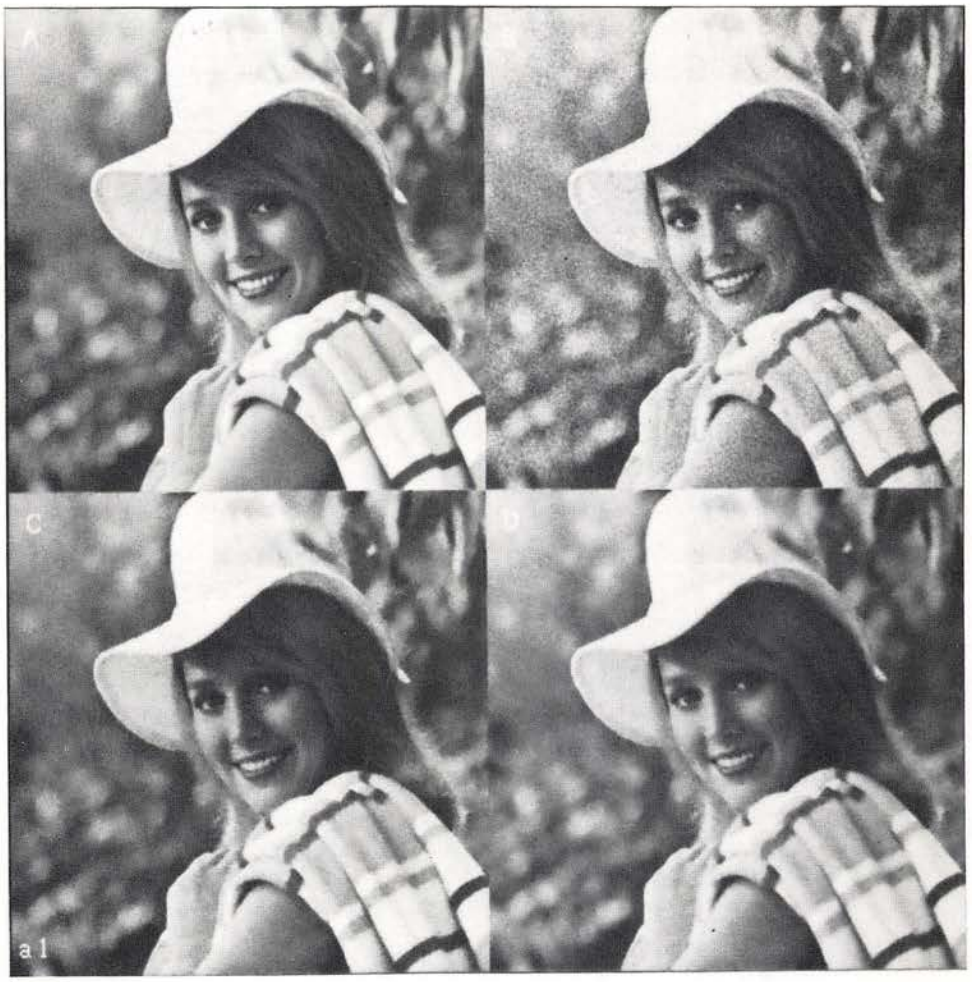

Figure 5.2 Adaptive noise smoothing filter for signal-independent additive noise

(A) Original image
(B) Original degraded by additive noise with $\sigma_v^2=100$
(C) Adaptive noise smoothing estimate with local variance of Eq. (5.16)
(D) Adaptive noise smoothing estimate with local variance of Eq. (5.18)

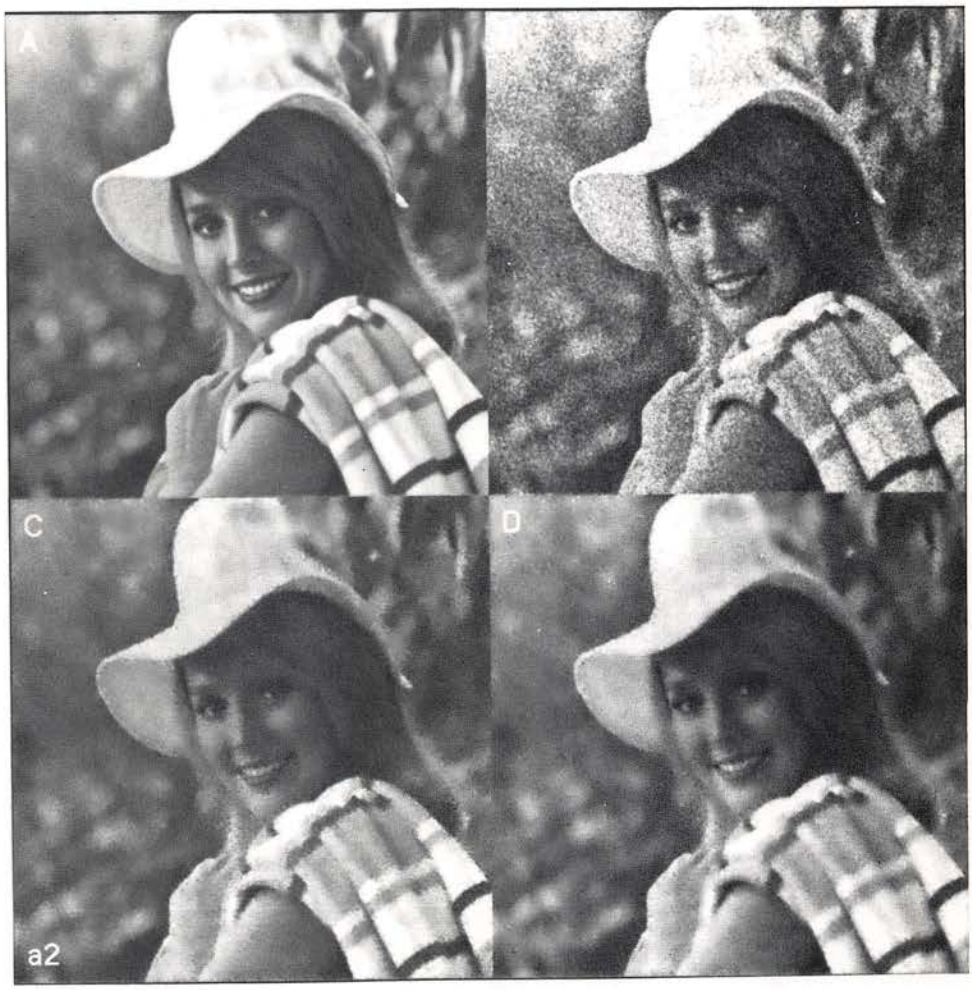

Figure 5.3 Adaptive noise smoothing filter for signal-independent additive noise

(A) Original image
(B) Original degraded by additive noise with $\sigma_v^2=400$
(C) Adaptive noise smoothing estimate with local variance of Eq.(5.16)
(D) Adaptive noise smoothing estimate with local variance of Eq.(5.18)

5.4 Adaptive Noise Smoothing Filter for Various Signal-Dependent Noise Models

The general form of the adaptive noise smoothing filter for a class of signal-dependent noise is shown in Eq. (5.14). It is instructive to have the explicit structure of this filter for some physical noise models that are frequently encountered in practical imaging systems. In this section, we derive the explicit structure of the adaptive noise smoothing filter for multiplicative noise, film-grain noise, and Poisson noise.

5.4.1 Multiplicative Noise

For the multiplicative noise model discussed in section 2.5, the degradation model can be written as

$$g'(m,n) = u(m,n)f(m,n) \tag{5.19}$$

where $\bar{u}(m,n)=\bar{u}$ and $E[(u(m,n)-\bar{u})^2]=\sigma_u^2$. Define the normalized observation as

$$g(m,n) = g'(m,n)/\bar{u} \tag{5.20}$$

such that $\bar{g}(m,n)=\bar{f}(m,n)$. If we represent Eq. (5.19) in terms of the signal part and the noise part, we have

$$g(m,n) = f(m,n) + \frac{(u(m,n)-\bar{u})}{\bar{u}} f(m,n). \tag{5.21}$$

From Eq. (5.10), it is easy to see that

$$v(m,n)=(u(m,n)/\bar{u} - 1)f(m,n) \tag{5.22}$$

and

$$\sigma_v^2(m,n)= \frac{\sigma_u^2}{\bar{u}^2}(\bar{f}^2(m,n)+\sigma_f^2(m,n)). \tag{5.23}$$

From Eq. (5.17) and Eq. (5.23), the local variance of f(m,n) can be calculated from the local mean and local variance of g(m,n) and is given by

$$v_f(m,n) = \frac{v_g(m,n)- \sigma_u^2\mu_f^2(m,n)/\bar{u}^2}{1+(\sigma_u^2/\bar{u}^2)} \tag{5.24}$$

Substituting $v_v(m,n)$ into Eq. (5.14), we have the adaptive noise smoothing filter for the multiplicative noise model

$$\hat{f}(m,n) = \mu_f(m,n)+\frac{v_f(m,n)(g(m,n)-\mu_f(m,n))}{v_f(m,n)+\sigma_u^2(\mu_f^2(m,n)+v_f(m,n))/\bar{u}^2} \tag{5.25}$$

where g(m,n) is the normalized observation, and $\sigma_u^2/\bar{u}^2$ is the parameter characterizing the multiplicative noise level. The term $v_f(m,n)+\mu_f^2(m,n)$ in Eq. (5.25) shows the signal-dependent properties of multiplicative noise, and makes the adaptive noise smoothing filter change its characteristic adaptively to smooth the noise.

Comparing Eq. (5.25) with Lee's local statistics algorithm for multiplicative noise [5-6], we find that the term $\sigma_u^2 v_f(m,n)/\bar{u}^2$ is missing in Lee's algorithm. This arises from the linear approximation made for the nonlinear multiplicative noise model in Lee's heuristic

derivation and makes his filter suboptimal. The advantage of our approach is that by introducing the NMNV image model, we are able to derive the optimal linear filter for a class of signal-dependent noise in a systematic way, i.e., first represent the noise model in signal plus noise form and calculate the variance of the noise term. We also justify that the linear constraint should be applied to the estimator structure rather than the nonlinear observation model.

The simulation results are shown in Fig. 5.4. The original image is in Fig. 5.4(A). The image degraded by a multiplicative noise with unit mean and variance equal to 0.007 is shown in Fig. 5.4(B). Figure 5.4(C) is the adaptive noise smoothing estimate of the original image by using the sample mean and sample variance as local statistics. Figure 5.4(D) is the adaptive estimate using the new local variance estimate as in Fig. 5.2(D). These results are comparable with those of Fig. 5.2. Another set of simulation results for $\sigma_u^2=0.04$ are shown in Fig. 5.5.

5.4.2 Film-Grain Noise

Film-grain noise inherently exists in the process of photographic recording and reproduction. If we process the film in the linear region of the D-logE curve and ignore the blurring effect of the model, we have

$$g(m,n) = f(m,n)+cf^{1/3}(m,n)u(m,n) \qquad (5.26)$$

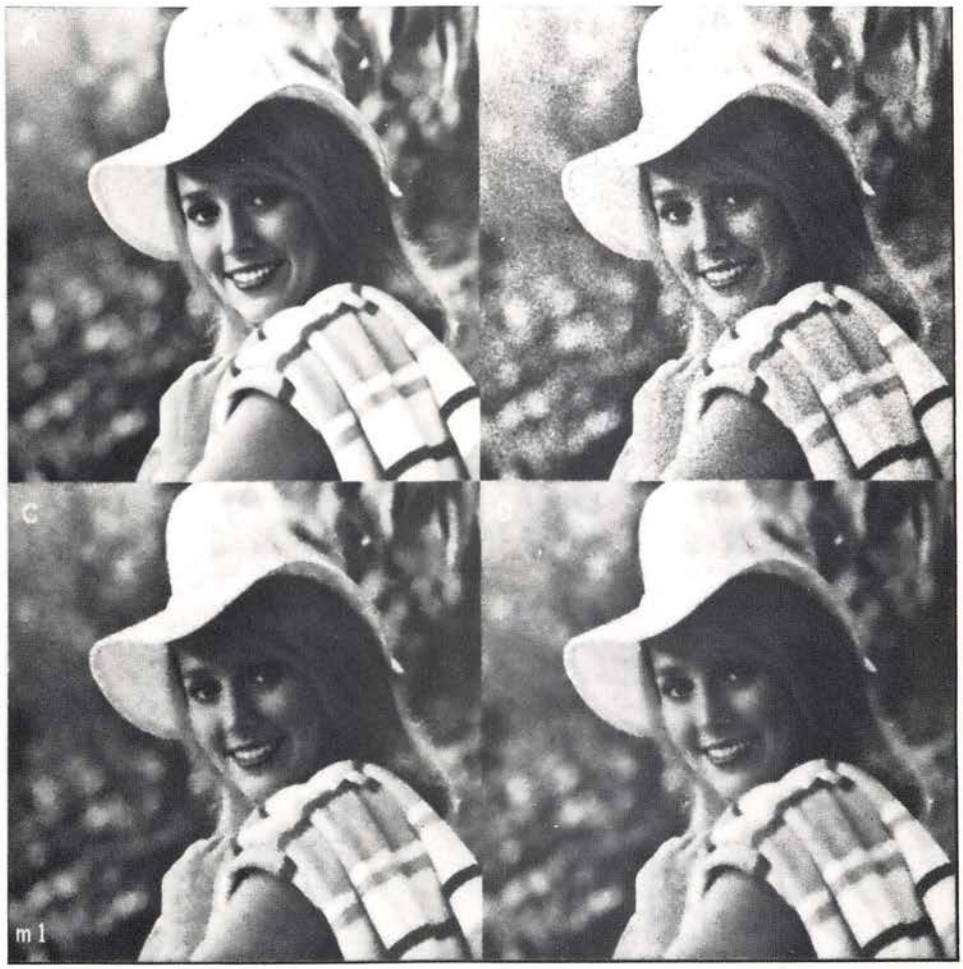

Figure 5.4 Adaptive noise smoothing filter for multiplicative noise

(A) Original image
(B) Original degraded by multiplicative noise with $\sigma_u^2=0.007$
(C) Adaptive noise smoothing estimate with local variance of Eq.(5.16)
(D) Adaptive noise smoothing estimate with local variance of Eq.(5.18)

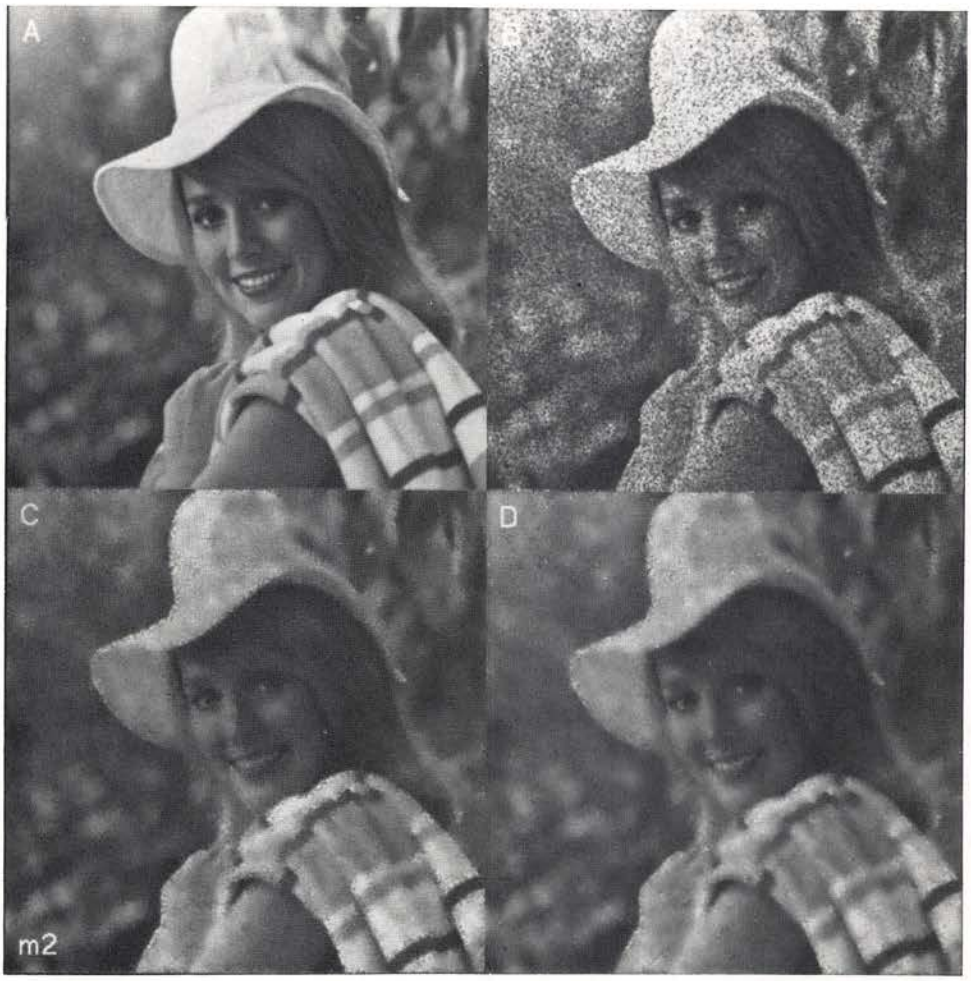

Figure 5.5 Adaptive noise smoothing filter for multiplicative noise

(A) Original image
(B) Original degraded by multiplicative noise with $\sigma_u^2=0.04$
(C) Adaptive noise smoothing estimate with local variance of Eq.(5.16)
(D) Adaptive noise smoothing estimate with local variance of Eq.(5.18)

where u(m,n) is a signal-independent noise. This model is very similar to the additive form of the multiplicative noise model except for the nonlinear effect of $f^{1/3}(m,n)$. Therefore, the derivation of the adaptive noise smoothing filter is straightforward with some knowledge of the statistics of $f^{1/3}(m,n)$, and is similar to the multiplicative noise case.

5.4.3 Poisson Noise

Photon noise is a fundamental limitation of images detected at low light levels. The degradation model of Poisson noise is given by

$$g'(m,n) = \text{Poisson}_{\lambda}(f(m,n)) \tag{5.27}$$

where λ is a proportionality factor. The statistics of the Poisson process were given in Eqs. (2.16), (2.17) and (2.18). Define the normalized observation as

$$g(m,n) = g'(m,n)/\lambda = \frac{\text{Poisson}_{\lambda}(f(m,n))}{\lambda}.$$

If we represent the normalized Poisson observation in terms of the signal part and the noise part, we have

$$g(m,n) = f(m,n) + (g(m,n) - f(m,n)). \tag{5.28}$$

Hence, the noise part is given by

$$v(m,n) = g(m,n) - f(m,n) = \frac{\text{Poisson}_{\lambda}(f(m,n))}{\lambda} - f(m,n)$$

and

$$\sigma_v^2(m,n) = \bar{f}(m,n)/\lambda \ .$$

From these equations, it is easy to show that the local variance of f(m,n) can be calculated from the local mean and local variance of g(m,n) by

$$v_f(m,n) = v_g(m,n) - \frac{\mu_f(m,n)}{\lambda} \qquad (5.29)$$

Therefore, the adaptive noise smoothing filter for Poisson noise can be written as

$$\hat{f}(m,n) = \mu_f(m,n) + \frac{v_f(m,n)\,(g(m,n)-\mu_f(m,n))}{v_f(m,n)+(\mu_f(m,n)/\lambda)} \qquad (5.30)$$

where g(m,n) is the normalized observation, and $\mu_f(m,n)/\lambda$ is an indication of the Poisson noise level at (m,n).

The simulation results are shown in Fig. 5.6. Figure 5.6(A) is the original image. Figure 5.6(B) is the original image degraded by a Poisson noise with $\lambda=1$. Figure 5.6(C) is the adaptive noise smoothing estimate of the original image obtained by using the sample mean and sample variance as local statistics. Figure 5.6(D) is the result of using the new local variance. The same seguence of simulation results for $\lambda=0.25$ are shown in Fig. 5.7.

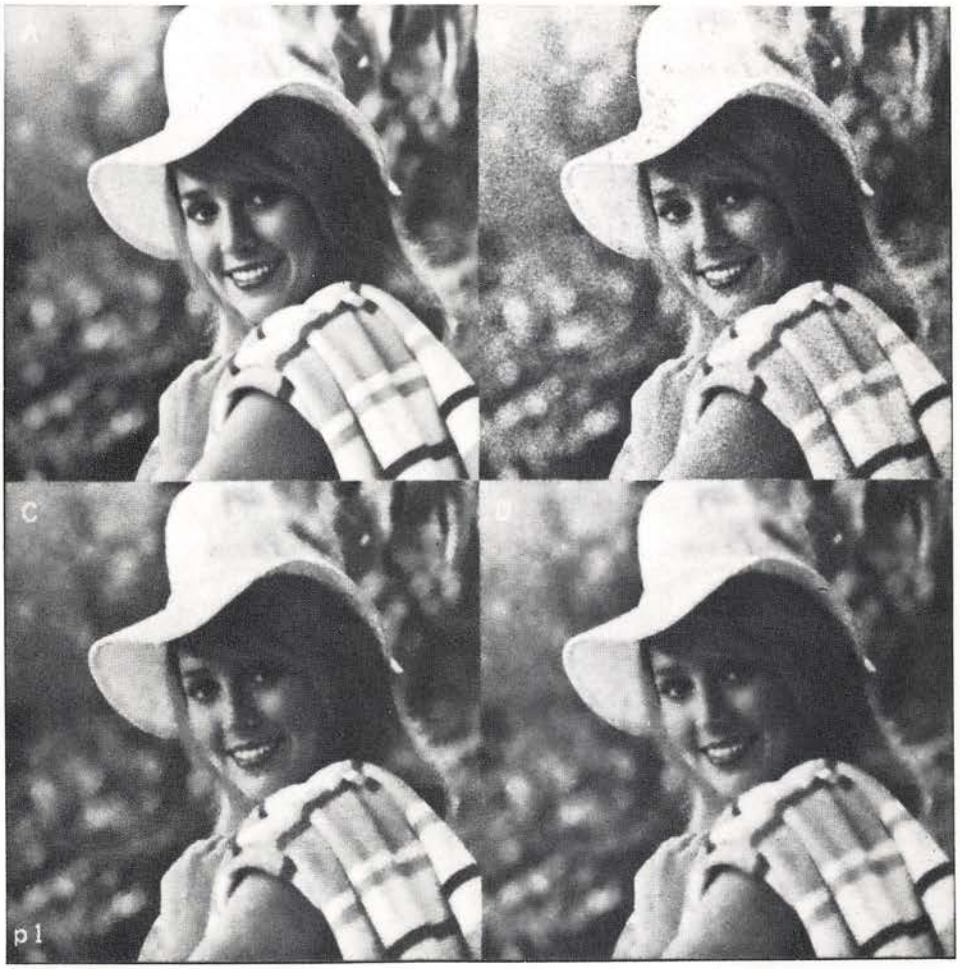

Figure 5.6 Adaptive noise smoothing filter for Poisson noise

(A) Original
(B) Original degraded by Poisson noise with $\lambda=1$
(C) Adaptive noise smoothing estimate with local variance of Eq.(5.16)
(D) Adaptive noise smoothing estimate with local variance of Eq.(5.18)

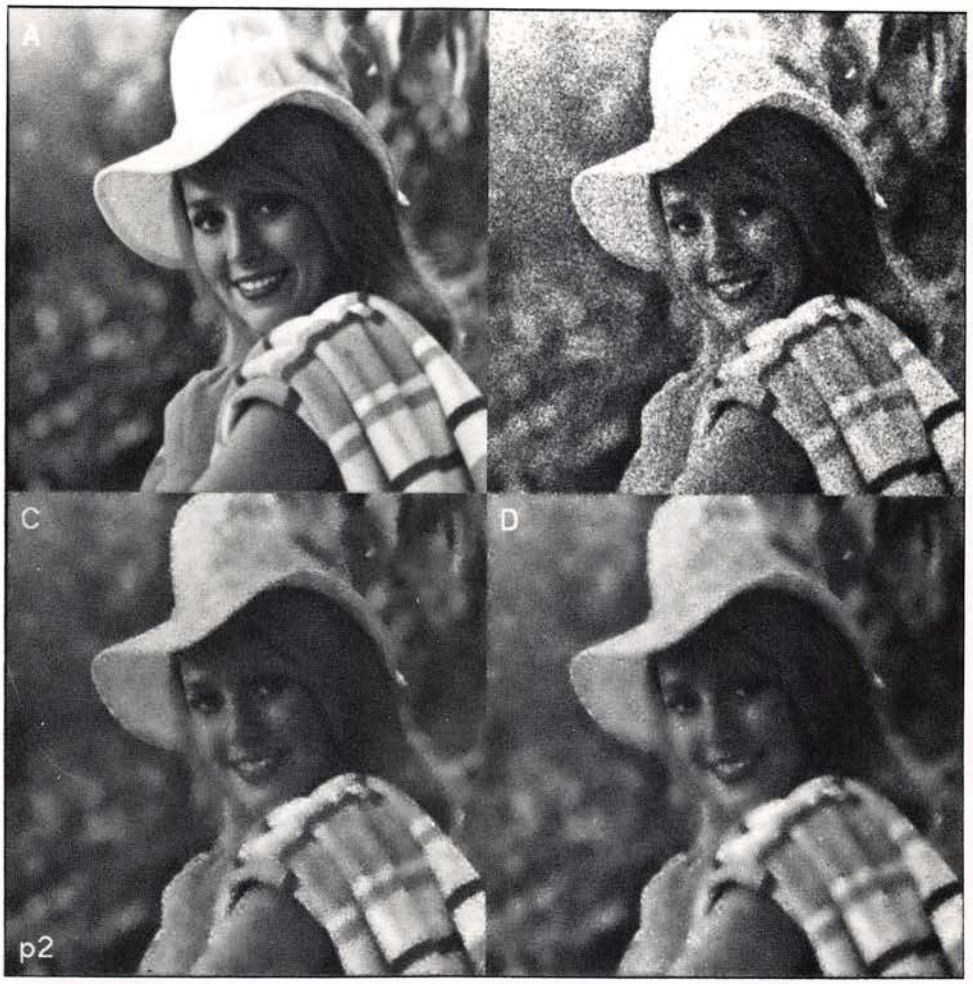

Figure 5.7 Adaptive noise smoothing filter for Poisson noise

(A) Original
(B) Original degraded by Poisson noise with $\lambda=0.25$
(C) Adaptive noise smoothing estimate with local variance of Eq.(5.16)
(D) Adaptive noise smoothing estimate with local variance of Eq.(5.18)

5.5 Conclusions

The adaptive noise smoothing filter has a very simple structure and does not require any *a priori* information from the original image. It uses a nonstationary image model and can easily deal with different types of signal-dependent noise. The mean square error criterion is used locally and has some of the desirable properties of a subjective error criterion.

The adaptive noise smoothing filter is adaptively linear and is similar to Lee's local statistics algorithm. However, there are two important differences in our approach:

1. Unlike Lee's heuristic arguments for using local mean and local variance, we introduce a NMNV Gaussian image model. With this image model, we can have a better understanding of the problem and the extension of this filter to image restoration becomes obvious. This problem will be discussed in the next chapter.

2. For the multiplicative noise model, our algorithm has a new term in the filter equation. This difference arises from the linear approximation made for the multiplicative noise model in Lee's heuristic

derivation, and shows that his algorithm is suboptimal for the multiplicative noise (signal-dependent noise in general).

The calculation of the local mean and local variance is critical to the quality of the restored image. The adaptive noise smoothing filter has the advantage of separating the estimation of statistics from the image restoration process. Thus, we can use various sophisticated methods to estimate the image statistics while fixing the restoration filter structure. Furthermore, the image statistics can be estimated by using a recursive filter to reduce the computation.

Chapter 6

NONSTATIONARY 2-D RECURSIVE IMAGE RESTORATION

6.1 Introduction

There have been many efforts to develop 2-D recursive image restoration algorithms in recent years. The difficulties with 2-D recursive image restoration are in establishing a suitable recursive model and the high dimensionality of the state vector. These factors make 2-D recursive algorithms computationally unattractive. Recent results on the reduced update Kalman filter by Woods et al. [6-1,6-2] seem to overcome some of these difficulties and have potential for real applications. Their algorithm uses a stationary image model and does not include any of the nonstationary image properties described in earlier chapters. Rajala et al. [6-3] derived a 2-D recursive filter based on a piecewise stationary image model. They first segment the image into disjoint regions according to the local spatial activity of the region and determine the covariance structure of different segments. Then they use a different Kalman filter for each segment. Ingle and Woods [6-4] modified the reduced update Kalman filter for a multiple image model. They used an identification-estimation approach in

which each point was assigned a stationary image model and filtered by the specific Kalman filter. Compared with Rajala's approach, this method emphasizes nonstationarity at edges in the scene rather than nonstationarity within regions.

In this chapter we develop a new recursive image restoration filter based on the NMNV image model. The algorithm is an extension of the adaptive noise smoothing filter, developed in Chapter 5, to image restoration. The state space model of the NMNV image model can be easily derived and is shown to be a shift operator. This simplifies the prediction step of the recursive filter considerably if we use indirect addressing techniques. The optimal filter requires excessive computation because of the high dimension of the state vector, thus a suboptimal filter similar to the reduced update Kalman filter [6-1] is used to reduce the computational effort. The nonstationary 2-D reduced update filter developed here is a numerical approximation to its nonrecursive formulation - the nonstationary Wiener filter. Boundary problems of recursive filtering that arise at the ends of a scan line can be easily resolved because of the image model assumed. Statistics needed for the filter are estimated from the local statistics of the degraded image. The extension of this recursive filter to signal-dependent noise, such as multiplicative noise and Poisson noise, is also derived.

6.2 State Space Model

Consider the linear space-invariant image degradation model

$$g(m,n)=\sum_{i=m-p}^{i=m+p}\sum_{j=n-q}^{j=n+q}h(i,j)f(m+i,n+j) + v(m,n) \qquad (6.1)$$

where $g(m,n)$ is the degraded image, $f(m,n)$ is the original image, $h(m,n)$ is the point spread function of the system, $2p+1$ and $2q+1$ indicate the extent of the blurring function, and $v(m,n)$ is assumed to be white noise with

$$E[v(m,n)]=0 \quad \text{and}$$

$$E[v(m_1,n_1)v(m_2,n_2)]=R(m_1,n_1)\delta(m_1-m_2,n_1-n_2).$$

Define the raster scanned state vector $\underline{x}_1(m,n)$ as

$$\underline{x}_1(m,n)=[f(m-p,n-q),f(m-p,n-q+1),\ldots f(m-p,N);$$
$$f(m-p+1,1),\ldots f(m-p+1,N);\ldots f(m+p,n+q-1)]^T$$

where N is the size of the image. The ordering of the state vector is similar to that of the lexicographic representation that converts the 2-D image into a 1-D vector. Therefore, we can treat Eq. (6.1) as a 1-D moving average process. The state space model of this process can be written as

$$\underline{x}_1(m,n+1)= F_1\underline{x}_1(m,n) + G_1w_1(m,n) \qquad (6.2)$$

$$z(m,n)= H_1\underline{x}_1(m,n) + D_1w_1(m,n) + v(m,n) \qquad (6.3)$$

where $w_1(m,n)=f(m+p,n+q)$ and $z(m,n)=g(m,n)$. The matrices in Eqs. (6.2) and (6.3) have the form

$$F_1=\begin{bmatrix} 0 & 1 & 0 & \cdots & 0 \\ 0 & 0 & 1 & 0 & \cdots & 0 \\ \cdot & & & & & \cdot \\ \cdot & & & & & \cdot \\ \cdot & & & & & 0 \\ \cdot & & & & & 1 \\ 0 & 0 & 0 & \cdots & & 0 \end{bmatrix} \qquad G_1=\begin{bmatrix} 0 \\ 0 \\ \cdot \\ \cdot \\ \cdot \\ 0 \\ 1 \end{bmatrix}$$

and

$$H_1=[h(-p,-q),h(-p,-q+1),\ldots h(-p,q),0,0,\ldots 0;$$

$$0,0,\ldots h(-p+1,-q),h(-p+1,-q+1),\ldots h(-p+1,q),0,0,.$$

$$0,0,\ldots \quad \cdots\cdots\cdots\cdots\cdots\cdots\cdots\cdots\cdots$$

$$0,0,\ldots h(p,-q),h(p,-q+1),\ldots,h(p,q-1)]$$

$$D_1=h(p,q).$$

Note that the state propagation matrix F_1 is a shift operator that propagates the state vector within the image. Due to the finite spatial extent of an image, the observation equation Eq. (6.3) is not a valid description of the degradation model near the image boundary and must be modified there. The vectors H_1 and D_1 account for the point spread function of the system and are raster scanned representations of the 2-D point spread function. Because all variables are spatial, the noncausal model is a shifted version of the causal model and is realizable.

The NMNV image model can be characterized by

$$w_1(m,n+1) = a*w_1(m,n) + w(m,n) \qquad (6.4)$$

where $a=0$ and $w(m,n)=f(m+p,n+q+1)$ is a shifted version of $w_1(m,n)$. Hence, the statistics of $w(m,n)$ are given by

$$E[w(m,n)]=\bar{f}(m+p,n+q+1) \text{ and}$$

$$E[(w(m_1,n_1)-\bar{w}(m_1,n_1))(w(m_2,n_2)-\bar{w}(m_2,n_2))]$$

$$=Var[f(m_1,n_1)]\delta(m_1-m_2,n_1-n_2).$$

The major difficulty of recursive image restoration in a conventional stationary image model is in establishing a suitable recursive image model. This problem does not occur for the NMNV image model because there is no correlation between adjacent pixels in the residual image and the output is simply a delayed version of the input. The nonstationary correlation existing in an image is effectively imbedded in the nonstationary mean and the nonstationary variance.

In order to combine the degradation model in Eqs. (6.2) and (6.3) with the image model in Eq. (6.4), we define the augmented state vector

$$\underline{x}(m,n)=\begin{bmatrix}\underline{x}_1(m,n)\\ w_1(m,n)\end{bmatrix}$$

$$=[f(m-p,n-q),f(m-p,n-q+1),\ldots f(m-p,N);f(m-p+1,1),$$

$$f(m+p,1),f(m+p,2),\ldots f(m+p,n+q)]^T. \qquad (6.5)$$

The augmented model of Eqs. (6.2), (6.3) and (6.4) can now be written as

$$\begin{bmatrix} \underline{x}_1(m,n+1) \\ w_1(m,n+1) \end{bmatrix} = \begin{bmatrix} F_1 & G_1 \\ 0 & 0 \end{bmatrix} \begin{bmatrix} \underline{x}_1(m,n) \\ w_1(m,n) \end{bmatrix} + \begin{bmatrix} \underline{0} \\ 1 \end{bmatrix} w(m,n) \quad (6.6)$$

$$z(m,n) = [H_1, h(p,q)] \begin{bmatrix} \underline{x}_1(m,n) \\ w_1(m,n) \end{bmatrix} + v(m,n), \quad (6.7)$$

or

$$\underline{x}(m,n+1) = F\underline{x}(m,n) + Gw(m,n) \quad (6.8)$$

$$z(m,n) = H\underline{x}(m,n) + v(m,n) \quad (6.9)$$

where

$$F = \begin{bmatrix} F_1 & G_1 \\ 0 & 0 \end{bmatrix} \quad (6.10)$$

and

$$H = [h(-p,-q), h(-p,-q+1), \ldots h(-p,q), 0, 0, \ldots 0;$$
$$0, 0, \ldots h(-p+1,-q), h(-p+1,-q+1), \ldots h(-p+1,q), 0, 0, .$$
$$0, 0, \ldots h(p,-q), h(p,-q+1), \ldots h(p,q)]. \quad (6.11)$$

The relative positions of the state vector $\underline{x}(m,n)$ and input $w(m,n)$ is illustrated in Fig. 6.1. Note that the F matrix remains a shift operator. It is interesting to see that the state propagation matrix F is space-invariant even we consider a nonstationary image model. The nonstationarity of the image is described by the nonstationary mean and nonstationary variance of the input process rather than by a space-variant matrix.

The nonstationary mean of the augmented model can be

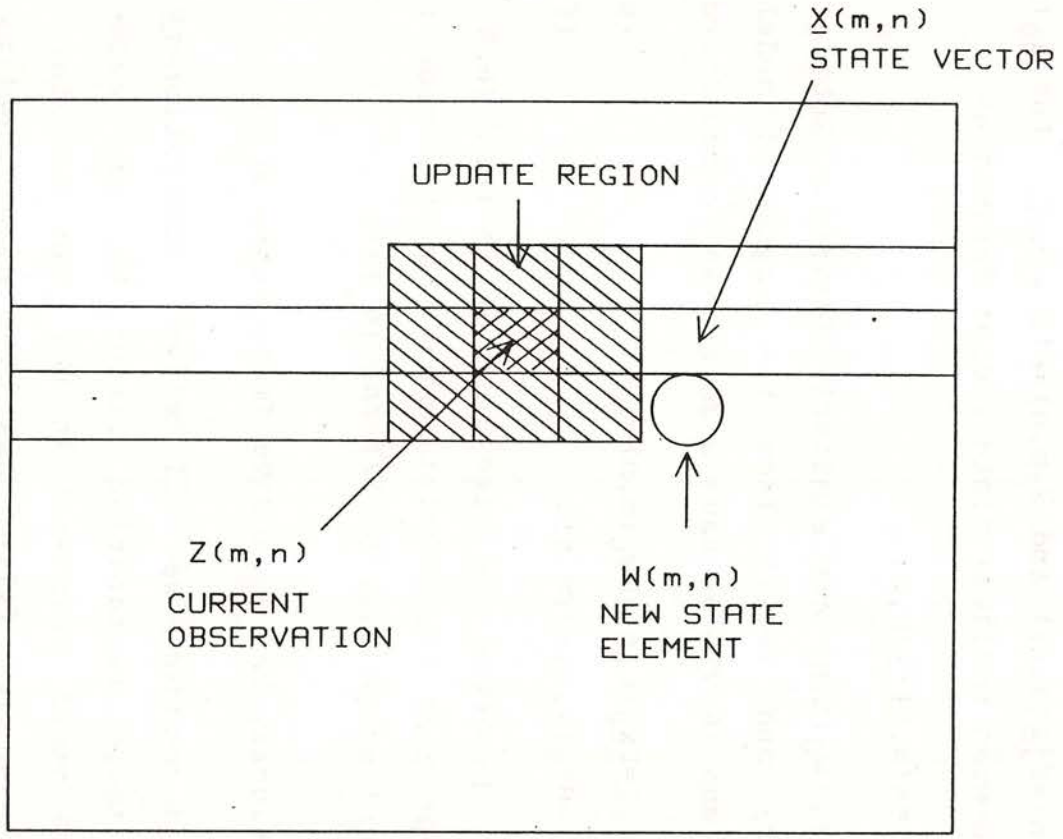

Figure 6.1 State space model of the nonstationary 2-D recursive restoration filter

obtained by taking the expectation on both sides of Eqs. (6.8), (6.9) and we have

$$\bar{\underline{x}}(m,n+1)=F\bar{\underline{x}}(m,n)+G\bar{w}(m,n) \tag{6.12}$$

$$\bar{z}(m,n)=H\bar{\underline{x}}(m,n) \tag{6.13}$$

where $\bar{\underline{x}}(m,n)=E[\underline{x}(m,n)]$ and $\bar{z}(m,n)=E[z(m,n)]$. Let $\underline{x}_0(m,n)$ be the zero-mean residual state vector defined as

$$\underline{x}_0(m,n)=\underline{x}(m,n)-\bar{\underline{x}}(m,n)$$

and $z_0(m,n)$, $w_0(m,n)$ are similarly defined. Subtracting Eqs. (6.12) and (6.13) from the augmented model in Eqs. (6.8) and (6.9), we have a zero-mean residual model

$$\underline{x}_0(m,n+1)=F\underline{x}_0(m,n)+Gw_0(m,n) \tag{6.14}$$

$$z_0(m,n)=H\underline{x}_0(m,n)+v(m,n). \tag{6.15}$$

This model preserves the same form as in Eqs. (6.8) and (6.9) except that the nonstationary mean has been taken out as described in Eqs. (6.12) and (6.13).

6.3 Nonstationary 2-D Recursive Image Restoration

In this section, we will derive a nonstationary 2-D recursive image restoration filter for the augmented state space model discussed in the last section. The resulting recursive filter has high dimensionality and the amount of computation makes it unattractive for practical applications. To overcome this problem, a reduced update idea similar to Woods' reduced update filter [6-1] is used to ease the computation requirements.

6.3.1 Derivation

To derive the Kalman filter equations, we follow the procedure used in Meditch [6-5]. Let $\underline{\hat{x}}_{0f}(m,n)$ be the optimal filtered estimate of $\underline{x}_0(m,n)$ based on the observations $z_0(1,1)$, $z_0(1,2)$, ..., $z_0(m,n)$, and $\underline{\hat{x}}_{0p}(m,n)$ be the optimal predicted estimate of $\underline{x}_0(m,n)$ based on $z_0(1,1)$, $z_0(1,2)$, ..., $z_0(m,n-1)$. We have

$$\underline{\hat{x}}_{0f}(m,n)=E[\underline{x}_0(m,n)\,|\,z_0(1,1),\ldots,z_0(m,n)]$$

and

$$\underline{\hat{x}}_{0p}(m,n)=E[\underline{x}_0(m,n)\,|\,z_0(1,1),\ldots,z_0(m,n-1)].$$

Taking conditional expectations on both sides of Eq. (6.14) for given observations $z_0(1,1)$, $z_0(1,2)$, ..., $z_0(m,n-1)$, and reducing the index by one, we have the relation

$$E[\underline{x}_0(m,n)\,|\,z_0(1,1),\ldots,z_0(m,n-1)]$$

$$=E[F\underline{x}_0(m,n-1)+Gw_0(m,n-1)\,|\,z_0(1,1),\ldots,z_0(m,n-1)]$$

or

$$\underline{\hat{x}}_{0p}(m,n)=F\underline{\hat{x}}_{0f}(m,n-1)$$

where we use the fact that $w_0(m,n-1)$ is independent of $z_0(1,1)$, ..., $z_0(m,n-1)$ and is zero mean. The predicted covariance matrix $P_p(m,n)$ is given by

$$
\begin{aligned}
&P_p(m,n)\\
&=E[(\underline{x}_0(m,n)-\hat{\underline{x}}_{0p}(m,n))(\underline{x}_0(m,n)-\hat{\underline{x}}_{0p}(m,n))^T]\\
&=E[(F\underline{x}_0(m,n-1)+Gw_0(m,n-1)-F\hat{\underline{x}}_{0f}(m,n-1))\\
&\quad(F\underline{x}_0(m,n-1)+Gw_0(m,n-1)-F\hat{\underline{x}}_{0f}(m,n-1))^T]\\
&=FP_f(m,n-1)F^T+GQ(m,n-1)G^T
\end{aligned}
$$

where $Q(m,n-1)=E[w_0^2(m,n-1)]$ is the nonstationary variance of the original image, and $P_f(m,n-1)$ is the filtered covariance matrix. This is the prediction step.

The optimal filtered estimate $\hat{\underline{x}}_{0f}(m,n)$ can be obtained by using the projection theorem [6-5] and we have

$$
\begin{aligned}
&\hat{\underline{x}}_{0f}(m,n)=E[\underline{x}(m,n)\,|\,z_0(1,1),z_0(1,2),\ldots,z_0(m,n)]\\
&=E[\underline{x}(m,n)\,|\,z_0(1,1),z_0(1,2),\ldots,z_0(m,n-1),\tilde{z}_{0p}(m,n)]\\
&=E[\underline{x}(m,n)\,|\,z_0(1,1),z_0(1,2),\ldots,z_0(m,n-1)]+\\
&\quad E[\underline{x}(m,n)\,|\,\tilde{z}_{0p}(m,n)]\\
&=\hat{\underline{x}}_{0p}(m,n)+E[\underline{x}(m,n)\,|\,\tilde{z}_{0p}(m,n)] \qquad (6.16)
\end{aligned}
$$

where $\tilde{z}_{0p}(m,n)$ is known as the innovation process and is defined as

$$
\begin{aligned}
&\tilde{z}_{0p}(m,n)=z_0(m,n)-E[z_0(m,n)\,|\,z_0(1,1),\ldots,z_0(m,n-1)]\\
&=H\underline{x}_0(m,n)+v(m,n)-H\hat{\underline{x}}_{0p}(m,n)\\
&=H\tilde{\underline{x}}_{0p}(m,n)+v(m,n). \qquad (6.17)
\end{aligned}
$$

Here we use the fact that $v(m,n)$ is independent of $z_0(1,1)$, ..., $z_0(m,n-1)$, and $\tilde{\underline{x}}_{0p}(m,n)=\underline{x}_0(m,n)-\hat{\underline{x}}_{0p}(m,n)$.

From Eq. (6.16) and Eq. (5.4) in Chapter 5, the filtered estimate of $\underline{x}_0(m,n)$ can be written as

$$\hat{\underline{x}}_{0f}(m,n)=\hat{\underline{x}}_{0p}(m,n)+\underline{k}(m,n)\tilde{z}_{0p}(m,n)$$

where $\underline{k}(m,n)=P_{x_0\tilde{z}_{0p}}(m,n)P^{-1}_{\tilde{z}_{0p}\tilde{z}_{0p}}(m,n)$. The cross-covariance matrix $P_{x_0\tilde{z}_{0p}}(m,n)$ has the form

$$\begin{aligned}
&P_{x_0\tilde{z}_{0p}}(m,n) = E[\underline{x}_0(m,n)\tilde{z}^T_{0p}(m,n)]\\
&=E[(\hat{\underline{x}}_{0p}(m,n)+\tilde{\underline{x}}_{0p}(m,n))(H\tilde{\underline{x}}_{0p}(m,n)+v(m,n))^T]\\
&=P_p(m,n)H^T
\end{aligned}$$

where we use the orthogonality principle [6-5] in the simple form

$$E[\hat{\underline{x}}_{0p}(m,n)\tilde{\underline{x}}_{0p}(m,n)] = 0.$$

The covariance matrix of the innovation process can be calculated as

$$\begin{aligned}
&P_{\tilde{z}_{0p}\tilde{z}_{0p}}(m,n)= E[\tilde{z}_{0p}(m,n)\tilde{z}_{0p}(m,n)]\\
&=HP_p(m,n)H^T + R(m,n).
\end{aligned}$$

The filtered covariance matrix $P_f(m,n)$ is given by

$$\begin{aligned}
&P_f(m,n)=E[(\underline{x}_0(m,n)-\hat{\underline{x}}_{0f}(m,n))(\underline{x}_0(m,n)-\hat{\underline{x}}_{0f}(m,n))^T]\\
&=E[(\underline{x}_0(m,n)-\hat{\underline{x}}_{0p}(m,n)-\underline{k}(m,n)\tilde{z}_{0p}(m,n))\\
&\qquad(\underline{x}_0(m,n)-\hat{\underline{x}}_{0p}(m,n)-\underline{k}(m,n)\tilde{z}_{0p}(m,n))^T]\\
&=E[(\tilde{\underline{x}}_{0p}(m,n)-\underline{k}(m,n)(H\tilde{\underline{x}}_{0p}(m,n)+v(m,n)))\\
&\qquad(\tilde{\underline{x}}_{0p}(m,n)-\underline{k}(m,n)(H\tilde{\underline{x}}_{0p}(m,n)+v(m,n)))^T]\\
&=(I-\underline{k}(m,n)H)P_p(m,n)(I-\underline{k}(m,n)H)^T+\underline{k}(m,n)R(m,n)\underline{k}^T(m,n)\\
&=[I-\underline{k}(m,n)H]P_p(m,n).
\end{aligned}$$

In summary, we have the following Kalman filter equations:

Prediction step:

$$\underline{\hat{x}}_{0p}(m,n)=F\underline{\hat{x}}_{0f}(m,n-1) \tag{6.18}$$

$$P_p(m,n)=FP_f(m,n-1)F^T+GQ(m,n-1)G^T \tag{6.19}$$

Filtering step:

$$\underline{k}(m,n)=P_p(m,n)H^T[HP_p(m,n)H^T+R(m,n)]^{-1} \tag{6.20}$$

$$\underline{\hat{x}}_{0f}(m,n)=\underline{\hat{x}}_{0p}(m,n)+\underline{k}(m,n)[z_0(m,n)-H\underline{\hat{x}}_{0p}(m,n)] \tag{6.21}$$

$$P_f(m,n)=(I-\underline{k}(m,n)H)P_p(m,n). \tag{6.22}$$

6.3.2 Computational Aspects

The dimensionality of the nonstationary recursive filter is equal to (2p*N+2q+1) where 2p+1 and 2q+1 are the widths of the blurring function in the vertical and horizontal directions respectively. Here, N is the image size which is usually a large number. Due to the high dimensionality of the state vector, the computational and memory requirements make the optimal Kalman filter approach impractical. A suboptimal approach similar to the reduced update Kalman filter is used here. The update region of a point (m,n) is specified as those points within the point spread function of the blurring degradation. Instead of updating the whole state vector, the reduced update Kalman filter updates only those points in the update region that make a direct contribution to the observation g(m,n) in Eq. (6.1). The gain vector $\underline{k}(m,n)$ is therefore constrained to be zero

outside the update region of the "present" point (m,n). The same principle is used to update the filtered covariance matrix $P_f(m,n)$. These modifications virtually reduce the dimension of the state vector from (2p*N+2q+1) to (2p+1)*(2q+1) and make the number of computations per pixel independent of the image size N.

The computation for the prediction step of the reduced update Kalman filter is straightforward. The predicted state estimate $\hat{\underline{x}}_{0p}(m,n)$ takes one matrix-vector multiplication as in Eq. (6.18). Because the state propagation matrix F is only a shift operator, we can use indirect addressing techniques and no real multiplication is required. The predicted covariance matrix in Eq. (6.19) can be similarly obtained by using the same techniques. It is interesting to see that the NMNV image model not only decouples the state equation but also facilitates the prediction step of the recursive filter with the indirect addressing techniques.

In the filtering step, we use the reduced update constraint and the gain vector $\underline{k}(m,n)$ is set to zero outside the update region of the current point (m,n). This approximation reduces the computation dramatically and we only need to calculate (2p+1)*(2q+1) elements of the gain vector. The matrix inversion required in Eq. (6.20) is only a scalar inverse. The filtered state estimate is calculated according to Eq. (6.21), and only (2p+1)*(2q+1) elements of $\hat{\underline{x}}_{0f}(m,n)$ are updated. The same

reduced update principle applies to the filtered covariance matrix $P_f(m,n)$ and the filtered covariance matrix only has effective dimension $(2p+1)*(2q+1)$. Thus the total computation of the nonstationary 2-D recursive filter is on the order of $O(N^2)$ and the computation at each point is proportional to $[(2p+1)*(2q+1)]^2$.

Due to the raster scanned ordering of a 2-D image, the observation equation (6.15) is not valid near the boundary of the image and causes the boundary problems. The prediction step of the reduced update Kalman filter remains the same at the boundary since it only depends on the state equation which is a valid description everywhere in the image. The filtering step has to be modified since the observation equation is incorrect at the boundary, and the filtering operation may contribute error to the filtered estimate. To resolve the boundary problem, we only use the prediction equations to propagate the predicted estimates in the boundary region and turn off the filtering equations until the filter passes the boundary region and the observation equation becomes valid again.

The local mean of the degraded image $z(m,n)$ is readily calculated from the noisy image. However, the nonstationary 2-D recursive filter requires the nonstationary mean and nonstationary variance of the input process $w(m,n)$. One way to get the local mean of $w(m,n)$ is to use the inverse system of Eqs. (6.12) and

(6.13) on the local mean estimate of z(m,n). The quality of this estimate depends on the stability of the inverse system and problems of error accumulation may occur due to the inexact knowledge of the blurring function and the instability of the inverse system. Another local mean estimate of w(m,n) can be obtained by using the blurring function as the weighting function for calculating the local mean of z(m,n) and using the inverse filter to calculate the local mean of w(m,n). It is easy to see that the net effect is to set the local mean of w(m,n) equal to z(m,n). Another method is to estimate E[w(m,n)] from z(m,n) by local averaging, then convolve the local mean estimate of w(m,n) with the blurring function to get a consistent estimate of E[z(m,n)] satisfying Eq. (6.13). Principles of calculating the local statistics discussed in Chapter 5 also apply here.

6.3.3 Simulation Results

The original image in Fig. 6.2(A) is first blurred with a 5*5 Gaussian shape point spread function and then degraded by additive Gaussian noise with noise variance equal to 16. The degraded image is shown in Fig. 6.2(B). Figure 6.2(C) is the restored image obtained by using the degraded image as the local mean of the original image and calculating the local variance by using the same techniques as in Chapter 5. The restored image has sharp edges but seems noisy. Figure 6.2(D) is the restored image obtained by using a blurred version of the degraded

image as the local mean of the original image. The restored image has sharp edges and the noise is smoothed. From Fig. 6.2(C) and 6.2(D), we can see that the second method of calculating the local mean of the original image is better than the first method. This difference is especially clear when the noise variance is large. The simulation results for $\sigma_v^2=100$ are shown in Fig. 6.3. Figure 6.3(B) is the blurred image and Fig. 6.3(C) has both blur and additive noise. The restored image shown in Fig. 6.3(D) uses a 5*5 low-pass filtered version of the degraded image as the local mean of the original image.

6.4 Nonstationary 2-D Recursive Restoration of Images with Multiplicative Noise

The Kalman filter is usually derived for the signal-independent, additive, white noise case. In this section, we extend our 2-D nonstationary recursive image restoration filter to images degraded by blur and multiplicative noise.

The degradation model for an image degraded by blur and multiplicative noise can be written

$$g(m,n)=u(m,n)\left[\sum_{i=m-p}^{i=m+p}\sum_{j=n-q}^{j=n+q} h(i,j)\,f(m-i,n-j)\right] \qquad (6.23)$$

where $u(m,n)$ is a signal-independent multiplicative noise with

$$E[u(m,n)] = \bar{u}(m,n)$$

and

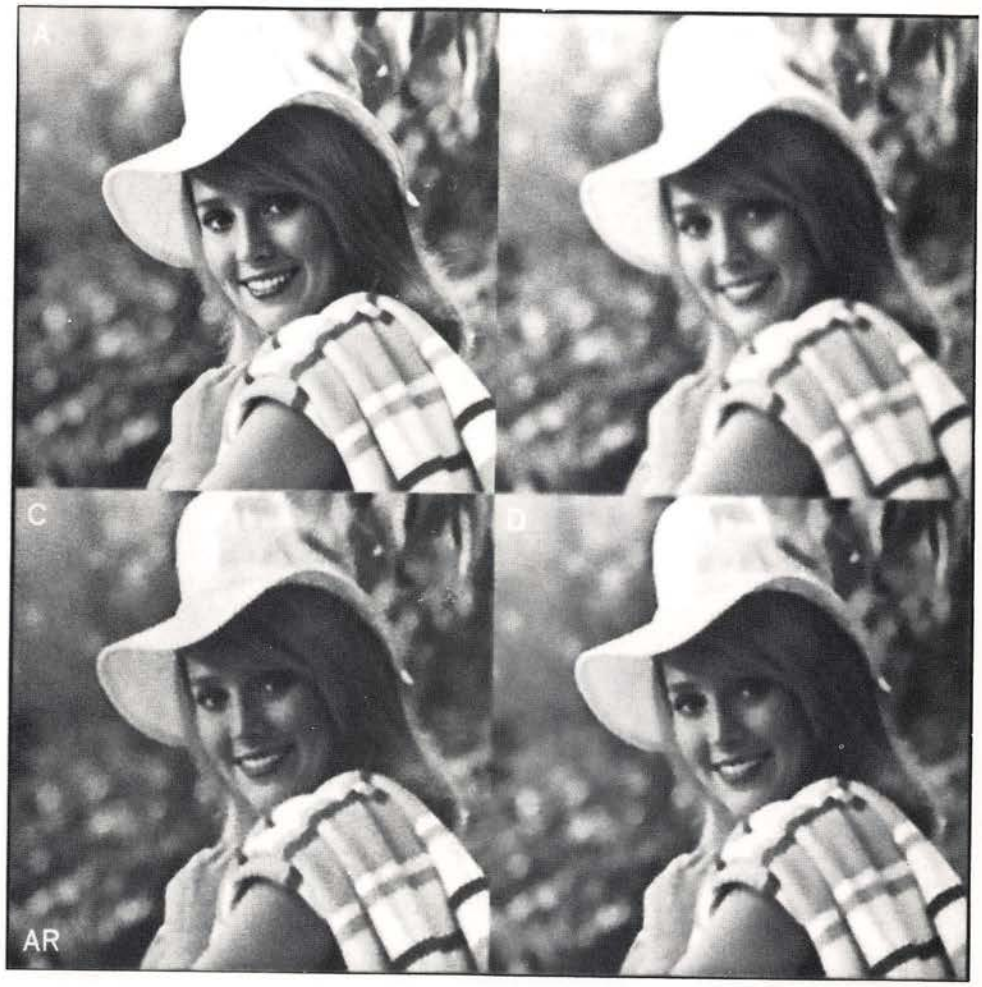

Figure 6.2 Restoration results for images with additive noise

(A) Original image
(B) Original blurred with 5*5 Gaussian PSF and additive noise with σ_v^2=16
(C) Recursive restoration using degraded original as local mean
(D) Recursive restoration using smoothed degraded original as local mean

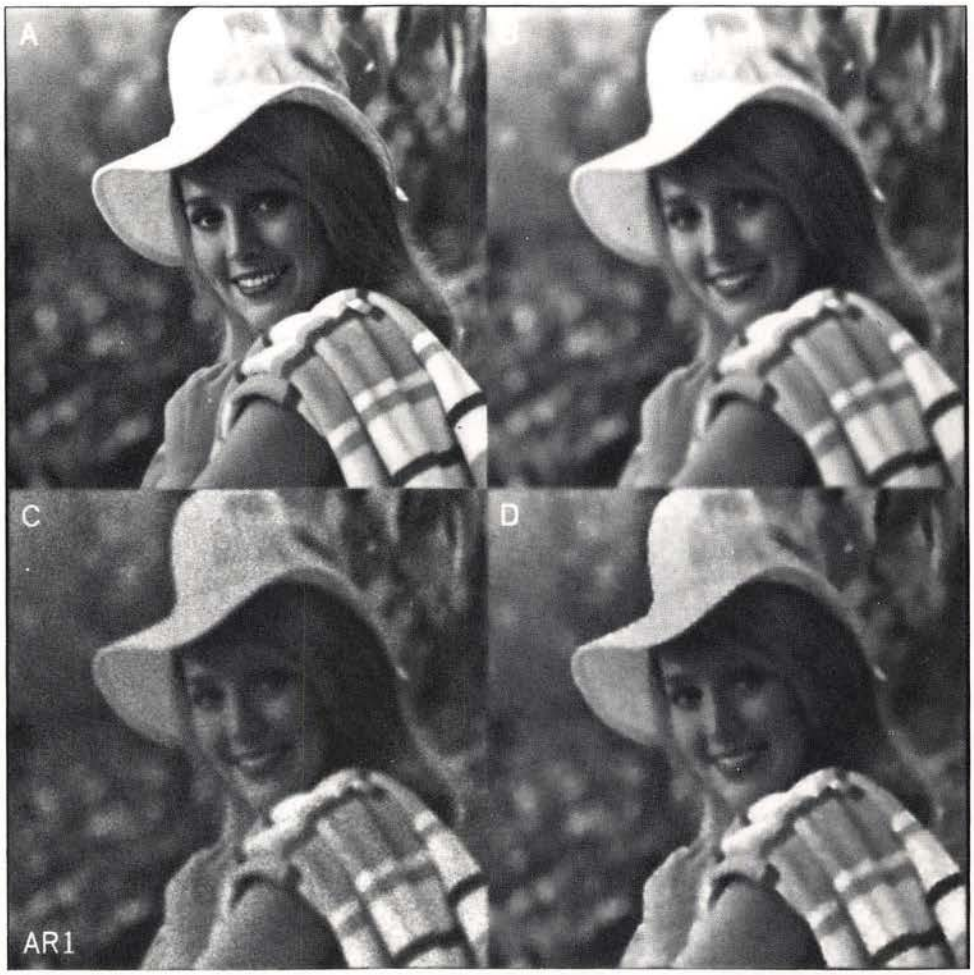

Figure 6.3 Restoration results for images with blur and additive noise

(A) Original image
(B) Original blurred with 5*5 Gaussian PSF
(C) Blurred image in (B) plus additive noise with σ_v^2=100
(D) Recursive restoration result

$$E[(u(m,n)-\bar{u}(m,n))(u(m_1,n_1)-\bar{u}(m_1,n_1))]$$
$$=R_u(m,n)\,\delta(m-m_1,n-n_1).$$

The augmented state space model of this degradation model can be written as

$$\underline{x}(m,n+1)= F\underline{x}(m,n)+ Gw(m,n) \tag{6.24}$$

$$z(m,n)= u(m,n)H\underline{x}(m,n) \tag{6.25}$$

where matrices F and G are the same as in Eqs. (6.8) and (6.9). Note that the state equation remains the same as in Eq. (6.8) because we use the same image model, but the observation equation has a nonlinear form due to the multiplicative noise. The nonstationary mean of the multiplicative noise model can be obtained by taking the expectation of Eqs. (6.24) and (6.25), and we have

$$\bar{\underline{x}}(m,n+1)=F\bar{\underline{x}}(m,n)+G\bar{w}(m,n) \tag{6.26}$$

$$\bar{z}(m,n)=\bar{u}(m,n)H\bar{\underline{x}}(m,n). \tag{6.27}$$

Subtracting the nonstationary mean from the augmented state space model, we have the zero-mean residual model

$$\underline{x}_0(m,n+1)=F\underline{x}_0(m,n)+Gw_0(m,n) \tag{6.28}$$

$$z_0(m,n)=u(m,n)H\underline{x}_0(m,n)+u_0(m,n)H\bar{\underline{x}}(m,n) \tag{6.29}$$

where $\underline{x}_0(m,n)=\underline{x}(m,n)-\bar{\underline{x}}(m,n)$, and $z_0(m,n)$, $u_0(m,n)$, $w_0(m,n)$ are similarly defined.

The prediction step of this model is the same as the additive noise model because the state equations are the same. Hence, we have

$$\underline{\hat{x}}_{0p}(m,n)=F\underline{\hat{x}}_{0f}(m,n-1)$$

$$P_p(m,n)=FP_f(m,n-1)F^T + GQ(m,n-1)G^T.$$

The innovation process can be written as

$$\begin{aligned}\tilde{z}_{0p}(m,n)&=z_0(m,n)-\hat{z}_{0p}(m,n)\\&=z_0(m,n)-E^*[z_0(m,n)\,|\,z_0(1,1),\ldots z_0(m,n-1)]\\&=z_0(m,n)-\bar{u}(m,n)H\underline{\hat{x}}_{0p}(m,n)\\&=\bar{u}(m,n)H\underline{\tilde{x}}_{0p}(m,n)+u_0(m,n)H(\underline{x}_0(m,n)+\underline{\bar{x}}(m,n))\end{aligned} \qquad (6.30)$$

where $E^*[.|.]$ represents the linear minimum mean square error estimate of $z_0(m,n)$ based on the past observations, and we use the fact that $u(m,n)$ is independent of observations $z(1,1)$, $z(1,2)$, ..., $z(m,n-1)$. As in section 6.3, the filtered estimate is given by

$$\underline{\hat{x}}_{0f}(m,n)=\underline{\hat{x}}_{0p}(m,n)+\underline{k}(m,n)\tilde{z}_{0p}(m,n)$$

where $\underline{k}(m,n)=P_{x_0\tilde{z}_{0p}}(m,n)P^{-1}_{\tilde{z}_{0p}\tilde{z}_{0p}}(m,n)$. The cross-covariance matrix can be calculated as

$$\begin{aligned}P_{x_0\tilde{z}_{0p}}(m,n) &= E[\underline{x}_0(m,n)\tilde{z}_{0p}(m,n)]\\&=E\{[\underline{\hat{x}}_{0p}(m,n)+\underline{\tilde{x}}_{0p}(m,n)][\bar{u}(m,n)H\underline{\tilde{x}}_{0p}(m,n)+\\&\quad u_0(m,n)H(\underline{x}_0(m,n)+\underline{\bar{x}}(m,n))]^T\}\\&=\bar{u}(m,n)P_p(m,n)H^T\end{aligned}$$

where we use the orthogonality principle and the knowledge that $u_0(m,n)$ is independent of the original image and the predicted estimate.

The covariance matrix of the innovation process is given by

$$P_{\tilde{z}_{0p}\tilde{z}_{0p}}(m,n) = E[\tilde{z}_{0p}(m,n)\tilde{z}_{0p}^T(m,n)]$$
$$=\bar{u}^2(m,n)HP_p(m,n)H^T + R_u(m,n)H\underline{\bar{x}}(m,n)\underline{\bar{x}}^T(m,n)H^T$$
$$+ R_u(m,n)HC_f(m,n)H^T$$

where $C_f(m,n)$ is the covariance matrix of the original image. For the NMNV image model, we have

$$C_f(m,n)=\begin{bmatrix} \sigma_f^2(m-p,n-q) & & & 0 \\ & \sigma_f^2(m-p,n-q+1) & & \\ & & \ddots & \\ 0 & & & \sigma_f^2(m+p,n+q) \end{bmatrix}.$$

The filtered covariance matrix is given by

$$P_f(m,n)=E\{[\underline{x}_0(m,n)-\underline{\hat{x}}_{0f}(m,n)][\underline{x}_0(m,n)-\underline{\hat{x}}_{0f}(m,n)]^T\}$$
$$=E\{[\underline{\tilde{x}}_{0p}(m,n)-\underline{k}(m,n)\tilde{z}_{0p}(m,n)][\underline{\tilde{x}}_{0p}(m,n)-\underline{k}(m,n)\tilde{z}_{0p}(m,n)]$$
$$=(I-\bar{u}(m,n)\underline{k}(m,n)H)P_p(m,n).$$

In summary, we have the following Kalman filter equations for multiplicative noise model:

Prediction step:

$$\underline{\hat{x}}_{0p}(m,n)=F\underline{\hat{x}}_{0f}(m,n-1) \tag{6.31}$$

$$P_p(m,n)=FP_f(m,n-1)F^T + GQ(m,n-1)G^T \tag{6.32}$$

Filtering step:

$$\underline{k}(m,n)= \bar{u}(m,n)P_p(m,n)H^T[\bar{u}^2(m,n)HP_p(m,n)H^T$$
$$+R_u(m,n)H(\underline{\bar{x}}(m,n)\underline{\bar{x}}^T(m,n)+C_f(m,n))H^T]^{-1} \tag{6.33}$$

$$\underline{\hat{x}}_{0f}(m,n)=\underline{\hat{x}}_{0p}(m,n)+\underline{k}(m,n)[z_0(m,n)-\bar{u}(m,n)H\underline{\hat{x}}_{0p}(m,n)] \quad (6.34)$$

$$P_f(m,n)=(I-\bar{u}(m,n)\underline{k}(m,n)H)P_p(m,n) \quad (6.35)$$

6.4.1 Simulation Results

The original image in Fig. 6.4(A) is first blurred by a 5*5 Gaussian shape point spread function and is shown Fig. 6.4(B). Then it is degraded by a signal-independent Gaussian multiplicative noise with mean 1 and variance 0.00083. The degraded image is shown in Fig. 6.4(C). The restored image is shown in Fig. 6.4(D). Here the local mean of the original image is estimated by blurring the degraded image with a 5*5 window. The same set of simulation results for $\sigma_u^2=0.007$ are shown in Fig. 6.5.

6.5 Nonstationary 2-D Recursive Restoration of Images with Poisson Noise

For images detected at low light levels, photon noise is a fundamental limitation. The degradation model for an image degraded by blur and photon noise can be written

$$g(m,n)=\text{Poisson}_\lambda\left(\sum_i\sum_j h(i,j)f(m-i,n-j)\right) \quad (6.36)$$

where $\text{Poisson}_\lambda(.)$ is the Poisson random number generator with proportionality factor λ as defined in section 2.4. The augmented state space model of Eq. (6.36) can be expressed as

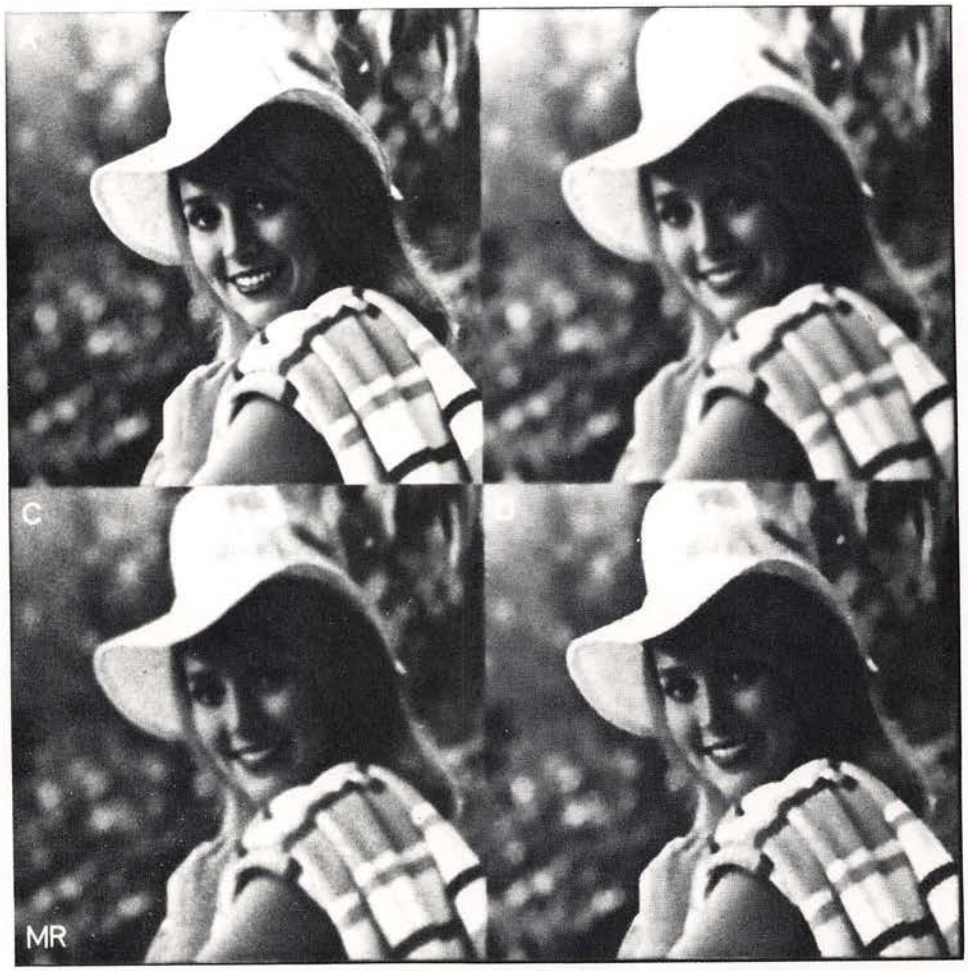

Figure 6.4 Restoration results for images with blur and multiplicative noise

(A) Original image
(B) Original blurred with 5*5 Gaussian PSF
(C) Image (B) degraded by multiplicative noise with σ_u^2=0.00083
(D) Recursive restoration result

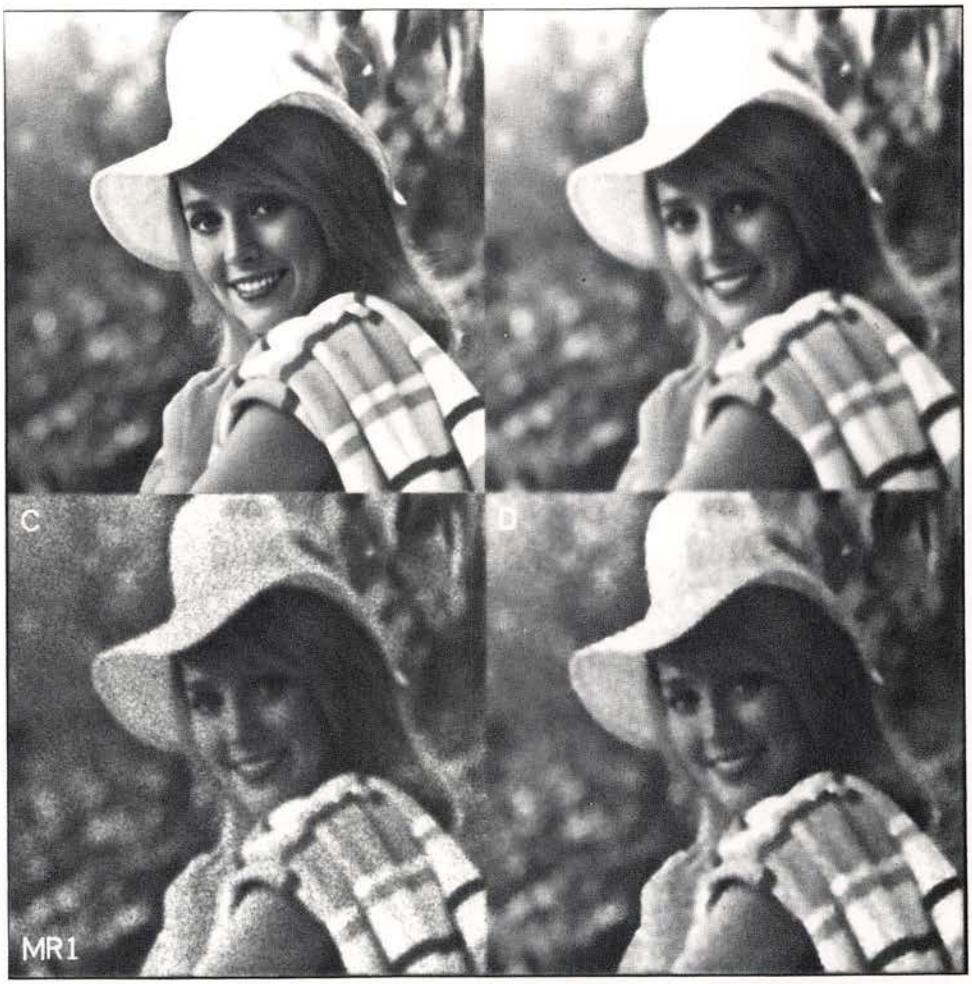

Figure 6.5 Restoration results for images with blur and multiplicative noise

(A) Original image
(B) Original blurred with 5*5 Gaussian PSF
(C) Image (B) degraded by multiplicative noise with $\sigma_u^2=0.007$
(D) Recursive restoration result

$$\underline{x}(m,n+1)=F\underline{x}(m,n)+Gw(m,n) \tag{6.37}$$

$$z(m,n)=\text{Poisson}_{\lambda}(H\underline{x}(m,n)). \tag{6.38}$$

The nonstationary mean of the augmented model can be obtained by taking the expectation of Eqs. (6.37) and (6.38), and we have

$$\bar{\underline{x}}(m,n+1)=F\bar{\underline{x}}(m,n)+G\bar{w}(m,n)$$

$$\bar{z}(m,n)=\lambda H\bar{\underline{x}}(m,n).$$

Subtracting the nonstationary mean from Eqs. (6.37) and (6.38), we have the zero-mean residual model

$$\underline{x}_0(m,n+1)=F\underline{x}_0(m,n)+Gw_0(m,n) \tag{6.39}$$

$$\begin{aligned} z_0(m,n) &= \lambda H\underline{x}_0(m,n)+[\text{Poisson}_{\lambda}(H\underline{x}(m,n))-\lambda H\underline{x}(m,n)] \\ &= \lambda H\underline{x}_0(m,n) + s_{\lambda}(m,n) \end{aligned} \tag{6.40}$$

where $s_{\lambda}(m,n)=\text{Poisson}_{\lambda}(H\underline{x}(m,n))-\lambda H\underline{x}(m,n)$ is the Poisson noise term. Note that

$$E[s_{\lambda}(m,n)\,|\,\underline{x}(m,n)]=0.$$

The prediction step is the same as in the additive noise model. The innovation process is given by

$$\begin{aligned} \tilde{z}_{0p}(m,n) &= z_0(m,n)-\hat{z}_{0p}(m,n) \\ &= z_0(m,n)-E^*[z_0(m,n)\,|\,z_0(1,1),\ldots z_0(m,n-1)] \\ &= z_0(m,n)-\lambda H\hat{\underline{x}}_{0p}(m,n)-E^*[s_{\lambda}(m,n)\,|\,z_0(1,1),\ldots z_0(m,n-1)] \\ &= z_0(m,n)-\lambda H\hat{\underline{x}}_{0p}(m,n) \\ &= \lambda H\tilde{\underline{x}}_{0p}(m,n)+s_{\lambda}(m,n) \end{aligned} \tag{6.41}$$

where $E^*[.|.]$ represents the linear minimum mean square

error estimate based on the observations $z_0(1,1),\ldots,z_0(m,n-1)$, and we use the fact that $s_\lambda(m,n)$ is zero mean. The filtered estimate is given by

$$\underline{\hat{x}}_{0f}(m,n)=\underline{\hat{x}}_{0p}(m,n)+\underline{k}(m,n)\tilde{z}_{0p}(m,n)$$

where $\underline{k}(m,n)=P_{x_0\tilde{z}_{0p}}(m,n)P^{-1}_{\tilde{z}_{0p}\tilde{z}_{0p}}(m,n)$. The crosscovariance matrix is given by

$$\begin{aligned}
P_{x_0\tilde{z}_{0p}}(m,n) &= E[\underline{x}_0(m,n)\tilde{z}_{0p}(m,n)] \\
&= E[(\underline{\hat{x}}_{0p}(m,n)+\underline{\tilde{x}}_{0p}(m,n))(\lambda H\underline{\tilde{x}}_{0p}(m,n)+s_\lambda(m,n))^T] \\
&= \lambda P_p(m,n)H^T
\end{aligned}$$

where we use the orthogonality principle and the fact that

$$E[\underline{x}(m,n)s_\lambda(m,n)] = 0.$$

The variance of the innovation process is given by

$$\begin{aligned}
P_{\tilde{z}_{0p}\tilde{z}_{0p}}(m,n) &= E[\tilde{z}_{0p}(m,n)\tilde{z}_{0p}(m,n)] \\
&= \lambda^2 HP_p(m,n)H^T + \lambda H\bar{\underline{x}}(m,n).
\end{aligned}$$

The filtered covariance matrix is given by

$$\begin{aligned}
P_f(m,n) &= E[\underline{\tilde{x}}_{0f}(m,n)\underline{\tilde{x}}^T_{0f}(m,n)] \\
&= E[(\underline{\tilde{x}}_{0p}(m,n)-\underline{k}(m,n)\tilde{z}_{0p}(m,n))(\underline{\tilde{x}}_{0p}(m,n)-\underline{k}(m,n)\tilde{z}_{0p}(m,n))^T] \\
&= E\{[(I-\lambda\underline{k}(m,n)H)\underline{\tilde{x}}_{0p}(m,n)-\underline{k}(m,n)s_\lambda(m,n)] \\
&\quad [(I-\lambda\underline{k}(m,n)H)\underline{\tilde{x}}_{0p}(m,n)-\underline{k}(m,n)s_\lambda(m,n)]^T\} \\
&= (I-\lambda\underline{k}(m,n)H)P_p(m,n).
\end{aligned}$$

In summary, the Kalman filter equations for Poisson noise are given by

Prediction step:

$$\underline{\hat{x}}_{op}(m,n)=F\underline{\hat{x}}_{of}(m,n-1) \tag{6.42}$$

$$P_p(m,n)=FP_f(m,n-1)F^T + GQ(m,n-1)G^T \tag{6.43}$$

Filtering step:

$$\underline{\hat{x}}_{0f}(m,n)=\underline{\hat{x}}_{0p}(m,n)+\underline{k}(m,n)[z_0(m,n)-\lambda H\underline{\hat{x}}_{0p}(m,n)] \tag{6.44}$$

$$\underline{k}(m,n)= \lambda P_p(m,n)H^T(\lambda^2 HP_p(m,n)H^T+\lambda H\underline{\bar{x}}(m,n))^{-1} \tag{6.45}$$

$$P_p(m,n)=(I-\lambda\underline{k}(m,n)H)P_p(m,n) \tag{6.46}$$

6.5.1 Simulation Results

The original image is shown in Fig. 6.6(A). Figure 6.6(B) is the blurred image with a 5*5 Gaussian shape point spread function. Figure 6.6(C) has both blur and Poisson noise with $\lambda=8$. Note that Fig. 6.6(C) is normalized to have the same intensity level as the original image for display purposes. The restored image is shown in Fig. 6.6(D). Again, the local mean of the original image is estimated by blurring the degraded image with a 5*5 window. The same set of simulation results for $\lambda=1$ are shown in Fig. 6.7.

6.6 Conclusions

A nonstationary 2-D recursive restoration filter is derived based on the NMNV image model and the local minimum mean square error criterion. The filter has a simple, space-invariant structure and the nonstationary information of the image is described by a nonstationary

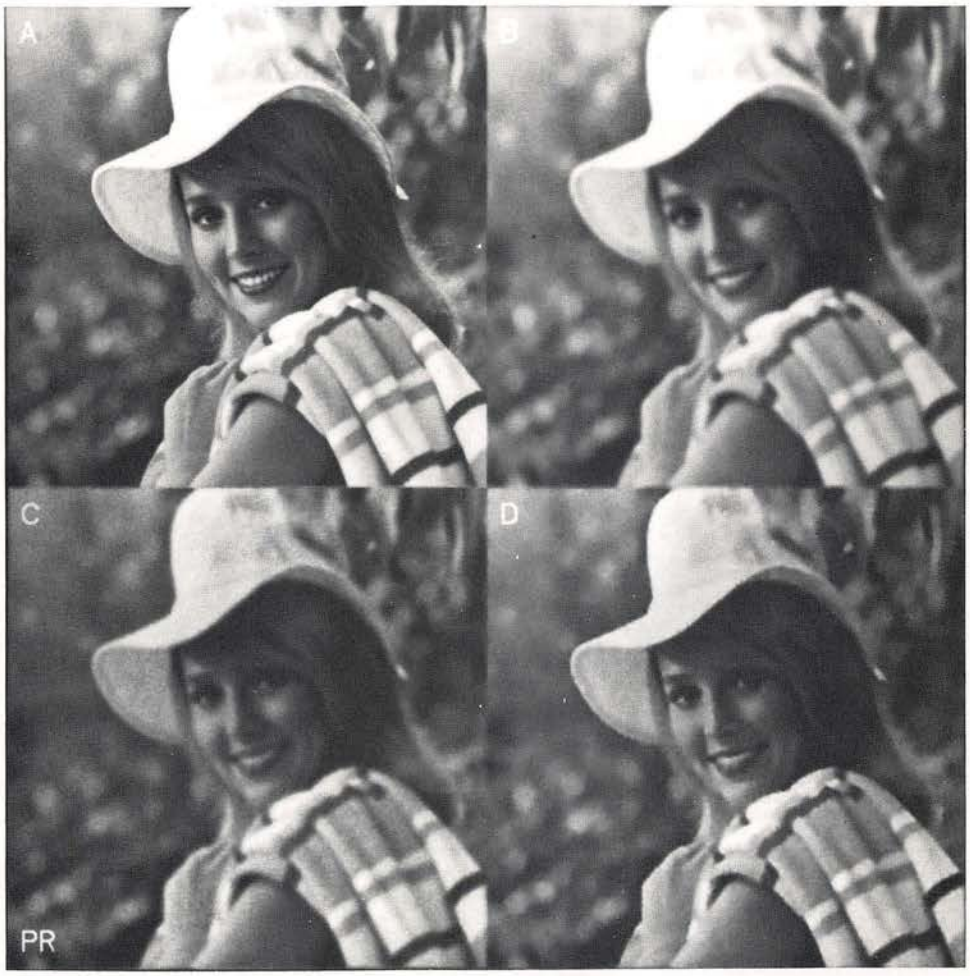

Figure 6.6 Restoration results for images with blur and Poisson noise

(A) Original image
(B) Original blurred with 5*5 Gaussian PSF
(C) Image (B) degraded by Poisson noise with $\lambda=8$
(D) Recursive restoration result

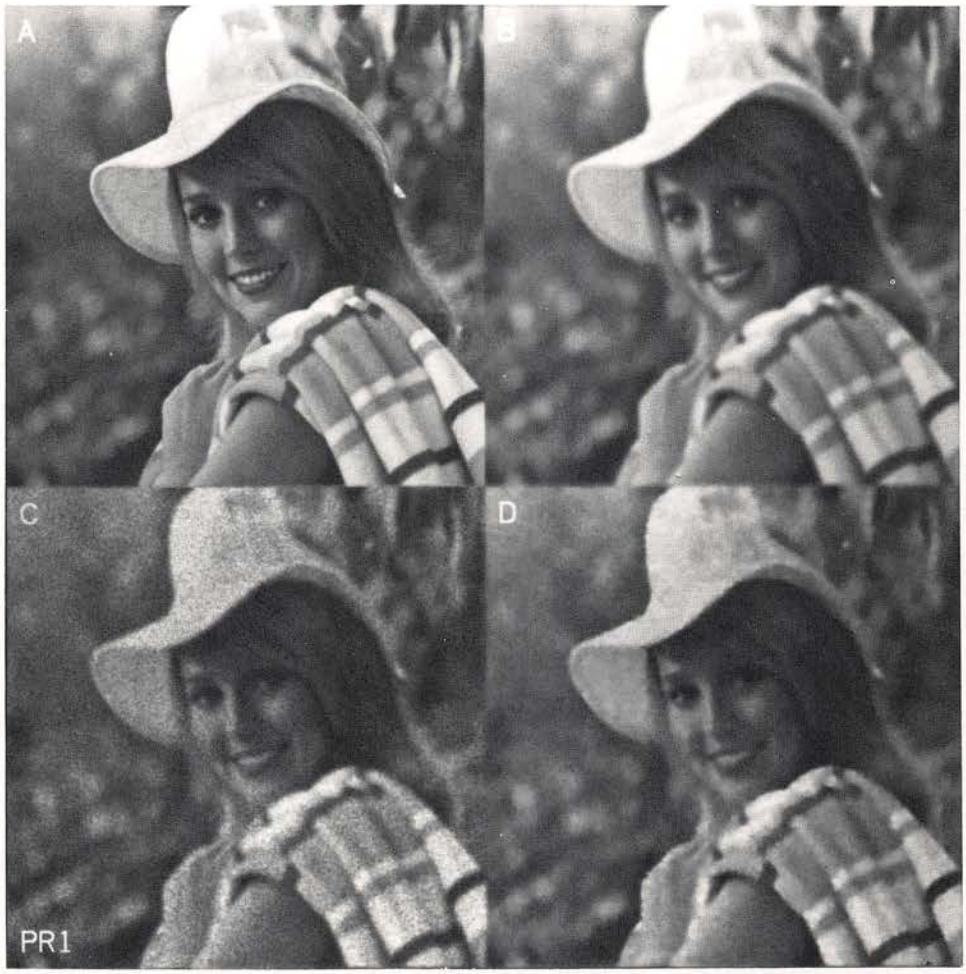

Figure 6.7 Restoration results for images with blur and Poisson noise

(A) Original image
(B) Original blurred with 5*5 Gaussian PSF
(C) Image (B) degraded by Poisson noise with $\lambda=1$
(D) Recursive restoration result

input process rather than a space-variant filter structure. Therefore, it is not necessary to build a space-variant dynamic model for each nonstationary image, and we only need to estimate the local mean and local variance of the nonstationary image. Similar to the adaptive noise smoothing filter, different local statistics estimates result in different filters.

A reduced update technique is used to reduce the computation efforts. With this approximation, the 2-D Kalman filter becomes practical for real-time application. The extension of the nonstationary 2-D recursive filter to signal-dependent noise is discussed and the filter has similar properties as the adaptive noise smoothing filter. The restoration filter produces better results than the conventional Wiener filter.

Chapter 7

SPECKLE REDUCTION TECHNIQUES FOR INTENSITY SPECKLE IMAGES

7.1 Introduction

Speckle occurs in all types of coherent imagery such as synthetic aperture radar (SAR) imagery, acoustic imagery and laser illuminated imagery. The origin of speckle and its statistical properties are now well understood and are discussed in Chapter 3. Unlike multiplicative noise or Poisson noise, speckle noise is not only signal-dependent but also correlated. The signal-to-noise ratio (SNR) of fully developed speckle is equal to one, and the correlation function of speckle noise depends on the coherent point spread function of the imaging system and the original image intensity. The presence of speckle in an image reduces the resolution of the image and the detectability of the target. Various speckle reduction techniques were devised using partially coherent illumination in the imaging system rather than coherent illumination [7-1]. Other methods used to reduce speckle have included observing speckle through a finite aperture, and moving an aperture while observing the time-averaged image. Similar processes were known to the radar community as the mixed integration techniques

[7-2,7-3]. While these methods are effective for speckle reduction, they require the modification of the imaging system and do not consider the image statistics.

In recent years, digital methods for processing SAR data and digitally processed SAR images have become available. Interests in applying digital image enhancement and restoration techniques to speckle reduction are high [7-4,7-5,7-6]. However, these approaches have assumed that speckle noise is multiplicative and used multiplicative noise filtering algorithms to suppress speckle noise. As shown in Chapter 3, the multiplicative model of speckle is based on the first order statistics of speckle and is only a rough approximation. In practice, the second order statistics of speckle are of fundamental importance for speckle reduction and the multiplicative noise filtering algorithms are not optimal for this purpose.

In this chapter, we model the speckle according to the exact physical process of coherent image formation. Thus, the model includes signal-dependent effects and accurately represents the higher order statistical properties of speckle that are important to the restoration procedure. Here, we only consider "fully developed" speckle and assume that only the speckle intensity is recorded and the phase information is lost through the recording process. We first derive an adaptive noise smoothing filter and a maximum a

posteriori (MAP) filter for a limiting situation when the discrete speckle samples can be assumed independent of each other. These filters are similar to the multiplicative noise filtering techniques used by other authors. A local linear minimum mean square error (LLMMSE) filter based on the nonstationary mean, nonstationary variance (NMNV) image model is derived. This filter adapts to the signal-dependent speckle noise and the nonstationary content of the image. More importantly, the correlation properties of speckle are taken into account. A 2-D recursive implementation of the LLMMSE filter is also developed as a fast computation algorithm. Simulation results on computer generated speckle images are presented.

7.2 Previous Approaches to Speckle Reduction

An important property of fully developed speckle is that the ensemble mean of the speckle image is equal to the incoherent image of the original object. This property serves as the basis of frame averaging techniques [7-7], where multiple frames of independent speckle images of the same object are generated and averaged on an intensity basis. This averaging process increases the SNR from 1, as in a single frame case, to $M^{1/2}$ where M is the number of independent speckle images. If M is very large, in theory, we can have a very good estimate of the incoherent image by averaging multiple frames of speckle images. However, cost and other system

limitations usually make it difficult to generate multiple frames of independent speckle images.

In the wavefront reconstruction process of the SAR system, it is possible to introduce frequency or angle diversity such that multiple frames of independent speckle images can be generated. The discrete frequency plane mixed-integration processor [7-3] subdivides the frequency plane into M cells, processes each cell coherently and incoherently sums the outputs. The purpose is to produce multiple frames of independent speckle images and the net effect is to increase SNR at the expense of resolution. The scanning frequency plane mixed-integration processor continuously scans the frequency plane with a subaperture which is 1/M times the size of the signal spectrum. The resulting image is coherently processed and incoherently time-averaged over the period of scanning. The processor is shown to be equivalent to smoothing the speckle intensity image with the incoherent point spread function of the scanning subaperture. While these mixed-integration processors are effective for speckle reduction, they do not consider the image statistics and are essentially space-invariant low-pass filters. The processors are implemented in the frequency domain because it is relatively easy to access the frequency spectrum when the SAR image is optically processed.

In recent years, digitally processed SAR images are

available, and there are tremendous amount of interest in applying digital image enhancement and restoration techniques to speckle reduction. Most authors applying digital image processing techniques to speckle reduction assumed the speckle noise is multiplicative. Arsenault [7-8] used the logarithmic transform to make the multiplicative noise become additive and applied noise smoothing filter in the transform domain. Lim et al. [7-4] and Lee [7-5] applied their multiplicative noise filtering algorithms to speckle images. Frost et al. [7-6] used an adaptive Wiener filter for multiplicative noise to smooth the speckle noise. The multiplicative model of speckle is based on the first order statistics of speckle and is only a rough approximation. In practice, the second order statistics of speckle are of fundamental importance for speckle reduction. Thus, these multiplicative noise filtering algorithms ignored the correlation properties of speckle and are not optimal for speckle reduction.

7.3 Speckle Reduction Techniques - Independent Speckle Samples

Unlike additive noise or Poisson noise, speckle noise is not only signal-dependent but also correlated. This can be observed from the coarseness, texture or the "speckle size" of a speckle image. The "speckle size" or the correlation region of a speckle image is approximately the size of the incoherent point spread

function of the system. If a speckle image has been undersampled such that the sampling interval is greater than the correlation length of the speckle, the covariance information of speckle is lost and the speckle samples are independent. Under this condition, speckle reduction becomes a noise smoothing problem.

In this section, we consider speckle reduction techniques for independent speckle samples. The adaptive noise smoothing filter for speckle reduction is shown to be the same as the multiplicative noise case. A nonlinear MAP filter which considers the negative exponential distribution of speckle intensity is then derived. The MAP estimate is a real root of a cubic equation and can be easily calculated. The extension of these filters to multiple frame case is developed and simulation results are presented.

7.3.1 Adaptive Noise Smoothing Filter

From Eq. (3.30), the first order conditional probability density function of the speckle intensity at point (m,n) is given by

$$P(g(m,n)|f)=$$
$$\begin{cases} (2\sigma^2(m,n))^{-1}\exp(-g(m,n)/2\sigma^2(m,n)) & \text{for } g(m,n)\geq 0 \\ 0 & \text{otherwise} \end{cases} \tag{7.1}$$

where

$$I(m,n)=2\sigma^2(m,n)=\sum_i\sum_j f(i,k)\,h^2(m-i,n-k) \tag{7.2}$$

is the incoherent image of f(m,n). Equation (7.1) can be represented by a multiplicative noise model and we have

$$g(m,n) = u(m,n)I(m,n) \tag{7.3}$$

where u(m,n) is signal-independent and has a normalized negative exponential distribution

$$P(u(m,n)) = \begin{cases} \exp(-u(m,n)) & \text{for } u(m,n) \geq 0 \\ 0 & \text{otherwise.} \end{cases}$$

Therefore, the adaptive noise smoothing filter for speckle reduction is the same as the adaptive noise smoothing filter for multiplicative noise with unit mean and unit variance.

7.3.2 MAP Filter

The adaptive noise smoothing filter only uses the local mean and local variance of speckle, and is the optimal MMSE filter for Gaussian statistics. Since the speckle intensity g(m,n) has a negative exponential distribution that is very different from the Gaussian distribution, it is useful to consider the nonlinear MAP filter for better performance.

If we use the NMNV image model for the incoherent image I(m,n), the joint conditional probability function of g(m,n) for independent speckle samples can be written as

$$P(\underline{g}|\underline{I}) =$$

$$P(g(1,1)|I(1,1))P(g(1,2)|I(1,2))\ldots(g(N,N)|I(N,N)) \quad (7.4)$$

where $\underline{g}$ and $\underline{I}$ are the lexicographic representations of $g(m,n)$ and $I(m,n)$ respectively. The MAP estimate of $\underline{I}$ is obtained by maximizing the *a posteriori* probability density function

$$P(\underline{I}|\underline{g}) = \frac{P(\underline{g}|\underline{I})P(\underline{I})}{P(\underline{g})} \quad (7.5)$$

with respect to $\underline{I}$. Because the logarithm function is a monotonically increasing function, we can take the logarithm on both sides of Eq. (7.5) and then differentiate it with respect to $\underline{I}$. Thus, we have the MAP equation

$$\left.\frac{\partial \ln P(\underline{g}|\underline{I})}{\partial \underline{I}} + \frac{\partial \ln P(\underline{I})}{\partial \underline{I}}\right|_{\underline{I}=\hat{\underline{I}}_{MAP}} = \underline{0} \quad (7.6)$$

where we use the fact that $P(\underline{g})$ is a constant with respect to $\underline{I}$. The first term in Eq. (7.6) is the maximum likelihood (ML) term, and the second term is the *a priori* term of the incoherent image. For the NMNV image model, $P(\underline{I})$ can be written as

$$P(\underline{I})=P(I(1,1))P(I(1,2))\ldots P(I(m,n))\ldots P(I(N,N)) \quad (7.7)$$

and

$$P(I(m,n)) = \frac{1}{\sqrt{2\pi\sigma_I^2(m,n)}} \exp\left[-\frac{(I(m,n)-\bar{I}(m,n))^2}{2\sigma_I^2(m,n)}\right].$$

Here, $\sigma_I^2(m,n)$ and $\bar{I}(m,n)$ are the nonstationary variance and mean of $I(m,n)$. From Eqs. (7.4), (7.6) and (7.7), the MAP equation can be expressed as a set of scalar equations

$$\left.\frac{\partial \ln P(g(m,n)|I(m,n))}{\partial I(m,n)} + \frac{\partial \ln P(I(m,n))}{\partial I(m,n)}\right|_{I(m,n)=\hat{I}_{MAP}(m,n)} = 0 \tag{7.8}$$

The first term of Eq. (7.8) can be written as

$$\frac{\partial \ln P(g(m,n)|I(m,n))}{\partial I(m,n)}$$

$$= -1/I(m,n) + g(m,n)/I^2(m,n). \tag{7.9}$$

Setting Eq. (7.9) to zero, we have the ML estimate

$$-1/I(m,n)+g(m,n)/I^2(m,n) \;|_{I(m,n)=\hat{I}_{ML}(m,n)} = 0$$

or

$$\hat{I}_{ML}(m,n)=g(m,n). \tag{7.10}$$

It is interesting to see that the ML estimate of the incoherent image is the speckle image itself. The second term of Eq. (7.8) can be written as

$$\frac{\partial \ln P(I(m,n))}{\partial I(m,n)}$$

$$= -(I(m,n)-\bar{I}(m,n))/\sigma^2_{I(m,n)}. \tag{7.11}$$

From Eqs. (7.8), (7.9) and (7.11), we have the MAP equation

$$\left.\frac{g(m,n)}{I^2(m,n)} - \frac{1}{I(m,n)} - \frac{(I(m,n)-\bar{I}(m,n))}{\sigma_I^2(m,n)}\right|_{I(m,n)=\hat{I}_{MAP}(m,n)} = 0$$

or

$$-\hat{I}^2_{MAP}(m,n)[\hat{I}_{MAP}(m,n)-\bar{I}(m,n)]+$$
$$\sigma_I^2(m,n)[g(m,n)-\hat{I}_{MAP}(m,n)]=0. \qquad (7.12)$$

It is easy to see from Eq. (7.12) that $\hat{I}_{MAP}(m,n)$ is the real root of a cubic equation whose value is between $\bar{I}(m,n)$ and $g(m,n)$. Because the MAP estimate of the independent speckle samples case depends only on the speckle observation and statistics at one point, we will call it a "one-point" MAP estimate.

7.3.3 MAP Filter for Multiple Frame Speckle

In some applications, we may have several independent speckle images of the same object. Frame averaging technique can be applied to these images to increase the signal-to-noise ratio. It is easy to see that the average of M independent speckle images

$$g^{(a)}(m,n) = \frac{1}{M}\sum_i g^{(i)}(m,n) \qquad (7.13)$$

is the ML estimate of the incoherent image of the object [7-4], where $g^{(i)}(m,n)$ is the ith speckle image frame. This simple averaging technique does not consider the image statistics. It is expected that further speckle reduction could be achieved by using the speckle reduction techniques developed for the single frame case.

The average of M independent negative exponential

random variables has a gamma probability density function and can be written as

$$P(g^{(a)}(m,n)|I(m,n)) =$$

$$\begin{cases} \left(\frac{M}{I(m,n)}\right)^{M} \frac{g^{(a)M-1}(m,n)}{\Gamma(L)} \exp\left[-M \frac{g^{(a)}(m,n)}{I(m,n)}\right] & \text{for } I(m,n)\geq 0 \\ 0 & \text{otherwise} \end{cases}$$

where $\Gamma(.)$ is the gamma function. The conditional mean and variance of $g^{(a)}(m,n)$ are given by

$$E[g^{(a)}(m,n)|I(m,n)] = I(m,n)$$

and

$$Var[g^{(a)}(m,n)|I(m,n)] = I^2(m,n)/M.$$

Therefore, the adaptive noise smoothing filter for the multiple frame averaged speckle image is the same as the adaptive noise smoothing filter for multiplicative noise with unit mean and variance equal to 1/M.

The MAP filter for multiple frames of independent speckle images can be derived by following the standard procedure of formulating the MAP equation as in the single frame case. Our objective is to maximize

$$\frac{P(\underline{g}^{(1)},\underline{g}^{(2)},\ldots\underline{g}^{(i)}|\underline{I})P(\underline{I})}{P(\underline{g}^{(1)},\underline{g}^{(2)},\ldots\underline{g}^{(i)})}$$

with respect to $\underline{I}$. It is easy to see that we have the following MAP equation

$$-\hat{I}_{MAP}(m,n)[\hat{I}_{MAP}(m,n)-\bar{I}(m,n)] + M\sigma_I^2(m,n)[g^{(a)}(m,n)-\hat{I}_{MAP}(m,n)]=0 \quad (7.14)$$

where $g^{(a)}(m,n)$ is defined in Eq. (7.13). This equation is similar to the one-point MAP equation except that the frame number M puts a weight on the difference between $g^{(a)}(m,n)$ and $\hat{I}_{MAP}(m,n)$. When M=1, Eq. (7.14) is the same as the MAP equation for the single frame case.

7.3.4 Simulation Results

In this section, we show some simulation results for different speckle reduction filters for the independent speckle case. The discrete speckle image is generated according to the multiplicative speckle model. The original image of an aerial photograph is shown in Fig. 7.1(A). The speckle image is shown is Fig. 7.1(B). The signal-to-noise ratio of this image is equal to one and the speckle samples are independent. The local mean estimate of Fig. 7.1(B) is calculated by using a 7*7 uniform weight moving average window and is shown in Fig. 7.1(C). In this picture, the noise is smoothed at the expense of resolution and the results are similar to the results of using a low-pass filter. The one-point MAP estimate is obtained by solving the cubic MAP equation where the coefficients of the equation are determined from the local mean and local variance estimates, and the result is shown in Fig. 7.1(D). The MAP estimate has much better resolution and most regions are clearly defined.

Because of the low signal-to-noise ratio of a speckle image, we will not have a good estimate of the local mean and local variance. This fact explains the noisy appearance in Fig. 7.1(D). If we estimate the local mean and local variance from the MAP estimate in Fig. 7.1(D) and use these values as the coefficients of a new MAP equation, the solution is a new MAP estimate shown in Fig. 7.2(D). Comparing this picture with the old MAP estimate as shown in Fig. 7.2(C), we can see that the noise is further smoothed without much loss of image resolution.

The same procedure is carried out by using the adaptive noise smoothing filter. The original image is shown in Fig. 7.3(A). Figure 7.3(B) is the same speckle image as in Fig. 7.1(B). The first iteration adaptive estimate is shown in Fig. 7.3(C). Comparing this picture with Fig. 7.2(C), we note that the MAP estimate seems to put a lot of black dots on the sharp transition region of the image while the adaptive noise smoothing estimate puts white dots. This difference is because the MAP filter considers the negative exponential distribution of speckle intensity and tends to "guess" on the low intensity side if the local variance estimate is large.

The multiple frames case is shown in Fig. 7.4. The average of 4 independent speckle images is shown in Fig. 7.4(B). The signal-to-noise ratio of this picture increases from 1 to 2 due to the averaging process and

this should improve the local statistics estimates. The adaptive noise smoothing estimate is shown in Fig. 7.4(C) and the MAP estimate is shown in Fig. 7.4(D). The improvement of using our speckle reduction techniques after the 4 frames averaging process justifies the usefulness of considering the image statistics in the filtering process.

7.4 Speckle Reduction Techniques - Correlated Speckle Samples

The speckle reduction techniques discussed in the last section assume that the discrete samples of a speckle intensity image are statistically independent and that only the first order statistics of speckle are used for speckle reduction. The correlation properties of speckle are ignored and we only have an estimate of the incoherent image rather than the original object intensity.

In this section, we derive an optimal local minimum mean square error (LLMMSE) estimate of the original image which takes into account the second order statistics of speckle. This approach is different from all the past work on applying digital image processing techniques to reduce speckle noise. The MAP filter for correlated speckle samples should also be valuable for speckle reduction. However, we are not able to obtain the explicit form of the joint probability density function

Figure 7.1 MAP speckle reduction filter for the case of independent speckle samples

(A) Original image
(B) Speckle image - single frame, independent speckle samples
(C) 7*7 local mean of (B)
(D) One-point MAP estimate

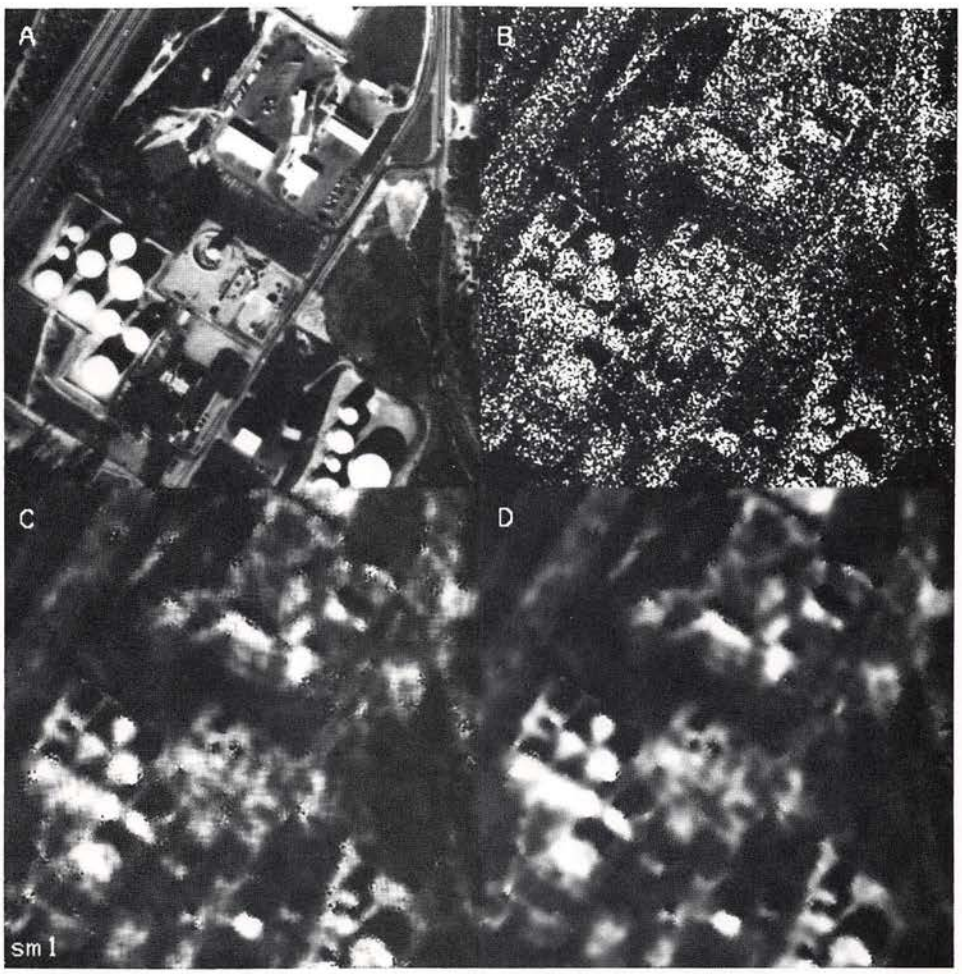

Figure 7.2 MAP speckle reduction filter with improved local statistics

(A) Original image
(B) Speckle image - single frame, independent speckle samples
(C) One-point MAP estimate (first iteration)
(D) One-point MAP estimate with improved local statistics (second iteration)

Figure 7.3 Adaptive noise smoothing filter for the case of independent speckle samples

(A) Original image
(B) Speckle image - single frame, independent speckle samples
(C) Adaptive noise smoothing estimate (first iteration)
(D) Adaptive noise smoothing estimate with improved local statistics (second iteration)

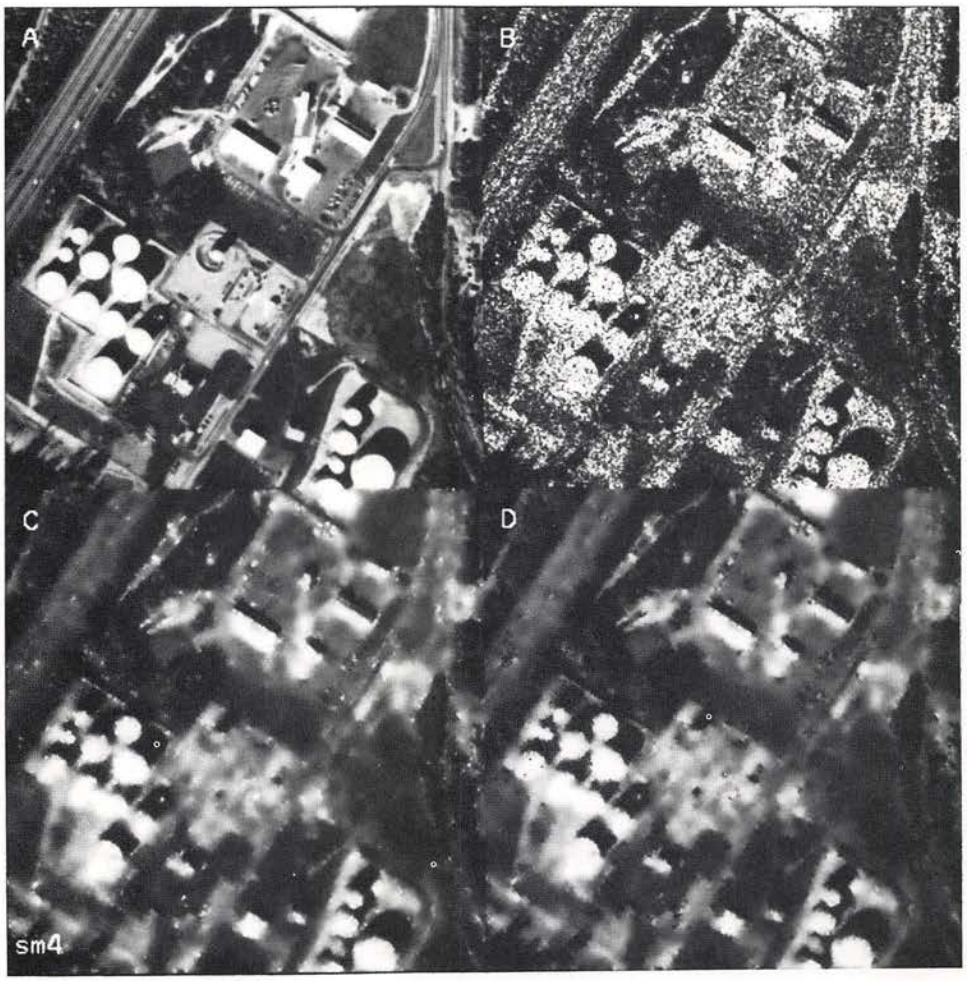

Figure 7.4 Speckle reduction filter for multiple frames, independent speckle samples

(A) Original image
(B) Speckle image - 4 frames average, independent speckle samples
(C) Adaptive noise smoothing estimate
(D) One-point MAP estimate

of speckle intensities. The difficulties in deriving the MAP filter even if we have the required information are explained.

7.4.1 MAP Filter

If a speckle intensity image is adequately sampled such that the covariance structure of speckle is preserved, in principle, this information can be used to further reduce speckle noise. In order to derive the MAP restoration filter for the correlated speckle sample case, we should first have the joint probability density function for speckle intensity.

For "fully developed" speckle, the complex amplitude speckle image $\underline{b}(m,n)$ is assumed to be complex circular Gaussian, and the conditional probability density function of $\underline{b}$ is given by

$$P(\underline{b}|\underline{f}) = (\pi^{N^2}|R_{b(f)}|)^{-1}\exp(-\underline{b}^* R_{b(f)}^{-1}\underline{b}) \qquad (7.15)$$

where $\underline{b}$ is the lexicographic representation of the complex amplitude speckle image $\underline{b}(m,n)$, $\underline{b}^*$ is the complex conjugate and transpose of $\underline{b}$, $R_{b(f)}$ is the conditional autocorrelation matrix of $\underline{b}$, $|R_{b(f)}|$ is the determinant of matrix $R_{b(f)}$, and N is the size of the image. In order to find the joint probability density function of the speckle intensity $\underline{g}$ and phases $\underline{\theta}$, we make the following transformation of variables

$$b_j^{(r)} = g^{1/2}\cos\theta_j$$

$$b_j^{(i)} = g^{1/2}\sin\theta_j \qquad (7.16)$$

for $j=1,2,\ldots,N^2$.

Applying standard techniques for transformation of random variables, we have

$$P(\underline{g},\underline{\theta}|\underline{f}) = P(\underline{b}|\underline{f})|J| \qquad (7.17)$$

where the Jacobian of the transformation $|J|$ is easily found to be 2^{-N^2}. Substituting this into Eq. (7.17), we have

$$P(\underline{g},\underline{\theta}|\underline{f})$$
$$=[(2\pi)^{N^2}|R_{b(f)}|]^{-1}\exp(-\sum_i\sum_j u_{ij}g_i^{1/2}g_j^{1/2}e^{j(\theta_j-\theta_i)}) \qquad (7.18)$$

where u_{ij} is the (i,j)th element of matrix $R_{b(f)}$. To find the joint probability density function of $\underline{g}$ alone, we integrate Eq. (7.18) over $\underline{\theta}$ and obtain

$$P(\underline{g}|\underline{f})=\int\int\cdots\int\int P(\underline{g},\underline{\theta}|\underline{f})\,d\underline{\theta}. \qquad (7.19)$$

In general, there is no explicit analytic form for this density function [7-9] . If we only consider two pixels in the image, we have

$$P(g_1,g_2|\underline{f})=\int\int P(g_1,g_2,\theta_1,\theta_2|\underline{f})\,d\theta_1 d\theta_2$$
$$=(u_{11}u_{22}-u_{12}^2)\exp[-(g_1u_{11}+g_2u_{22})]\ I_0(2\sqrt{g_1g_2}u_{12}) \qquad (7.20)$$

where $I_0(.)$ is the zero order modified Bessel function of the first kind. This is as far as we can go. The two-point MAP filter is very complicated already, let alone the optimal N^2 points MAP filter.

7.4.2 LLMMSE Filter for Speckle Reduction

From Eq. (5.4), the LLMMSE filter for speckle reduction has the form

$$\hat{\underline{f}}_{LLMMSE} = \bar{\underline{f}} + C_{fg} C_g^{-1} (\underline{g} - \bar{\underline{g}}). \tag{7.21}$$

Note that in this formulation, our objective is to estimate the object intensity rather than the incoherent image of the object. From Eq. (3.19), the conditional and unconditional means of $\underline{g}$ can be expressed as

$$E[\underline{g}|\underline{f}] = H_I \underline{f} \text{ and } E[\underline{g}] = H_I \bar{\underline{f}} \tag{7.22}$$

where H_I is the incoherent point spread matrix of the system. The cross-covariance matrix of $\underline{f}$ and $\underline{g}$ is given by

$$\begin{aligned} C_{fg} &= E[(\underline{f}-\bar{\underline{f}})(\underline{g}-\bar{\underline{g}})^T] \\ &= E[(\underline{f}-\bar{\underline{f}})(\underline{g}-H_I\underline{f}+H_I\underline{f}-H_I\bar{\underline{f}})^T] \\ &= E[(\underline{f}-\bar{\underline{f}})(\underline{g}-H_I\underline{f})^T] + E[(\underline{f}-\bar{\underline{f}})(\underline{f}-\bar{\underline{f}})^T H_I^T] \\ &= C_f H_I^T \end{aligned} \tag{7.23}$$

where C_f is the covariance matrix of $\underline{f}$. The covariance matrix of $\underline{g}$ is given by

$$\begin{aligned} C_g &= E[(\underline{g}-\bar{\underline{g}})(\underline{g}-\bar{\underline{g}})^T] \\ &= E[(\underline{g}-H_I\underline{f}+H_I\underline{f}-H_I\bar{\underline{f}})(\underline{g}-H_I\underline{f}+H_I\underline{f}-H_I\bar{\underline{f}})^T] \\ &= E[(\underline{g}-H_I\underline{f})(\underline{g}-H_I\underline{f})^T] + H_I C_f H_I^T. \end{aligned} \tag{7.24}$$

The first part of Eq. (7.24) is the speckle noise term and the second part is the signal term. The (i,j)th element of the first term in Eq. (7.24) is equal to

$E[C_g(m,n;m_1,n_1|f)]$, where (m,n) is the spatial coordinate and $i=(m-1)*N+n$, $j=(m_1-1)*N+n_1$. From Eqs. (3.34) and (3.36), we have

$$
\begin{aligned}
&E[C_g(m,n;m_1,n_1|f)] \\
&= E[\sum_i\sum_k\sum_r\sum_s h(m-i,n-k)h(m_1-i,n_1-k)f(i,k)h(m-r,n-s) \\
&\quad h(m_1-r,n_1-s)f(r,s)] \\
&=\sum_i\sum_k\sum_r\sum_s h(m-i,n-k)h(m_1-i,n_1-k)h(m-r,n-s) \\
&\quad h(m_1-r,n_1-s)E[f(i,k)f(r,s)]. \qquad (7.25)
\end{aligned}
$$

If we assume that the object intensity can be modeled by its nonstationary mean and nonstationary variance, then Eq. (7.25) can be expressed as

$$
\begin{aligned}
&E[C_g(m,n;m_1,n_1|f)] \\
&=\sum_i\sum_k\sum_r\sum_s h(m-i,n-k)h(m_1-i,n_1-k)h(m-r,n-s) \\
&\quad h(m_1-r,n_1-s)[\bar{f}(i,k)\bar{f}(r,s)+\sigma_f^2(i,k)\delta(i-r,k-s)] \\
&=\sum_i\sum_k\sum_r\sum_s h(m-i,n-k)h(m_1-i,n_1-k)h(m-r,n-s) \\
&\quad h(m_1-r,n_1-s)\bar{f}(i,k)\bar{f}(r,s)+ \\
&\quad \sum_i\sum_k h^2(m-i,n-k)h^2(m_1-i,n_1-k)\,\sigma_f^2(i,k) \\
&= |\sum_i\sum_k h(m-i,n-k)h(m_1-i,n_1-k)\bar{f}(i,k)|^2 + \\
&\quad \sum_i\sum_k h^2(m-i,n-k)h^2(m_1-i,n_1-k)\,\sigma_f^2(i,k). \qquad (7.26)
\end{aligned}
$$

From Eqs. (7.25) and (7.26), Eq. (7.24) can be expressed as

$$C_g = [H\bar{F}H^T]^2+H_IC_fH_I^T+H_IC_fH_I^T \qquad (7.27)$$

where the operator $[A]^2$ takes the magnitude square of each element of matrix A, and $\bar{F}$ matrix is defined as

$$\bar{\underline{F}} = \begin{bmatrix} \bar{f}(1,1) & & & 0 \\ & \bar{f}(1,2) & & \\ & & \ddots & \\ 0 & & & \bar{f}(N,N) \end{bmatrix}.$$

Substituting these statistics into Eq. (7.21), we have the LLMMSE speckle reduction filter for the case of correlated speckle.

The LLMMSE speckle reduction filter requires the inverse of C_g which is of dimension N^2 by N^2. For a common image size N=256, this task will take tremendous amount of computation and memory space. Therefore, we have to use sectioning methods to reduce the computation load.

7.4.3 LLMMSE Filter for Multiple Frame Speckle

Assume that we have M independent speckle images of the same object. Let

$$g^{(a)}(m,n) = \frac{1}{M}\sum_i g^{(i)}(m,n) \qquad (7.28)$$

where $g^{(i)}(m,n)$ is the ith frame speckle image. We also assume that each speckle image has the same average intensity level. The LLMMSE filter derived for the single frame case can be easily modified to deal with multiple frames of independent speckle images if the statistics of $g^{(a)}(m,n)$ are available. The covariance matrix of $\underline{g}^{(a)}$ is given by

$$
\begin{aligned}
C_g(a) &= E[(\underline{g}^{(a)}-\bar{\underline{g}}^{(a)})(\underline{g}^{(a)}-\bar{\underline{g}}^{(a)})^T] \\
&= E\{\frac{1}{M^2}[\sum_i(\underline{g}^{(i)}-\bar{\underline{g}}^{(i)})][\sum_i(\underline{g}^{(j)}-\bar{\underline{g}}^{(j)})]^T\} \\
&= \frac{1}{M^2}\sum_i E[(\underline{g}^{(i)}-\bar{\underline{g}}^{(i)})(\underline{g}^{(i)}-\bar{\underline{g}}^{(i)})^T] \\
&\quad + \frac{1}{M^2}\sum_i\sum_{i\neq j} E[(\underline{g}^{(i)}-\bar{\underline{g}}^{(i)})(\underline{g}^{(j)}-\bar{\underline{g}}^{(j)})^T] \\
&= \frac{1}{M}C_g + \frac{(M-1)}{M} H_I C_f H_I^T \\
&= \frac{1}{M}\{[H\bar{F}H^T]^2 + H_I C_f H_I^T\} + H_I C_f H_I^T
\end{aligned} \tag{7.29}
$$

where C_g is the covariance matrix of a single speckle image as shown in Eq. (7.27), and we use the fact that

$$
\begin{aligned}
&E[(\underline{g}^{(i)}-\bar{\underline{g}}^{(i)})(\underline{g}^{(j)}-\bar{\underline{g}}^{(j)})^T] \\
&= E[(\underline{g}^{(i)}-E[\underline{g}^{(i)}|\underline{f}]+E[\underline{g}^{(i)}|\underline{f}]-\bar{\underline{g}}^{(i)}) \\
&\quad (\underline{g}^{(j)}-E[\underline{g}^{(j)}|\underline{f}]+E[\underline{g}^{(j)}|\underline{f}]-\bar{\underline{g}}^{(j)})^T] \\
&= H_I C_f H_I^T.
\end{aligned}
$$

Note that in Eq. (7.29), the signal term is the same as the single frame case, but the speckle noise correlation term is reduced by a factor 1/M. Similarly, the cross-covariance matrix is given by

$$
C_{fg}(a) = C_f H_I^T. \tag{7.30}
$$

Substituting these statistics into Eq. (7.21), we have the LLMMSE filter for multiple frame speckle.

7.4.4 Simulation Results

In this section, we show some simulation results using the LLMMSE speckle reduction filter for correlated speckle samples. The original image is shown in Fig. 7.5(A). The discrete speckle image in Fig. 7.5(B) is generated according to the multiple phase speckle model as discussed in Chapter 3. The coherent point spread function used in the generation process is a 5*5 separable triangular shape window. The correlation properties of this speckle image can be shown by comparing the speckle size in Fig. 7.5(B) and Fig. 7.1(B). We use a 7*7 uniform weight moving average window to calculate the local mean of Fig. 7.5(B) and the result is shown in Fig. 7.5(C). The LLMMSE filter is implemented by using a sectioning method to reduce computation and memory requirements. The restored image is shown in Fig. 7.5(D). In this case, we separate the image into sections of size 12*12, and adjacent sections are overlapped to avoid boundary effects. The image is of size 256*256 and it takes 4 hours CPU time on a DEC KL-10 system. The restored image has better resolution than the low-pass filter results.

The simulation results for multiple frame processing are shown in Fig. 7.6. The average of 4 independent frames of speckle images is shown in Fig. 7.6(B). The local mean is estimated by using a 7*7 window and the result is shown in Fig. 7.6(C). The restored image using

Figure 7.5 LLMMSE speckle reduction filter for the case of correlated speckle samples

(A) Original image
(B) Speckle image - single frame, correlated speckle samples (5 by 5 coherent PSF)
(C) 7*7 local mean of (B)
(D) Restored image

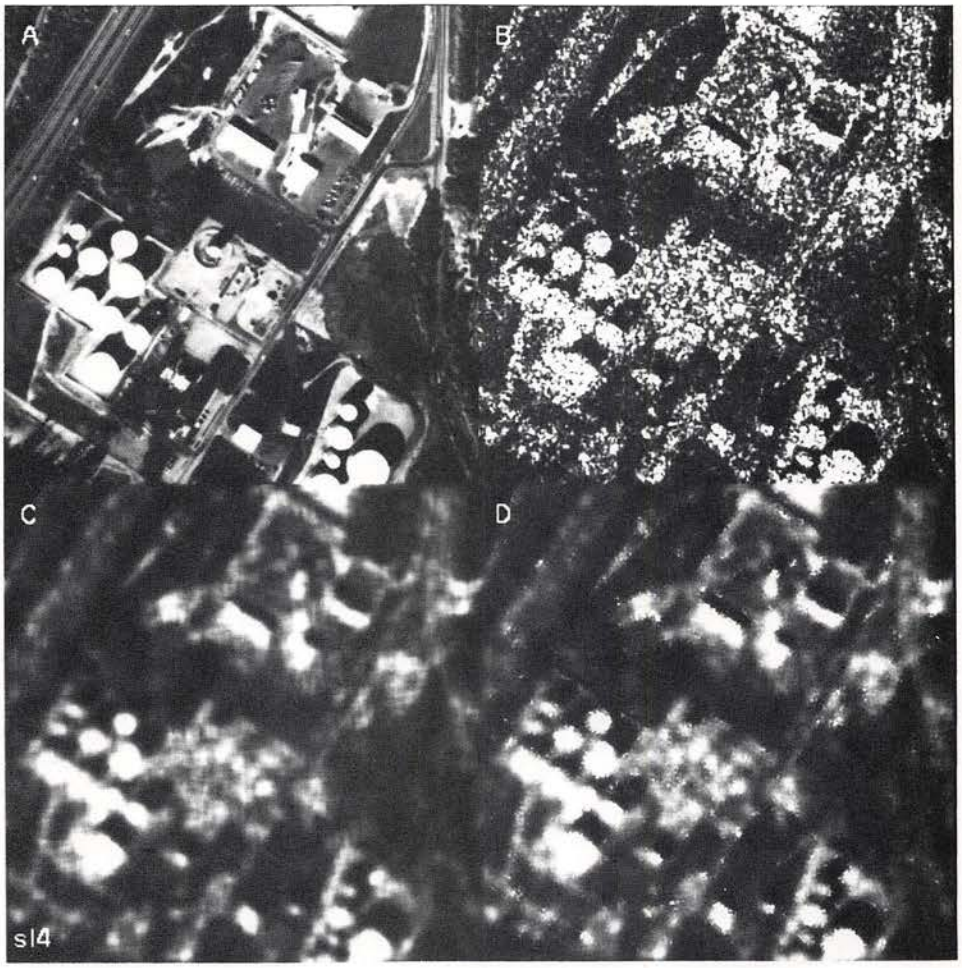

Figure 7.6 LLMMSE speckle reduction filter for multiple frames, correlated speckle samples

(A) Original image
(B) Speckle image - 4 frames average, correlated speckle samples (5 by 5 coherent PSF)
(C) 7*7 local mean of (B)
(D) Restored image

the LLMMSE speckle reduction filter and sectioning methods is shown in Fig. 7.6(D).

7.5 Nonstationary 2-D Recursive Filter for Speckle Reduction

The LLMMSE filter for speckle reduction introduced in the last section is nonrecursive and computationally demanding even if we use a sectioning method. It is valuable to consider a recursive implementation of this filter both for fast computation and local processing.

The nonstationary 2-D recursive filter developed in Chapter 6 is not applicable directly for speckle reduction because speckle noise is correlated. The correlation of speckle depends on the signal statistics and is nonstationary. These factors make the development of a recursive speckle reduction filter difficult.

7.5.1 Derivation

The dynamic model of a speckle image can be represented as

$$\underline{x}(m,n+1) = F\underline{x}(m,n) + Gw(m,n) \tag{7.31}$$

$$z(m,n) = \text{speckle}_H(\underline{x}(m,n)). \tag{7.32}$$

Equation (7.31) is the state equation of the NMNV image model as in Eq. (6.14). The observation equation is described by a speckle generator, $\text{speckle}_H(\underline{x}(m,n))$, which

produces the speckle intensity at point (m,n) from $\underline{x}(m,n)$ with a coherent point spread matrix H according to the discrete speckle generation model discussed in Chapter 3. The ensemble mean of speckle observation z(m,n) is given by

$$\bar{z}(m,n) = E[z(m,n)] = E[\text{speckle}_H(\underline{x}(m,n))]$$
$$= E\{E[\text{speckle}_H(\underline{x}(m,n))|\underline{x}(m,n)]\}$$
$$= E\{H_I\underline{x}(m,n)\} = H_I\bar{\underline{x}}(m,n) \qquad (7.33)$$

where H_I is the incoherent point spread matrix, and we used the fact that the conditional mean of speckle intensity is equal to the incoherent image of the object. If we subtract the nonstationary mean from Eqs. (7.31) and (7.32), we have the zero-mean residual model of speckle

$$\underline{x}_o(m,n+1) = F\underline{x}_o(m,n) + Gw_o(m,n) \qquad (7.34)$$
$$z_o(m,n) = H_I\underline{x}_o(m,n)+[\text{speckle}_H(\underline{x}(m,n))-H_I\underline{x}(m,n)]. \qquad (7.35)$$

If we define the speckle noise term as

$$s(m,n) = \text{speckle}_H(\underline{x}(m,n))-H_I\underline{x}(m,n), \qquad (7.36)$$

then Eq. (7.35) can be written as

$$z_o(m,n) = H_I\underline{x}_o(m,n) + s(m,n). \qquad (7.37)$$

It is easy to see that s(m,n) has a zero mean and the covariance function of s(m,n) is the same as $E[C_g(m,n;m_1,n_1|f)]$. Therefore, from Eq. (7.26), we have

$$
\begin{aligned}
&E[s(m,n)s(m_1,n_1)] \\
&= E[\sum_i\sum_k\sum_p\sum_q h(m-i,n-k)h(m_1-i,n_1-k)h(m-p,n-q) \\
&\quad h(m_1-p,n_1-q)f(i,k)f(p,q)] \\
&= |\sum_i\sum_k h(m-i,n-k)h(m_1-i,n_1-k)\bar{f}(i,k)|^2 + \\
&\quad \sum_i\sum_k h^2(m-i,n-k)h^2(m_1-i,n_1-k)\sigma_f^2(i,k). \qquad (7.38)
\end{aligned}
$$

Note that the speckle noise s(m,n) is signal-dependent and correlated. The correlation of s(m,n) depends on the local statistics of the original image and the coherent point spread function (PSF) of the system. The correlation region of s(m,n) is roughly 4 times the size of the coherent PSF. For example, if the PSF is of size (2p+1)*(2q+1), then the correlation region of speckle is (4p+1)*(4q+1). The cross correlation of $\underline{x}_o(m,n)$ and s(m,n) is given by

$$
\begin{aligned}
&E[\underline{x}_o(m,n)s^T(m,n)] \\
&=E[\underline{x}_o(m,n)(\text{speckle}_H(\underline{x}(m,n))-H_I\underline{x}(m,n))^T] \\
&=E[\underline{x}_o(m,n)(\text{speckle}_H(\underline{x}(m,n)))^T]-E[\underline{x}_o(m,n)\underline{x}^T(m,n)H_I^T] \\
&=E[\underline{x}_o(m,n)\underline{x}^T(m,n)H_I^T]-E[\underline{x}_o(m,n)\underline{x}^T(m,n)H_I^T] \\
&=0. \qquad (7.39)
\end{aligned}
$$

Thus there is no correlation between the speckle noise and the residual state vector $\underline{x}_o(m,n)$, and as a result there is no correlation between the speckle noise and the input process $w_o(m,n)$. These properties reduce the complexity of the recursive filter.

The prediction step of the speckle model is the same as that for the nonstationary 2-D recursive filter for additive noise discussed in Chapter 6 because the state equations are the same. Hence

$$\underline{\hat{x}}_{op}(m,n) = F\underline{\hat{x}}_{of}(m,n-1) \tag{7.40}$$

$$P_p(m,n) = FP_f(m,n-1)F^T + GQ(m,n-1)G^T \tag{7.41}$$

where $\underline{\hat{x}}_{op}(m,n)$ and $\underline{\hat{x}}_{of}(m,n)$ are the predicted and filtered estimates of $\underline{x}_o$, P_p and P_f are the predicted and filtered covariance matrices, and Q is the variance of input w_o. The innovation process is given by

$$\begin{aligned}
\tilde{z}_{op}(m,n) &= z_o(m,n) - \hat{z}_{op}(m,n) \\
&= z_o(m,n) - E^*[H_I\underline{x}_o(m,n) + s(m,n) \mid z_o(1,1), z_o(1,2), \ldots \\
&\quad \ldots, z_o(m,n-1)] \\
&= z_o(m,n) - H_I\underline{\hat{x}}_{op}(m,n) - \hat{s}_p(m,n) \\
&= H_I\underline{\tilde{x}}_{op}(m,n) + \tilde{s}_p(m,n)
\end{aligned} \tag{7.42}$$

where $E^*[.|.]$ represents the linear minimum mean square error estimator rather than the conditional expectation operator, and

$$\begin{aligned}
\hat{s}_p(m,n) &= E^*[s(m,n) \mid z_o(1,1), z_o(1,2), \ldots, z_o(m,n-1)] \\
\tilde{s}_p(m,n) &= s(m,n) - \hat{s}_p(m,n).
\end{aligned} \tag{7.43}$$

Note that due to the correlation property of speckle noise, we need to estimate the noise term s(m,n) at each point in order to estimate the signal $\underline{x}_o(m,n)$. The filtered estimate has the form

$$\underline{\hat{x}}_{of}(m,n)=\underline{\hat{x}}_{op}(m,n)+P_{\underline{x}_o\tilde{z}_{op}}(m,n)P^{-1}_{\tilde{z}_{op}}(m,n)\tilde{z}_{op}(m,n) \quad (7.44)$$

where

$$P_{\underline{x}_o\tilde{z}_{op}}(m,n) = E[\underline{x}_o(m,n)\tilde{z}_{op}(m,n)]$$
$$= E[(\underline{\hat{x}}_{op}(m,n)+\underline{\tilde{x}}_{op}(m,n))(H_I\underline{\tilde{x}}_{op}(m,n)+\tilde{s}_p(m,n))^T]$$
$$= P_p(m,n)H_I^T + E[\underline{\tilde{x}}_{op}(m,n)\tilde{s}_p^T(m,n)] \quad (7.45)$$

and

$$P_{\tilde{z}_{op}}(m,n) = E[\tilde{z}_{op}(m,n)\tilde{z}_{op}(m,n)]$$
$$= E[(H_I\underline{\tilde{x}}_{op}(m,n)+\tilde{s}_p(m,n))(H_I\underline{\tilde{x}}_{op}(m,n)+\tilde{s}_p(m,n))^T]$$
$$= H_IP_p(m,n)H_I^T+P_p^{(s)}(m,n)+2H_IE[\underline{\tilde{x}}_{op}(m,n)\tilde{s}_p^T(m,n)] \quad (7.46)$$

and $P_p^{(s)}(m,n)=E[\tilde{s}_p(m,n)\tilde{s}_p(m,n)]$. Define

$$P_p^{xs}(m,n) = E[\underline{\tilde{x}}_{op}(m,n)\tilde{s}_p(m,n)],$$

now Eq. (7.44) can be expressed as

$$\underline{\hat{x}}_{of}(m,n) = \underline{\hat{x}}_{op}(m,n) + \underline{k}(m,n)\tilde{z}_{op}(m,n) \quad (7.47)$$

and

$$\underline{k}(m,n) = (P_p(m,n)H_I^T + P_p^{xs}(m,n))$$
$$(H_IP_p(m,n)H_I^T+P_p^s(m,n)+2H_IP_p^{xs}(m,n))^{-1}. \quad (7.48)$$

To find the estimate and prediction covariance functions of s(m,n), we need to construct a propagation model for s(m,n). Since s(m,n) has only a finite correlation region and the extent of the coherent point spread function is usually small, we define the model

$$\underline{S}(m,n+1) = F_s\underline{S}(m,n) + G_s s(m+2p,n+2q+1) \qquad (7.49)$$

where

$$\underline{S}(m,n) = [s(m-2p,n-2q), s(m-2p,n-2q+1), \ldots s(m-2p,N);$$
$$s(m-2p+1,1), s(m-2p+1,2), \ldots s(m-2p+1,N); \ldots;$$
$$s(m+2p,1), \ldots s(m+2p,n+2q)],$$

and

$$F_s = \begin{bmatrix} 0 & 1 & 0 & 0 & \ldots\ldots & 0 \\ 0 & 0 & 1 & 0 & \ldots\ldots & 0 \\ \cdot & & & & & \cdot \\ \cdot & & & & & \cdot \\ \cdot & & & & & 0 \\ \cdot & & & & & 1 \\ 0 & 0 & \ldots\ldots\ldots & & & 0 \end{bmatrix} \qquad G_s = \begin{bmatrix} 0 \\ 0 \\ \cdot \\ \cdot \\ \cdot \\ 0 \\ 1 \end{bmatrix}.$$

Note that this model accounts only for the propagation of $s(m,n)$ with the state vector $\underline{x}_o(m,n)$ and does not describe the correlation structure of $\underline{S}(m,n)$. The function of this model is to form a 2-D recursive structure and stack all the speckle noise components which are correlated with $z_o(m,n)$. The relationship between $\underline{x}(m,n)$ and $\underline{S}(m,n)$ is illustrated in Fig. 7.7.

Let $\hat{\underline{S}}_f(m,n)$ be the filtered estimate of $\underline{S}(m,n)$. From Eq. (7.49), the prediction estimate of $\underline{S}(m,n)$ is given by

$$\hat{\underline{S}}_p(m,n) = F_s\hat{\underline{S}}_f(m,n-1) \qquad (7.50)$$

and

$$P_p^S(m,n) = F_s P_f^S(m,n-1)F_s^T + G_s Q_s(m,n-1)G_s^T \qquad (7.51)$$

Figure 7.7 State space model of speckle noise reduction

where $Q_s(m,n)=E[s^2(m+2p,n+2q+1)]$. The filtered estimate of $\underline{S}(m,n)$ can be expressed as

$$\hat{\underline{S}}_f(m,n)=\hat{\underline{S}}_p(m,n)+P_{S\tilde{z}_{op}}(m,n)P_{\tilde{z}_{op}}^{-1}\tilde{z}_{op}(m,n). \tag{7.52}$$

The crosscovariance matrix is equal to

$$\begin{aligned}
P_{S\tilde{z}_{op}}(m,n) &= E[\underline{S}(m,n)\tilde{z}_{op}(m,n)] \\
&= E[\underline{S}(m,n)\tilde{\underline{x}}_{op}^T(m,n)H_I^T]+E[\underline{S}(m,n)\tilde{s}_p(m,n)] \\
&= E[(\hat{\underline{S}}_p(m,n)+\tilde{\underline{S}}_p(m,n))\tilde{\underline{x}}_{op}^T(m,n)H_I^T]+ \\
&\quad E[(\hat{\underline{S}}_p(m,n)+\tilde{\underline{S}}_p(m,n))\tilde{s}_p(m,n)] \\
&= P_p^{Sx}(m,n)H_I^T + P_p^{Ss}(m,n)
\end{aligned} \tag{7.53}$$

where we used the orthogonality principle. Therefore, from Eqs. (7.52) and (7.46), we have

$$\hat{\underline{S}}_f(m,n) = \hat{\underline{S}}_p(m,n) + \underline{k}^S(m,n)\tilde{z}_{op}(m,n) \tag{7.54}$$

where

$$\underline{k}^S(m,n)=(P_p^{Sx}(m,n)H_I^T+P_p^{Ss}(m,n))$$
$$(H_IP_p(m,n)H_I^T+P_p^{(s)}(m,n)+2H_IE[\tilde{\underline{x}}_{op}(m,n)\tilde{s}_p(m,n)])^{-1}. \tag{7.55}$$

The prediction crosscovariance matrix of $\underline{x}$ and $\underline{S}$ is given by

$$\begin{aligned}
P_p^{Sx}(m,n) &= E[\tilde{\underline{S}}_p(m,n)\tilde{\underline{x}}_{op}^T(m,n)] \\
&= E[(\underline{S}(m,n)-F_s\hat{\underline{S}}_f(m,n))(\underline{x}_o(m,n)-F\hat{\underline{x}}_{of}(m,n-1))^T] \\
&= F_sP_f^{Sx}(m,n-1)F_s^T.
\end{aligned} \tag{7.56}$$

Now, we calculate the filtered covariance matrices in order to complete the filter equations. We have

$$
\begin{aligned}
P_f(m,n) &= E[\underline{\tilde{x}}_{of}(m,n)\underline{\tilde{x}}_{of}^T(m,n)] \\
&= E[(\underline{\tilde{x}}_{op}(m,n)-\underline{k}(m,n)\tilde{z}_{op}(m,n)) \\
&\quad (\underline{\tilde{x}}_{op}(m,n)-\underline{k}(m,n)\tilde{z}_{op}(m,n))^T] \\
&= E\{[(I-\underline{k}(m,n)H_I)\underline{\tilde{x}}_{op}(m,n)-\underline{k}(m,n)\tilde{s}_p(m,n)] \\
&\quad [(I-\underline{k}(m,n)H_I)\underline{\tilde{x}}_{op}(m,n)-\underline{k}(m,n)\tilde{s}_p(m,n)]^T\}.
\end{aligned}
$$

It is straightforward to expand this equation and express it in terms of suitable prediction covariance matrices and $\underline{k}(m,n)$. After combining related terms and applying Eq. (7.48), we have the equation

$$
\begin{aligned}
&P_f(m,n) \\
&= (I-\underline{k}(m,n)H_I)P_p(m,n)-\underline{k}(m,n)P_p^{sx}(m,n) \\
&= P_p(m,n)-[P_p(m,n)H_I^T+P_p^{xs}(m,n)]\underline{k}^T(m,n). \qquad (7.57)
\end{aligned}
$$

Similarly, we can show that

$$
\begin{aligned}
&P_f^S(m,n) \\
&= P_p^S(m,n)-[P_p^{Ss}(m,n)+P_p^{Sx}(m,n)H_I^T]\underline{k}^{S^T}(m,n) \qquad (7.58)
\end{aligned}
$$

and

$$
\begin{aligned}
&P_f^{Sx}(m,n) \\
&= P_p^{Sx}(m,n)-[P_p^{Ss}(m,n)+P_p^{Sx}(m,n)H_I^T]\underline{k}^T(m,n). \qquad (7.59)
\end{aligned}
$$

Thus, we derived the nonstationary 2-D recursive filter for speckle reduction. The prediction and filtering steps are summarized in the following equations:

Prediction step:

$$\hat{\underline{x}}_{op}(m,n)=F\hat{\underline{x}}_{of}(m,n-1) \tag{7.60}$$

$$P_p(m,n)=FP_f(m,n-1)F^T+GQ(m,n-1)G^T \tag{7.61}$$

$$\hat{\underline{S}}_p(m,n)=F_s\hat{\underline{S}}_f(m,n-1) \tag{7.62}$$

$$P_p^S(m,n)=F_sP_f^S(m,n-1)F_s^T+G_sQ_s(m,n-1)G_s^T \tag{7.63}$$

$$P_p^{Sx}(m,n)=F_sP_f^{Sx}(m,n-1)F_s^T \tag{7.64}$$

Filtering step:

$$\tilde{z}_{op}(m,n)=z_o(m,n)-H_I\hat{\underline{x}}_{op}(m,n)-\hat{s}_p(m,n) \tag{7.65}$$

$$\hat{\underline{x}}_{of}(m,n)=\hat{\underline{x}}_{op}(m,n)+\underline{k}(m,n)\tilde{z}_{op}(m,n) \tag{7.66}$$

$$\hat{\underline{S}}_f(m,n)=\hat{\underline{S}}_p(m,n)+\underline{k}^S(m,n)\tilde{z}_{op}(m,n) \tag{7.67}$$

$$\underline{k}(m,n)=(P_p(m,n)H_I^T+P_p^{xs}(m,n))$$
$$(H_IP_p(m,n)H_I^T+P_p^s(m,n)+2H_IP_p^{xs}(m,n))^{-1} \tag{7.68}$$

$$\underline{k}^S(m,n)=(P_p^{Sx}(m,n)H_I^T+P_p^{Ss}(m,n))$$
$$(H_IP_p(m,n)H_I^T+P_p^{(s)}(m,n)+2H_IE[\tilde{\underline{x}}_{op}(m,n)\tilde{s}_p(m,n)])^{-1} \tag{7.69}$$

$$P_p(m,n)=P_p(m,n)-[P_p(m,n)H_I^T+P_p^{xs}(m,n)]\underline{k}^T(m,n) \tag{7.70}$$

$$P_f^S(m,n)=P_p^S(m,n)-[P_p^{Ss}(m,n)+P_p^{Sx}(m,n)H_I^T]\underline{k}^{S^T}(m,n) \tag{7.71}$$

$$P_f^{Sx}(m,n)=P_p^{Sx}(m,n)-[P_p^{Ss}(m,n)+P_p^{Sx}(m,n)H_I^T]\underline{k}^T(m,n). \tag{7.72}$$

7.5.2 Computational Aspects

The dimension of the state vector $\underline{x}_o(m,n)$ is $(2p*N+2q+1)$ where $2p+1$ and $2q+1$ are the widths of the coherent point spread function in the vertical and horizontal direction respectively, and N is the image size. The speckle state vector $\underline{S}(m,n)$ is larger than the signal state vector and has dimension $(4p*N+4q+1)$. Due to the large dimension of the state vectors, the amount

of computation and memory requirements make the optimal Kalman filter computationally unattractive. A reduced update suboptimal approach similar to the one discussed in Chapter 6 is used here.

The computation for the prediction step of the reduced update filter is straightforward and does not require any calculation if we use indirect addressing techniques. The inputs to the recursive speckle reduction filter are the local variances of the original image and the speckle noise. In the filtering step, we use the reduced update constraint and the gain vectors $\underline{k}(m,n)$, $\underline{k}^S(m,n)$ are set to zero outside the update region. This approximation reduces the computation dramatically and we only need to calculate $(2p+1)*(2q+1)$ elements of $\underline{k}(m,n)$ and $(4p+1)*(4q+1)$ elements of $\underline{k}^S(m,n)$. The same reduced update principle applies to the filtered covariance matrices $P_f(m,n)$, $P_f^S(m,n)$ and $P_f^{Sx}(m,n)$. Thus, the total computation for the nonstationary recursive speckle reduction filter is on the order of $O(N^2)$ and the computation at each point is proportional to $[(2p+1)*(2q+1)]^2+[(4p+1)*(4q+1)]^2$.

7.5.3 Simulation Results

The results of using recursive speckle reduction filter for correlated speckle intensity images are shown in Fig. 7.8. The original oil tank image in Fig. 7.8(A) has size 64*64. The correlated speckle intensity image

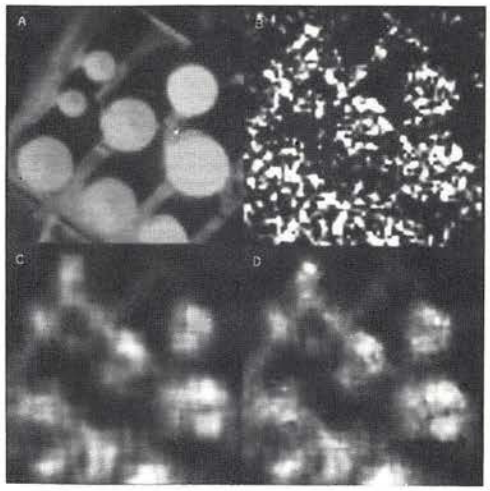

Figure 7.8 Nonstationary 2-D recursive speckle filter for correlated speckle samples

(A) Original oil tank image (portion of Fig. 7.1(A))
(B) Speckle image - single frame, correlated speckle samples (5 by 5 coherent PSF)
(C) 7*7 local mean of (B)
(D) Recursive restoration result

with a 3*3 coherent point spread function is shown in Fig. 7.8(B). Figure 7.8(C) is the local mean estimate calculated from Fig. 7.8(B) by using a 7*7 uniform weight moving average window. The restored image by using the nonstationary 2-D recursive speckle reduction filter is shown in Fig. 7.8(D).

7.6 Conclusions

In this Chapter, we developed several speckle reduction filters for intensity speckle images where only the speckle intensity is recorded and the phase information is lost in the recording process. For the case of independent speckle samples, speckle reduction becomes a noise smoothing problem and speckle can be modeled by a multiplicative noise with exponential distribution. The one-point MAP filter and adaptive noise smoothing filter that use both the image statistics and the first order statistics of speckle are shown to be effective for speckle reduction.

The second order statistics of speckle are of fundamental importance for speckle reduction. The LLMMSE filter developed here takes into account both the image statistics and the correlation of speckle which have been previously ignored. Because this filter requires extensive computation, a reduced update recursive filter is derived as a fast computation algorithm. These methods can be extended directly to process multiple frames of speckle intensity images.

Chapter 8

MAP SPECKLE REDUCTION FILTER FOR COMPLEX AMPLITUDE SPECKLE IMAGES

8.1 Introduction

In Chapter 7, we discussed various speckle reduction techniques for intensity speckle images where only the speckle intensity is recorded and the phase information is lost through the recording process. The loss of phase information is inevitable for synthetic aperture radar (SAR) images that are processed with a coherent optical system. The MAP speckle reduction filter for the correlated speckle samples in this case was shown to be analytically difficult to derive and implement.

In a digitally processed SAR image, both the amplitude and phase of the speckle image are preserved. Traditionally, only the intensity of the complex amplitude image was used for speckle reduction and the phase information was ignored. Here, we will show that with the extra phase information in the complex amplitude speckle image, the optimal nonlinear MAP filter can be derived easily compared with the intensity speckle case.

In this chapter, we discuss speckle reduction techniques for complex amplitude speckle images where both the amplitude and phase are preserved. We first derive the maximum likelihood (ML) estimate of the object intensity for complex amplitude speckle images. The ML equations are nonlinear and can only be solved by iterative algorithms. In each iteration, we have to invert a N^2 by N^2 matrix where N is the size of the image. The procedure is computationally demanding and convergence is not guaranteed. The MAP estimate is a balance between the ML estimate and the *a priori* mean. The MAP filter has the same computation problem as in the ML filter. Instead of trying to solve the nonlinear MAP equation directly, we represent the MAP equation in terms of the filtered estimate and filtered covariance matrix of the LLMMSE filter described in Chapter 6. The resulting MAP equation is a cubic equation and has the same form as the one-point MAP equation discussed in section 7.3.2. Thus, the MAP equation can be easily solved iteratively by using a nonstationary 2-D recursive filter as a fast computation algorithm and imposing a one-point MAP constraint (solution of a cubic equation) to optimize the estimate at each iteration. Simulation results are presented in the final section.

8.2 ML Estimate for Complex Amplitude Speckle Images

In this section, we derive a ML estimate of the original object intensity based on complex amplitude speckle observations. The complex amplitude speckle formation/reduction model is shown in Fig. 8.1. The complex amplitude speckle image $\underline{b}(m,n)$ can be expressed as

$$\underline{b}(m,n) = \sum_i \sum_k h(m-i,n-k) f^{1/2}(i,k) \underline{a}(i,k) + \underline{v}(m,n). \quad (8.1)$$

In this model, the random phasor $\underline{a}(i,k)$ is introduced by the roughness of the object surface. For the "single phase" speckle model discussed in Chapter 3, $\underline{a}(i,k)=\exp(i\phi(i,k))$, and for the "multiple phase" speckle model, $\underline{a}(i,k)$ is a complex circular Gaussian random process with zero mean and unit variance. Note that the complex amplitude noise process $\underline{v}(m,n)$ is included in the model and it may come from either the receiver or the processing procedure in a SAR system. Rewriting Eq. (8.1) using a lexicographic representation, we have

$$\underline{b} = H\underline{f}_a^{1/2} + \underline{v} \quad (8.2)$$

where H is the coherent point spread matrix and $\underline{f}_a^{1/2}$ is the lexicographic representation of the signal $f^{1/2}(i,k)\underline{a}(i,k)$. The conditional covariance matrix of $\underline{b}$ given $\underline{f}$ is denoted by $C_{b(f)}$ and has the form

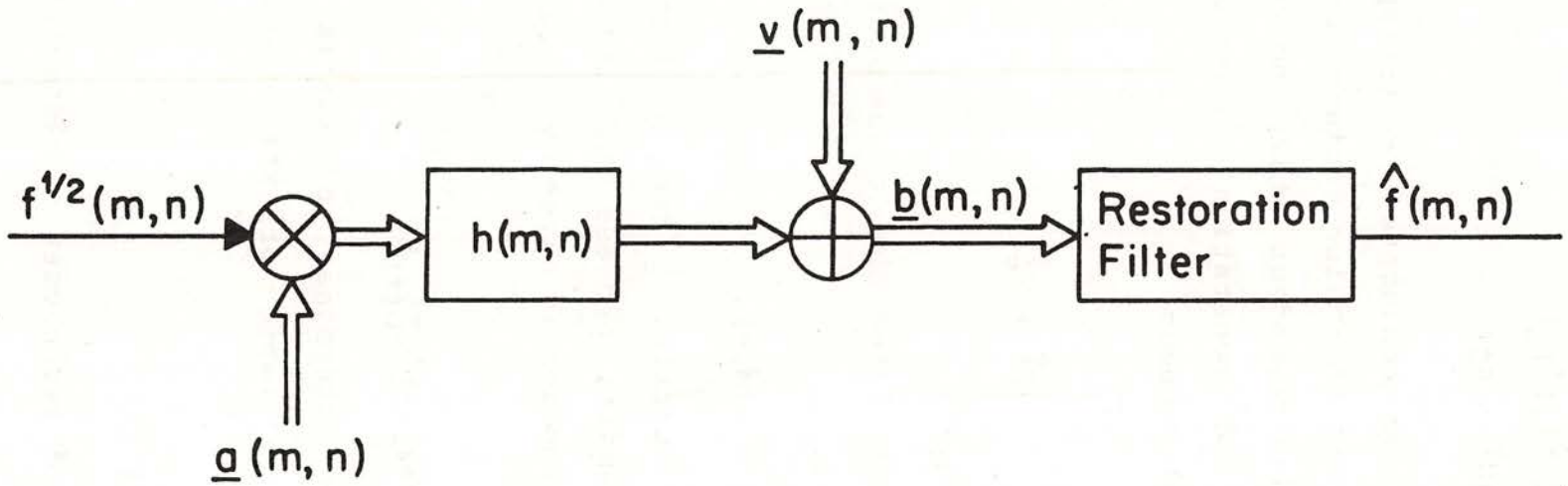

Figure 8.1 Complex amplitude speckle formation/restoration model

$$C_{b(f)} = E[\underline{b}\underline{b}^* | \underline{f}]$$
$$= E[(H\underline{f}_a^{1/2} + \underline{v})(H\underline{f}_a^{1/2} + \underline{v})^* | \underline{f}]$$
$$= HE[\underline{f}_a^{1/2}\underline{f}_a^{1/2*} | \underline{f}]H^T + \sigma_v^2 I \qquad (8.3)$$

where $\underline{b}^*$ is the complex conjugate and transpose of the complex vector $\underline{b}$, σ_v^2 is the noise variance and we assume that $\underline{v}$ is a signal-independent white noise. For the nonstationary mean and nonstationary variance (NMNV) image model, Eq. (8.3) becomes

$$C_{b(f)} = H \begin{bmatrix} f(1,1) & & 0 \\ & f(1,2) & \\ & \ddots & \\ 0 & & \ddots \\ & & f(N,N) \end{bmatrix} H^T + \sigma_v^2 I \qquad (8.4)$$

where we use the uncorrelated phasor assumption of fully developed speckle, i.e.,

$$E[\underline{a}(m,n)\underline{a}^*(m_1,n_1)] = \delta(m,n).$$

For fully developed speckle, $\underline{b}$ can be described by a complex circular Gaussian process and its conditional probability density function is given by

$$P(\underline{b}|\underline{f})$$
$$= (\pi^{N^2}|C_{b(f)}|)^{-1}\exp(-\underline{b}^* C_{b(f)}^{-1}\underline{b}) \qquad (8.5)$$

where $|C_{b(f)}|$ is the determinant of matrix $C_{b(f)}$. By definition, the ML estimate of the original object intensity $\hat{\underline{f}}_{ML}$ is

$$P(\underline{b}|\hat{\underline{f}}_{ML}) = \underset{\underline{f}}{\text{Max}}\ P(\underline{b}|\underline{f}). \qquad (8.6)$$

Following the standard techniques of formulating the ML

estimate, we take the logarithm on both sides of Eq. (8.5), differentiate it with respect to $\underline{f}$, and set it equal to zero, giving

$$\left.\frac{\partial \ln P(\underline{b}|\underline{f})}{\partial \underline{f}}\right|_{\underline{f}=\hat{\underline{f}}_{ML}} = -\left.\frac{\partial \ln|C_{b(f)}|}{\partial \underline{f}}\right|_{\underline{f}=\hat{\underline{f}}_{ML}} - \left.\frac{\partial}{\partial \underline{f}}(\underline{b}^* C_{b(f)}^{-1}\underline{b})\right|_{\underline{f}=\hat{\underline{f}}_{ML}} = \underline{0} \quad (8.7)$$

or in scalar equation form

$$-\frac{\partial \ln|C_{b(f)}|}{\partial f_i} - \frac{\partial}{\partial f_i}(\underline{b}^* C_{b(f)}^{-1}\underline{b})\Big|_{\underline{f}=\hat{\underline{f}}_{ML}} = 0 \quad (8.8)$$

for $i=1,2,3,\ldots,N^2$

From Theorem 2 of Appendix A, the first term in Eq. (8.8) can be written

$$\frac{\partial \ln|C_{b(f)}|}{\partial f_i} = \frac{1}{|C_{b(f)}|}\frac{\partial}{\partial f_i}|C_{b(f)}| = \mathrm{Tr}\left[C_{b(f)}^{-1}\frac{\partial C_{b(f)}}{\partial f_i}\right] \quad (8.9)$$

where Tr[.] is the trace operator. The second term of Eq. (8.8) can be expressed as

$$\frac{\partial(\underline{b}^* C_{b(f)}^{-1}\underline{b})}{\partial f_i} = \underline{b}^*\frac{\partial C_{b(f)}^{-1}}{\partial f_i}\underline{b} = -\underline{b}^* C_{b(f)}^{-1}\frac{\partial C_{b(f)}}{\partial f_i}C_{b(f)}^{-1}\underline{b} \quad (8.10)$$

according to Theorem 3 of Appendix A. Therefore, Eq. (8.8) can now be written as

$$-\mathrm{Tr}\left[C_{b(f)}^{-1}\frac{\partial C_{b(f)}}{\partial f_i}\right] + \underline{b}^* C_{b(f)}^{-1}\frac{\partial C_{b(f)}}{\partial f_i}C_{b(f)}^{-1}\underline{b}\Big|_{\underline{f}=\hat{\underline{f}}_{ML}} = 0 \quad (8.11)$$

for $i=1,2,3,\ldots,N^2$.

The differential of $C_{b(f)}$ can be calculated from Eq. (8.4) and is given by

$$\frac{\partial C_{b(f)}}{\partial f_i} = \frac{\partial}{\partial f_i}\left(H\begin{bmatrix} f(1,1) & & & \\ & f(1,2) & & 0 \\ & & \ddots & \\ & 0 & & f(N,N) \end{bmatrix} H^T + \sigma_v^2 I\right)$$

$$= H \begin{matrix} \\ \\ i \\ \\ \\ \end{matrix} \overbrace{\begin{bmatrix} 0 & \cdots & 0 & \cdots & 0 \\ \vdots & 0 & \vdots & & \vdots \\ 0 & \cdots & 1 & & \vdots \\ \vdots & & & \ddots & \vdots \\ 0 & \cdots & \cdots & & 0 \end{bmatrix}}^{i} H^T = \begin{bmatrix} 0 & \cdots & h_{1i} & \cdots & 0 \\ \vdots & & \vdots & & \vdots \\ \cdots & & h_{2i} & \cdots & \vdots \\ \vdots & & \vdots & & \vdots \\ 0 & \cdots & h_{N^2 i} & \cdots & 0 \end{bmatrix} H^T$$

$$= \begin{bmatrix} h_{1i}h_{1i}, & h_{1i}h_{2i}, & \cdots & h_{1i}h_{N^2 i} \\ h_{2i}h_{1i}, & h_{2i}h_{2i}, & \cdots & h_{2i}h_{N^2 i} \\ \vdots & \vdots & & \vdots \\ h_{N^2 i}h_{1i}, & h_{N^2 i}h_{2i}, & \cdots & h_{N^2 i}h_{N^2 i} \end{bmatrix}$$

$$= \underline{h}_i \underline{h}_i^T \qquad (8.12)$$

where $\underline{h}_i$ is the ith column of the coherent point spread matrix H. Substituting Eq. (8.12) into Eq. (8.11), we get the ML equations

$$-\mathrm{Tr}[C_{b(f)}^{-1}\underline{h}_i\underline{h}_i^T] + \underline{b}^* C_{b(f)}^{-1}\underline{h}_i\underline{h}_i^T C_{b(f)}^{-1}\underline{b}\,|_{\underline{f}=\hat{\underline{f}}_{ML}} = 0 \qquad (8.13)$$

for $i=1,2,3,\ldots,N^2$.

From Theorem 1 in Appendix A and the fact that $C_{b(f)}$ is a symmetric matrix, we have

$$\mathrm{Tr}[C_{b(f)}^{-1}\underline{h}_i\underline{h}_i^T] = \mathrm{Tr}[\underline{h}_i^T C_{b(f)}^{-1}\underline{h}_i]$$

$$= \underline{h}_i^T C_{b(f)}^{-1}\underline{h}_i .$$

The second term of Eq. (8.13) can be written as

$$\underline{b}^* C_{b(f)}^{-1} \underline{h}_i \underline{h}_i^T C_{b(f)}^{-1} \underline{b} = |\underline{b}^* C_{b(f)}^{-1} \underline{h}_i|^2$$
$$= \underline{h}_i^T C_{b(f)}^{-1} \underline{b}\underline{b}^* C_{b(f)}^{-1} \underline{h}_i .$$

From these equations, the ML equations in Eq. (8.13) can now be expressed as

$$-\underline{h}_i^T C_{b(f)}^{-1} \underline{h}_i + \underline{h}_i^T C_{b(f)}^{-1} \underline{b}\underline{b}^* C_{b(f)}^{-1} \underline{h}_i \Big|_{\underline{f}=\hat{\underline{f}}_{ML}} = 0 \qquad (8.14)$$

for $i=1,2,3,\ldots,N^2$.

8.3 MAP Speckle Reduction Filter for Complex Amplitude Speckle Images

In the ML estimation, we ignore the *a priori* information of the original image. This factor is considered in the MAP estimate

$$P(\hat{\underline{f}}_{MAP}|\underline{b}) = \max_{\underline{f}} P(\underline{f}|\underline{b}) . \qquad (8.15)$$

From the Bayes' law, we have

$$P(\underline{f}|\underline{b}) = \frac{P(\underline{b}|\underline{f})P(\underline{f})}{P(\underline{b})} \qquad (8.16)$$

If we use the NMNV image model, $P(\underline{f})$ can be written as

$$P(\underline{f}) = \prod_{i=1}^{N^2} \frac{1}{\sqrt{2\pi}\sigma_{f_i}} \exp\left[-\frac{(f_i-\bar{f}_i)^2}{2\sigma_{f_i}^2}\right] . \qquad (8.17)$$

Taking the logarithm on both sides of Eq. (8.16) and differentiating it with respect to $\underline{f}$, we have the MAP equation

$$\frac{\partial \ln P(\underline{b}|\underline{f})}{\partial \underline{f}} + \frac{\partial \ln P(\underline{f})}{\partial \underline{f}} \Bigg|_{\underline{f}=\hat{\underline{f}}_{MAP}} = \underline{0} \qquad (8.18)$$

where we use the fact that $P(\underline{b})$ is a constant with respect to $\underline{f}$. The first term in Eq. (8.18) is the ML term and is given in Eq. (8.14). The second term is given by

$$\frac{\partial \ln P(\underline{f})}{\partial f_i} = -\frac{1}{\sigma^2_{f_i}}(f_i - \bar{f}_i) \qquad (8.19)$$

for $i=1,2,3,\ldots,N^2$.

Therefore, the MAP equation can be expressed as

$$-\underline{h}_i^T C^{-1}_{b(f)} \underline{h}_i + \underline{h}_i^T C^{-1}_{b(f)} \underline{b}\underline{b}^* C^{-1}_{b(f)} \underline{h}_i - \frac{1}{\sigma^2_{f_i}}(f_i - \bar{f}_i)\Big|_{\underline{f}=\hat{\underline{f}}_{MAP}} = 0 \qquad (8.20)$$

for $i=1,2,\ldots,N^2$.

This equation is similar to the ML equation except for the a priori term. The MAP estimate is a balance between the ML estimate and the a priori mean. The ML and MAP equations can be solved, in principle, using iterative methods such as Newton-Raphson method or Picard method. However, in each iteration, we must numerically invert the matrix $C_{b(f)}$, which has dimension $N^2 * N^2$ where N is the size of the image. Even though we can use sectioning techniques to reduce the dimensionality of $C_{b(f)}$, the procedure is still very computationally demanding. We also need to find the optimal direction for updating the estimate in each iteration. This approach is still impractical even with fast computers.

8.4 The Relationship Between the MAP Estimate and the LLMMSE Filter

Before trying to solve the MAP equation, we first examine the LLMMSE estimate of $\underline{f}$. From Eq. (5.4), the LLMMSE estimate of $\underline{f}$ given observation $\underline{b}$ has the form

$$\hat{\underline{f}}_{LLMMSE} = \bar{\underline{f}} + C_{fb}C_b^{-1}\underline{b} \tag{8.21}$$

where $\bar{\underline{f}}$ is the local mean of $\underline{f}$, C_{fb} is the cross-covariance matrix of $\underline{f}$ and $\underline{b}$, and C_b is the covariance matrix of $\underline{b}$. The cross-covariance matrix can be calculated as

$$C_{fb} = E[(\underline{f}-\bar{\underline{f}})\underline{b}^*]$$
$$= E\{E[(\underline{f}-\bar{\underline{f}})\underline{b}^* | \underline{f}]\} = 0.$$

Therefore, we have

$$\hat{\underline{f}}_{LLMMSE} = \bar{\underline{f}}. \tag{8.22}$$

It is interesting to see that the complex amplitude speckle observations $\underline{b}$ do not help to estimate $\underline{f}$ if we use the LLMMSE criterion.

Instead of estimating $\underline{f}$ from $\underline{b}$, we can estimate $\underline{f}_a^{1/2}$ from $\underline{b}$. This is an image restoration problem on complex amplitude data. The LLMMSE filter for this case has the form

$$\hat{\underline{f}}_{a\ LLMMSE}^{1/2} = C_{f_a^{1/2}b}C_b^{-1}\underline{b} \tag{8.23}$$

where we use the fact that $\underline{b}$ is a zero-mean process and $\bar{f}_a^{1/2}=0$. From Eq. (8.4), we have

$$C_b = E[C_{b(f)}] = C_{b(\bar{f})}$$
$$= H\begin{bmatrix} \bar{f}(1,1) & & 0 \\ & \bar{f}(1,2) & \\ & & \ddots \\ 0 & & \bar{f}(N,N) \end{bmatrix} H^T + \sigma_v^2 I \qquad (8.24)$$

and

$$C_{\underline{f}_a^{1/2}\underline{b}} = E[\underline{f}_a^{1/2}\underline{b}^*] = E[\underline{f}_a^{1/2}(\underline{f}_a^{1/2}H^T+\underline{v})^*]$$
$$= \begin{bmatrix} \bar{f}(1,1) & & 0 \\ & \bar{f}(1,2) & \\ & & \ddots \\ 0 & & \bar{f}(N,N) \end{bmatrix} H^T \qquad (8.25)$$

Substituting Eqs. (8.24) and (8.25) into Eq. (8.23), we have

$$\hat{\underline{f}}_a^{1/2}{}_{LLMMSE} = \begin{bmatrix} \bar{f}(1,1) & & 0 \\ & \bar{f}(1,2) & \\ & & \ddots \\ 0 & & \bar{f}(N,N) \end{bmatrix} H^T C_b^{-1}\underline{b}$$
$$= \begin{bmatrix} \bar{f}(1,1) & & 0 \\ & \bar{f}(1,2) & \\ & & \ddots \\ 0 & & \bar{f}(N,N) \end{bmatrix} \begin{bmatrix} \underline{h}_1^T \\ \underline{h}_2^T \\ \vdots \\ \underline{h}_N^T 2 \end{bmatrix} C_b^{-1}\underline{b} \qquad (8.26)$$

This equation can be expressed in scalar form and we have

$$\underline{\hat{f}}_{a_i\ \mathrm{LLMMSE}}^{1/2} = \bar{f}_i \underline{h}_i^T C_b^{-1} \underline{b} \tag{8.27}$$

where $\bar{f}_i = \bar{f}(m,n)$ if $i=(m-1)*N+n$. Let $\hat{f}_i$ be an *ad hoc* estimate of f_i defined as

$$\hat{f}_i = ||\underline{\hat{f}}_{a_i\ \mathrm{LLMMSE}}^{1/2}||^2, \tag{8.28}$$

then we have

$$\begin{aligned}\hat{f}_i &= ||\bar{f}_i \underline{h}_i^T C_b^{-1} \underline{b}||^2 \\ &= \bar{f}_i^2 \underline{h}_i^T C_b^{-1} \underline{b}\underline{b}^* C_b^{-1} \underline{h}_i .\end{aligned} \tag{8.29}$$

To make the dependence of $\hat{f}_i$ on $\underline{\bar{f}}$ explicit, we denote $\hat{f}_i$ as

$$\hat{f}_i = \hat{f}_i(\underline{\bar{f}}) .$$

Comparing Eq. (8.29) with Eq. (8.20), we note that the second term in the MAP equation can be expressed as

$$\underline{h}_i^T C_{b(f)}^{-1} \underline{b}\underline{b}^* C_{b(f)}^{-1} \underline{h}_i = \frac{\hat{f}_i(\underline{f})}{f_i^2} . \tag{8.30}$$

Let $\underline{\tilde{f}}_a^{1/2}$ denote the error vector defined as

$$\underline{\tilde{f}}_a^{1/2} = \underline{f}_a^{1/2} - \underline{\hat{f}}_{a\ \mathrm{LLMMSE}}^{1/2}(\underline{\bar{f}}) . \tag{8.31}$$

The filtered covariance matrix of $\underline{\tilde{f}}_a^{1/2}$ is given by

$$\begin{aligned}P_{\underline{\tilde{f}}_a^{1/2}} &= E[(\underline{f}_a^{1/2} - \underline{\hat{f}}_{a\ \mathrm{LLMMSE}}^{1/2})(\underline{f}_a^{1/2} - \underline{\hat{f}}_{a\ \mathrm{LLMMSE}}^{1/2})^*] \\ &= E[(\underline{f}_a^{1/2} - C_{\underline{f}_a^{1/2} b} C_b^{-1} \underline{b})(\underline{f}_a^{1/2} - C_{\underline{f}_a^{1/2} b} C_b^{-1} \underline{b})^*]\end{aligned}$$

$$= E[\underline{f}_a^{1/2}\underline{f}_a^{1/2*}] - 2C_{f_a^{1/2}}{}_b C_b^{-1} C_{bf_a^{1/2}} + C_{f_a^{1/2}}{}_b C_b^{-1} E[\underline{b}\underline{b}^*] C_b^{-1} C_{bf_a^{1/2}}$$

$$= \begin{bmatrix} \bar{f}_1 & & 0 \\ & \bar{f}_2 & \\ & & \ddots \\ 0 & & \bar{f}_{N^2} \end{bmatrix} - C_{f_a^{1/2}}{}_b C_b^{-1} C_{bf_a^{1/2}} \qquad (8.32)$$

In order to make the dependence of $P_{\tilde{f}_a^{1/2}}$ on $\underline{\bar{f}}$ explicit, we use the notation $P_{\tilde{f}_a^{1/2}}(\underline{\bar{f}})$ to represent the filtered covariance matrix. From Eqs. (8.24) and (8.25), the second term in Eq. (8.32) can be written

$$C_{f_a^{1/2}}{}_b C_b^{-1} C_{bf_a^{1/2}} = \begin{bmatrix} \bar{f}_1 & & 0 \\ & \bar{f}_2 & \\ & & \ddots \\ 0 & & \bar{f}_{N^2} \end{bmatrix} \begin{bmatrix} \underline{h}_1^T \\ \underline{h}_2^T \\ \vdots \\ \underline{h}_{N^2}^T \end{bmatrix} C_b^{-1} \begin{bmatrix} \underline{h}_1^T \\ \underline{h}_2^T \\ \vdots \\ \underline{h}_{N^2}^T \end{bmatrix}^T \begin{bmatrix} \bar{f}_1 & & 0 \\ & \bar{f}_2 & \\ & & \ddots \\ 0 & & \bar{f}_{N^2} \end{bmatrix}$$

$$= \begin{bmatrix} \bar{f}_1 & & 0 \\ & \bar{f}_2 & \\ & & \ddots \\ 0 & & \bar{f}_{N^2} \end{bmatrix} \begin{bmatrix} \underline{h}_1^T C_b^{-1} \underline{h}_1, & \underline{h}_1^T C_b^{-1} \underline{h}_2, & \cdots & \underline{h}_1^T C_b^{-1} \underline{h}_{N^2} \\ \underline{h}_2^T C_b^{-1} \underline{h}_1, & \cdots\cdots & & \underline{h}_2^T C_b^{-1} \underline{h}_{N^2} \\ \vdots & & & \vdots \\ \underline{h}_{N^2}^T C_b^{-1} \underline{h}_1, & \cdots\cdots & & \underline{h}_{N^2}^T C_b^{-1} \underline{h}_{N^2} \end{bmatrix} \begin{bmatrix} \bar{f}_1 & & 0 \\ & \bar{f}_2 & \\ & & \ddots \\ 0 & & \bar{f}_{N^2} \end{bmatrix}$$

$$= \begin{bmatrix} \bar{f}_1^2 \underline{h}_1^T C_b^{-1} \underline{h}_1, & \bar{f}_1 \bar{f}_2 \underline{h}_1^T C_b^{-1} \underline{h}_2, & \cdots & \bar{f}_1 \bar{f}_{N^2} \underline{h}_1^T C_b^{-1} \underline{h}_{N^2} \\ \bar{f}_2 \bar{f}_1 \underline{h}_2^T C_b^{-1} \underline{h}_1, & \bar{f}_2^2 \underline{h}_2^T C_b^{-1} \underline{h}_2, & \cdots & \bar{f}_2 \bar{f}_{N^2} \underline{h}_2^T C_b^{-1} \underline{h}_{N^2} \\ \vdots & & & \vdots \\ \bar{f}_{N^2} \bar{f}_1 \underline{h}_{N^2}^T C_b^{-1} \underline{h}_1, & \cdots\cdots & & \bar{f}_{N^2}^2 \underline{h}_{N^2}^T C_b^{-1} \underline{h}_{N^2} \end{bmatrix} \qquad (8.33)$$

Note that the diagonal elements of $P_{\tilde{f}_a^{1/2}}(\underline{\bar{f}})$ are given by

$$P_{\tilde{f}_a^{1/2}(\underline{f})}(i,i) = \bar{f}_i - \bar{f}_i^2 \underline{h}_i^T C_b^{-1} \underline{h}_i \qquad (8.34)$$

for $i=1,2,\ldots,N^2$.

Hence, the first term of Eq. (8.19) can be expressed as

$$\underline{h}_i^T C_{b(f)}^{-1} \underline{h}_i = \frac{f_i - P_{\tilde{f}_a^{1/2}(\underline{f})}(i,i)}{f_i^2} \qquad (8.35)$$

for $i=1,2,\ldots,N^2$.

Substituting Eqs. (8.30) and (8.35) into the MAP equation Eq. (8.20), we have

$$\left. \frac{P_{\tilde{f}_a^{1/2}(\underline{f})}(i,i) - f_i}{f_i^2} + \frac{\| \hat{f}_{a_i\ \mathrm{LLMMSE}}^{1/2} \|^2}{f_i^2} - \frac{(f_i - \bar{f}_i)}{\sigma_{f_i}^2} \right|_{\underline{f}=\hat{\underline{f}}_{\mathrm{MAP}}} = 0$$

for $i=1,2,\ldots,N^2$. (8.36)

It is very interesting to see that the MAP equation can be expressed in terms of the filtered estimate and the filtered covariance matrix of the LLMMSE filter. The nonstationary 2-D recursive image restoration filter developed in Chapter 6 is the recursive implementation of the LLMMSE filter. Therefore, instead of inverting the large covariance matrix C_b of dimension $N^2 * N^2$, we can use the recursive filter as a fast computation algorithm to calculate the quantities needed in the MAP equation. This makes the MAP filter for the complex amplitude speckle images computationally feasible.

8.5 Iterative Scheme for Solving the MAP Equation

In the last section, we are able to represent the MAP equation in terms of the outputs of a nonstationary 2-D recursive filter. More importantly, this representation explicitly expresses the MAP equation in terms of f_i as a cubic equation. This becomes more clear if we rewrite Eq. (8.36) as

$$\left. \frac{(P_{\tilde{f}_a}^{1/2}(\underline{f})(i,i)+\|\hat{f}_{a_i\ \mathrm{LLMMSE}}^{1/2}\|^2)}{f_i^2} - \frac{1}{f_i} - \frac{(f_i-\bar{f}_i)}{\sigma_{f_i}^2} \right|_{\underline{f}=\hat{\underline{f}}_{\mathrm{MAP}}} = 0 \qquad (8.37)$$

for $i=1,2,\ldots,N^2$.

This equation has the same form as the one-point MAP equation discussed in section 7.3.2. The filtered estimate and the diagonal element of the filtered covariance matrix of the LLMMSE filter are combined and are treated as the independent speckle intensity in the one-point MAP equation. It is very helpful to view the function of the LLMMSE filter operating on the complex amplitude speckle observations as decorrelating the data similar to the function of an inverse filter. The outputs of the LLMMSE filter are combined to form an intensity image and processed by a one-point MAP filter that is derived by assuming the speckle intensity samples are statistically independent. With this in mind, a simple iterative algorithm is developed. In each iteration, we apply a nonstationary 2-D recursive filter on the complex amplitude speckle image. The filtered

estimate and the diagonal element of the filtered covariance matrix are combined to form a new intensity speckle image. The one-point MAP filter is then applied to this new intensity speckle image and we have a MAP estimate of the original object intensity. This new estimate is used as the local variance of the 2-D recursive filter and starts the next iteration. The block diagram of this algorithm is illustrated in Fig. 8.2. The one-point MAP estimate is the real solution of a cubic equation and its value is between the local mean estimate and the speckle intensity, and thus prevents the possibility of divergence in the iteration.

In this section, we present some simulation results for the MAP filter. The original image is shown in Fig. 8.3(A). The complex amplitude speckle image is generated using a 5*5 coherent point spread function and its intensity image is shown in Fig. 8.3(B). The local mean of the complex amplitude speckle image is zero because of the fully developed speckle assumption. Therefore, the local variance of the complex amplitude speckle image is equal to the local mean of its intensity image and is shown in Fig. 8.3(C). The first iteration MAP estimate is shown in Fig. 8.3(D). Then we use this estimate as the local variance of the complex amplitude speckle image and calculate the outputs of the nonstationary 2-D recursive filter. The second iteration MAP estimate is shown in Fig. 8.3(E). After the second iteration, the MAP estimate does not change significantly. As shown in the

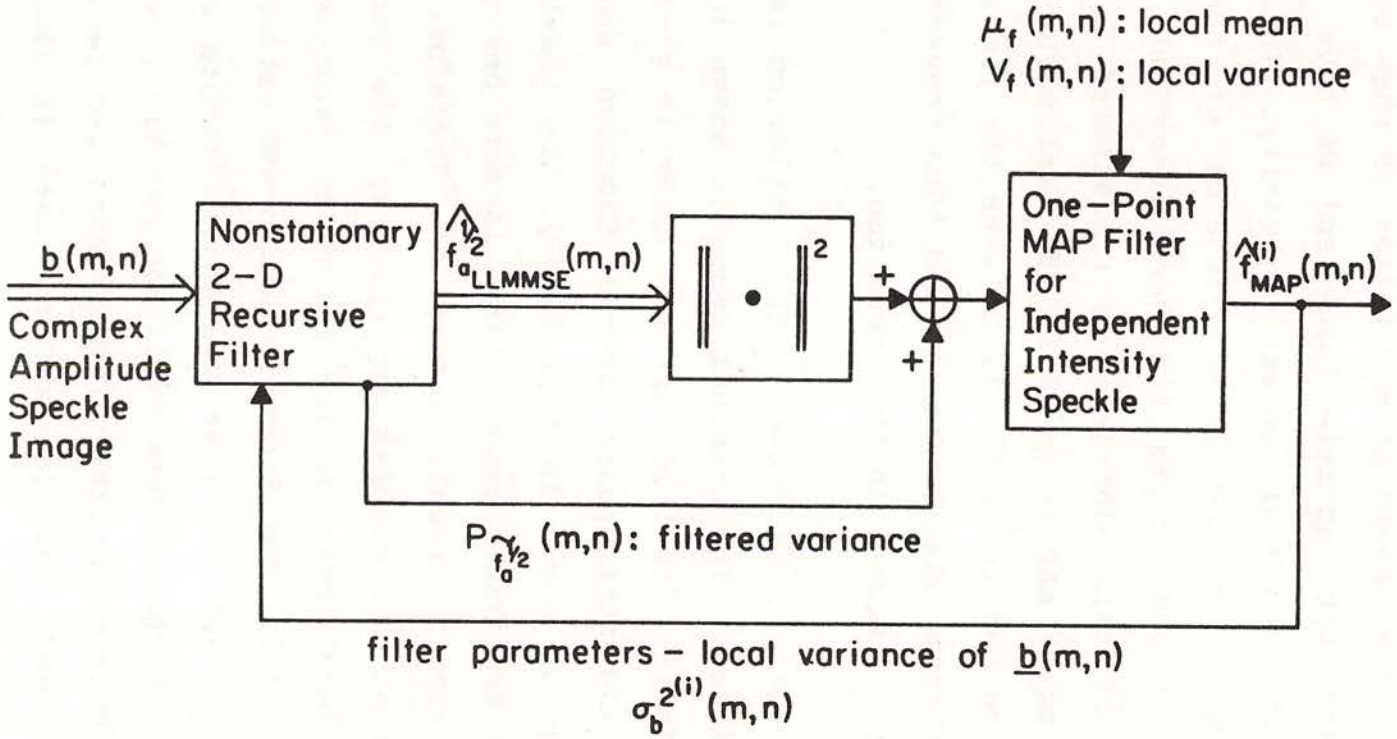

Figure 8.2 Iterative algorithm for MAP speckle reduction filter

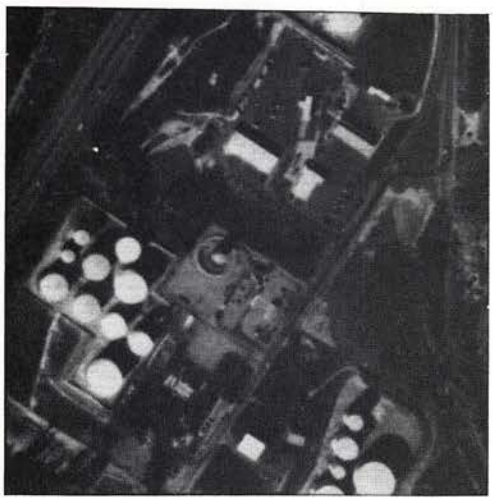

8.3(A) Original image

8.3(B) Speckle image - single frame, correlated samples (5 by 5 coherent PSF)

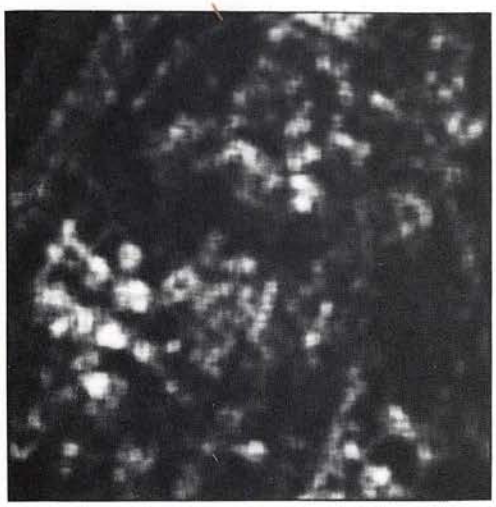

8.3(C) 7*7 local mean of (B)

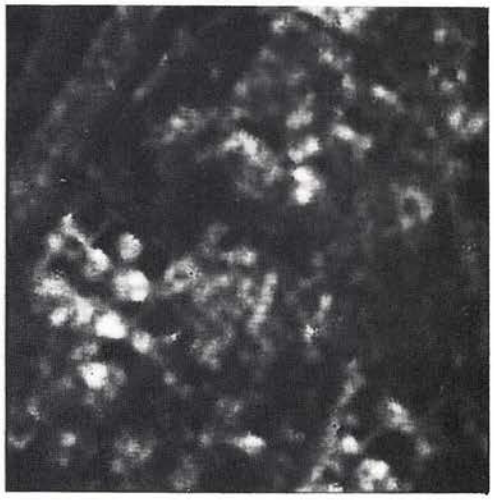

8.3(D) The first iteration MAP estimate

8.3(D) The second iteration MAP estimate

Figure 8.3 MAP speckle restoration filter for complex amplitude speckle images

picture, some regions of the processed image are enhanced and better defined.

8.6 Conclusions

This is the first attempt at using complex amplitude speckle data to reduce speckle noise. A MAP speckle reduction filter is derived in this chapter. The MAP filter is nonlinear and can be decomposed into two parts, a deconvolution component and a one-point MAP component. The deconvolution component can be implemented with a nonstationary 2-D recursive filter. The one-point MAP estimate is a real root of a cubic equation. This decomposition not only simplifies the computation but also suggests a simple constrained iteration algorithm to solve the MAP equation. The structure of this algorithm shows the optimal way of processing complex amplitude speckle images.

Chapter 9

SUMMARY AND CONCLUSIONS

In this dissertation a nonstationary 2-D recursive restoration filter for images with signal-dependent noise was developed. Speckle noise was modeled according to the exact physical process of coherent image formation and speckle reduction techniques based on intensity and complex amplitude speckle data were presented.

In contrast to the conventional stationary image model, we introduced a nonstationary mean and nonstationary variance (NMNV) image model in which the nonstationary mean is used to describe the gross structure of the image and the nonstationary variance is used to describe the edge information. The validation of this image model is verified through experiments. For images degraded by a class of uncorrelated, signal-dependent noise including multiplicative noise and Poisson noise, an adaptive noise smoothing filter that minimizes the local linear minimum mean square error (LLMMSE) is derived. The filter has very simple structure and is a point processor. This parallel nature enables the possibility of using VLSI techniques for real time

processing. The filter is able to adapt itself to the nonstationary content of the image and different types of signal-dependent noise. All the parameters needed for the filter are the nonstationary mean and nonstationary variance which can be estimated from the degraded image. Various ways of estimating these statistics combined with the fixed structure LLMMSE filter correspond to different nonlinear adaptive noise smoothing filters.

The adaptive noise smoothing filter can be extended to image restoration where the image is degraded by blur and signal-dependent noise. The filter is no longer a point processor due to the blur degradation, and requires extensive computation. A 2-D recursive implementation of this filter with reduced update concept is developed to reduce the computational requirements. This recursive filter can handle space-variant blur easily and is suitable for real-time processing. Because of the special structure of the NMNV image model, the prediction step of the filter requires no real computation if we use indirect addressing techniques. The same filter structure can be used for noise smoothing problem where we have a nonstationary mean and finite nonstationary covariance image model. This will correspond to a restoration problem with space-variant blur and a NMNV image model.

Speckle is a granular noise inherently exists in all types of coherent imagery such as synthetic aperture radar (SAR) imagery. In this work, we modeled the speckle

according to the exact physical process of coherent image formation. Thus, the model includes signal-dependent effects and accurately represents the higher order statistical properties of speckle that are important for the speckle reduction procedure. Unlike multiplicative noise, speckle noise is not only signal-dependent but also correlated where the correlation depends on the signal statistics and is nonstationary.

Speckle reduction can be achieved by averaging multiple frames of uncorrelated speckle images of the same object on an intensity basis. While this method is effective when multiple frames of uncorrelated speckle images are available, it does not consider the image statistics and the correlation of speckle. We derived the nonstationary speckle statistics based on the NMNV image model and developed a local linear minimum mean square error (LLMMSE) speckle reduction filter that considers the second order statistics of speckle. The filter is able to adapt itself to the nonstationary content of the image and use the correlation properties of speckle to further reduce speckle noise. Recursive implementation of this filter is presented as a fast computation algorithm. In a limiting situation where the speckle intensity samples are statistically independent within a single frame, speckle reduction becomes a noise smoothing problem and the adaptive noise smoothing filter for multiplicative noise can be applied. The maximum a posteriori (MAP) estimate in this case is the real root

of a cubic equation, and its value is between the local mean and the speckle intensity image. we call it a one-point MAP filter because the MAP equations are decoupled. All these speckle reduction techniques are later extended to process multiple frames of speckle intensity images with good restoration results.

In a digitally processed SAR image, both the amplitude and phase of the speckle image are preserved. Traditionally, only the intensity of the complex amplitude image is used for speckle reduction and the phase information is ignored. Here, we developed a MAP speckle reduction filter for complex amplitude speckle images. The MAP equation is nonlinear and requires extensive computation. Fortunately, we are able to represent the MAP equations in terms of the outputs of a nonstationary 2-D recursive restoration filter and the resulting MAP equation has the same form as the one-point MAP equation. This decomposition not only simplifies the computational aspects of the MAP filter, but also suggests a practical algorithm to calculate the MAP estimate iteratively. The extension of this algorithm to multiple frames of complex amplitude speckle images is straightforward.

APPENDIX A

In this appendix, we summarize three matrix theorems which are useful for the derivation of the MAP filter for complex amplitude speckle images.

Theorem 1:

Let A be an m×n matrix and B an n×m matrix, then

Tr[AB] = Tr[BA] where Tr[·] is the trace operator.

Proof: From the definition of the trace operator, we have

$$\mathrm{Tr}[AB] = \sum_{i=1}^{m}\left(\sum_{j=1}^{n} a_{ij}b_{ji}\right) = \sum_{i=1}^{m}\sum_{j=1}^{n} a_{ij}b_{ji}$$

$$= \sum_{j=1}^{n}\sum_{i=1}^{m} a_{ij}b_{ji} = \sum_{j=1}^{n}\left(\sum_{i=1}^{m} b_{ji}a_{ij}\right) = \mathrm{Tr}[BA]$$

Theorem 2:

Let f_i be a real variable and assume that $C(f_i)$ is a continuously differentiable nonsingular Hermitian matrix, then

$$\frac{\partial \ln|C|}{\partial f_i} = \mathrm{Tr}\left[C^{-1}\frac{\partial C}{\partial f_i}\right]$$

where $|C|$ is the determinant of matrix C.

Proof: Since $|C|$ is a scalar function of variable f_i, we have

$$\frac{\partial}{\partial f_i} \ln|C| = |C|^{-1} \frac{\partial |C|}{\partial f_i} \tag{A.1}$$

From the assumption that C is a Hermitian matrix, there exists a unitary matrix U such that

$$U^* C U = D \tag{A.2}$$

where U^* is the Hermitian of matrix U, and D is a diagonal matrix whose diagonal elements are real functions of f_i, i.e.

$$D = \begin{bmatrix} d_1 & & 0 \\ & d_2 & \\ & & \ddots \\ 0 & & d_N \end{bmatrix}$$

Substituting equation (A.2) into (A.1), we have

$$\frac{\partial}{\partial f_i} \ln|C| = |C|^{-1} \frac{\partial |C|}{\partial f_i} = |UDU^*|^{-1} \frac{\partial |UDU^*|}{\partial f_i}$$

$$= (|U||D||U^*|)^{-1} \frac{\partial (|U||D||U^*|)}{\partial f_i}$$

$$= |D|^{-1} \frac{\partial |D|}{\partial f_i} = (d_1 d_2 \cdots d_N)^{-1}$$

$$\left(\frac{\partial d_1}{\partial f_i} d_2 d_3 \cdots d_N + d_1 \frac{\partial d_2}{\partial f_i} d_3 \cdots d_N + \cdots + \right.$$

$$\left. d_1 d_2 \cdots \frac{\partial d_N}{\partial f_i}\right)$$

$$= d_1^{-1} \frac{\partial d_1}{\partial f_i} + d_2^{-1} \frac{\partial d_2}{\partial f_i} + \ldots + d_N^{-1} \frac{\partial d_N}{\partial f_i}$$

$$= \mathrm{Tr}[D^{-1} \frac{\partial D}{\partial f_i}] . \qquad (A.3)$$

Substituting Eq.(A.2) into the final result of Eq.(A.3), we get

$$\frac{\partial}{\partial f_i} \ln|C| = \mathrm{Tr}[D^{-1} \frac{\partial D}{\partial f_i}]$$

$$= \mathrm{Tr}[U^* C^{-1} U (\frac{\partial U^*}{\partial f_i} CU + U^* \frac{\partial C}{\partial f_i} U + U^* C \frac{\partial U}{\partial f_i})]$$

$$= \mathrm{Tr}[U^* C^{-1} U \frac{\partial U^*}{\partial f_i} CU + U^* C^{-1} \frac{\partial C}{\partial f_i} U + U^* \frac{\partial U}{\partial f_i}]$$

$$= \mathrm{Tr}[U^* C^{-1} U \frac{\partial U^*}{\partial f_i} CU] + \mathrm{Tr}[U^* C^{-1} \frac{\partial C}{\partial f_i} U] + \mathrm{Tr}[U^* \frac{\partial U}{\partial f_i}] .$$

If we apply theorem 1, $\frac{\partial}{\partial f_i} \ln|C|$ becomes

$$\frac{\partial}{\partial f_i} \ln|C| = \mathrm{Tr}[U \frac{\partial U^*}{\partial f_i} + C^{-1} \frac{\partial C}{\partial f_i} + U^* \frac{\partial U}{\partial f_i}]$$

$$= \mathrm{Tr}[\frac{\partial}{\partial f_i} (UU^*) + C^{-1} \frac{\partial C}{\partial f_i}]$$

$$= \mathrm{Tr}[C^{-1} \frac{\partial C}{\partial f_i}] .$$

Theorem 3: Let $C(f_i)$ be a continuous differentiable nonsingular matrix, then

$$\frac{\partial C^{-1}}{\partial f_i} = -C^{-1}\frac{\partial C}{\partial f_i}C^{-1} \quad .$$

Proof: Because C is nonsingular, C^{-1} exists and

$$CC^{-1} = I \quad . \tag{A.4}$$

Differentiating both sides of Eq.(A.4), we get

$$\frac{\partial}{\partial f_i}(CC^{-1}) = \frac{\partial C}{\partial f_i} C^{-1} + C\frac{\partial C^{-1}}{\partial f_i} = 0$$

Therefore

$$\frac{\partial C^{-1}}{\partial f_i} = -C^{-1} \frac{\partial C}{\partial f_i} C^{-1} \quad .$$

REFERENCES

[1-1] H.C. Andrews and B.R. Hunt, Digital Image Restoration, Englewood Cliff, NJ. Prentice-Hall, 1977.

[1-2] W.K. Pratt, Digital Image Processing, Wiley-Interscience, New York, 1978.

[1-3] J.W. Woods, and C.H. Radewan, "Kalman filtering in two dimensions," IEEE Trans. Information Theory, vol. IT-23, pp. 473-482, July 1977.

[1-4] J.W. Woods, and V.K. Ingle, "Kalman filtering in two dimensions: further results," IEEE Trans. Acoustics, Speech, and Signal Processing, vol. ASSP-29, pp. 188-196, April 1981.

[1-5] B.R. Hunt, and T.M. Cannon, "Nonstationary assumptions for Gaussian models of images," IEEE Trans. System, Man and Cybernetics, vol. 6, pp. 876-881, Dec. 1976.

[1-6] H.T. Trussell, and B.R. Hunt, "Sectioned methods for image restoration," IEEE Trans. Acoustics, Speech, and Signal Processing, vol. ASSP-26, pp. 157-164, April 1978.

[1-7] C.M. Lo, and A.A. Sawchuk, "Nonlinear restoration of filtered images with Poisson noise," Proc. SPIE Tech. Symp. - Application of Digital Image Processing-III, vol. 207, pp. 84-95, San Diego, August 1979.

[1-8] D.T. Kuan, A.A. Sawchuk, T.C. Strand, and P. Chavel, "Nonstationary 2-D recursive image restoration," 1981 Annual Meeting Optical Society of America, Olando, Florida, October 1981.

[1-9] J.W. Goodman, "Some fundamental properties of speckle," J. Opt. Soc. Am., vol. 66, pp. 1145-1149, Nov. 1976.

[1-10] J.S. Lee, "Speckle analysis and smoothing of synthetic aperture radar images," Computer Graphics and Image Processing, vol. 17, pp. 24-32, 1981.

[1-11] J.S. Lim, and H. Nawab, "Techniques for speckle noise removal," Optical Engineering, vol.20, pp. 472-480, May/June 1981.

[1-12] V.S. Frost, J.A. Stiles, K.S. Shanmugan, and J.C. Holtzman, "A model for radar images and its application to adaptive digital filtering for multiplicative noise," IEEE Trans. Pattern Analysis and Machine Intelligence, vol.PAMI-4, pp. 157-166, March 1982.

[1-13] D.T. Kuan, A.A. Sawchuk, T.C. Strand, and P. Chavel, "Discrete speckle modeling and restoration," J. Opt. Soc. Am., vol. 71, pp. 1585-1586, Dec. 1981.

[1-14] D.T. Kuan, A.A. Sawchuk, T.C. Strand, and P. Chavel, "Nonstationary 2-D recursive filter for speckle reduction," Proc. of 1982 IEEE International Conference on Acoustics, Speech, and Signal Processing, Paris, France, May 1982.

[2-1] J.W. Goodman, Introduction to Fourier Optics, McGraw-Hill, New York, 1968.

[2-2] W.K. Pratt, Digital Image Processing, Wiley-Interscience, New York, 1978.

[2-3] D.S. Lebedev, and L.I. Mirkin, "Digital nonlinear smoothing of images," Institute for Information Transmission Problems, Academy of Sciences, USSR, pp. 150-157, 1975.

[2-4] V.K. Ingle, and J.W. Woods, "Multiple model recursive estimation of images," Proc. IEEE, ICASSP 79, pp. 642-645, Washington, D.C., April 1979.

[2-5] B.R. Hunt, and T.M. Cannon, "Nonstationary assumptions for Gaussian models of images," IEEE Trans. System, Man and Cybernetics, vol. 6, pp. 876-881, Dec. 1976.

[2-6] B.R. Hunt, "Bayesian methods in nonlinear digital image restoration," IEEE Trans. Computer, vol. C-26, pp. 219-229, March 1977.

[2-7] H.T. Trussell, and B.R. Hunt, "Sectioned methods for image restoration," IEEE Trans. Acoustics, Speech, and Signal Processing, vol. ASSP-26, pp. 157-164, April 1978.

[2-8] T.S. Huang, "Some notes on film-grain noise," Appendix 14, in Restoration of Atmospherically Degraded Images, NSF Summer Study Report, Woods Hole, Mass. 1966, pp. 105-109.

[2-9] F. Naderi, and A.A. Sawchuk, "Estimation of images degraded by film-grain noise," Applied Optics, vol. 17, pp. 1228-1237, April 1978.

[2 -10] C.M. Lo, and A.A. Sawchuk, "Nonlinear restoration of filtered images with Poisson noise," Proc. SPIE Tech. Symp. - Application of Digital Image Processing-III, vol. 207, pp. 84-95, San Diego, August 1979.

[2-11] J.W. Goodman, "Some fundamental properties of speckle," J. Opt. Soc. Am., vol. 66, pp. 1145-1149, Nov. 1976.

[3-1] J.W. Goodman, "Statistical properties of laser speckle patterns," in Laser Speckle and Related Phenomena, edited by J.C. Dainty. Springer-Verley, Heidelberg, 1975. Vol. 9, Topics in Applied Physics.

[3-2] S. Lowenthal, and H. Arsenault, "Image formation for coherent diffuse objects : statistical properties," J. Opt. Soc. Am., vol.60, pp. 1478-1483, Nov. 1970.

[3-3] H. Fujii, T. Asakura, and Y. Shindo, "Measurement of surface roughness properties by using image speckle contrast," J. Opt. Soc. Am., vol.66, pp. 1217-1222, Nov. 1976.

[3-4] H.M. Pedersen, "The roughness dependence of partially developed, monochromatic speckle patterns," Opt. Commun., vol.12, pp. 156-159, 1974.

[3-5] B.D. Guenther, C.R. Christensen, and A. Jain, "Digital processing of speckle images," Proc. IEEE Conf. on Pattern Recognition and Image Processing, Chicago, IL. May 1978.

[3-6] H. Fujii, J. Uozumi, and T. Asakura, "Computer simulation study of image speckle patterns with relation to object surface profile," J. Opt. Soc. Am., vol.66, pp. 1222-1236, Nov. 1976.

[3-7] J.W. Goodman, Introduction to Fourier Optics, McGraw-Hill, New York, 1968.

[4-1] N.E. Nahi and T. Assefi, "Baysian recursive image estimation," IEEE Trans. Computer, vol C-12, pp. 734-738, July 1972.

[4-2] A.O. Aboutalib, M.S. Murphy, and L.M. Silverman, "Digital Restoration of image degraded by general motion blurs," IEEE Trans. Automat. Contr. vol. AC-22, pp. 294-302, June 1977.

[4-3] J.W. Woods, and C.H. Radewan, "Kalman filtering in two dimensions," IEEE Trans. Information Theory, vol. IT-23, pp. 473-482, July 1977.

[4-4] B.R. Hunt, and T.M. Cannon, "Nonstationary assumptions for Gaussian models of images," IEEE Trans. System, Man and Cybernetics, vol. 6, pp. 876-881, Dec. 1976.

[4-5] D.S. Lebedev, and L.I. Mirkin, "Smoothing of two dimensional images using the composite model of a fragment," Iconics, Institute for problems in information transmission, Academy of Science.

[4-6] F. Naderi, and A.A. Sawchuk, "Estimation of images degraded by film grain noise," Applied Optics, vol. 17, pp. 1228-1237, April 1978.

[4-7] C.M. Lo, and A.A. Sawchuk, "Nonlinear restoration of filtered images with Poisson noise," Proc. SPIE Tech. Symp. - Application of Digital Image Processing-III, vol. 207, pp. 84-95, San Diego, August 1979.

[4-8] C.L. Anderson, and A.N. Netravali, "Image restoration based on a subjective criterion," IEEE Trans. System, Man, and Cybernetics, vol. SMC-6, pp. 845-853, Dec. 1976.

[4-9] C.W. Helstrom, "Image restoration by the method of least squares," J. Opt. Soc. Am., vol.57, pp. 297-303, March 1967.

[4-10] N.E. Nahi, "Role of recursive estimation in statistical image enhancement," Proc. IEEE, vol. 60, pp. 872-877, July 1972.

[4-11] M.S. Murphy, and L.M. Silverman, "Image model representation and line-by-line recursive restoration," IEEE Trans. Automatic Control, vol. AC-23, pp. 809-816, Oct. 1978.

[4-12] M.P. Ekstrom, and J.W. Woods, "Two dimensional spectral factorization with applications in recursive digital filtering," IEEE Trans. Acoustics, Speech, and Signal Processing, vol. ASSP-24, pp. 115-128, April 1976.

[4-13] A.P. Sage, and J.L. Melsa, Estimation Theory with Applications to Communications and Control. New York, McGraw-Hill, 1971.

[4-14] J.S. Lee, "Digital image enhancement and noise filtering by use of local statistics," IEEE Trans. Pattern Anal. and Machine Intell., vol. PAMI-2, pp. 165-168, March 1980.

[4-15] H.T. Trussell, and B.R. Hunt, "Sectioned methods for image restoration," IEEE Trans. Acoustics, Speech, and Signal Processing, vol. ASSP-26, pp. 157-164, April 1978.

[4-16] J.F. Walkup, and R.C. Choens, "Image processing in signal dependent noise," Opt. Eng. vol. 13, pp. 258-266, May/June 1974.

[4-17] K.Kondo, Y.Ichioka, and T. Suzuki, "Image restoration by Wiener filtering in the presence of signal dependent noise," Applied Optics, vol. 16, pp. 2554-2558, Sept. 1977.

[4-18] J.W. Goodman, and J.F. Belsher, "Fundamental limitations in linear invariant restoration of atmospherically degraded images," Proc. SPIE 75, pp. 141-154, 1976.

[4-19] W.A. Pearlman, "A visual system model and a new distortion measure in the context of image processing," J. Opt. Soc. Am., vol. 68, pp. 374-385, March 1978.

[4-20] J.F. Abramatic, and L.M. Silverman, "Nonlinear restoration of noisy images," IEEE Trans. Pattern Anal. Machine Intell., vol. PAMI-4, pp. 141-149, March 1982.

[5-1] J.W. Woods, and C.H. Radewan, "Kalman filtering in two dimensions," IEEE Trans. Information Theory, vol. IT-23, pp. 473-482, July 1977.

[5-2] V.K. Ingle, and J.W. Woods, "Multiple model recursive estimation of images," Proc. IEEE, ICASSP 79, pp. 642-645, Washington, D.C., April 1979.

[5-3] H.T. Trussel, and B.R. Hunt, "Sectioned methods for image restoration," IEEE Trans. Acoustics, Speech, and Signal Processing, vol. ASSP-26, pp. 157-164, April 1978.

[5-4] C.L. Anderson, and A.N. Netravali, "Image restoration based on a subjective criterion," IEEE Trans. System, Man, and Cybernetics, vol. SMC-6, pp. 845-853, Dec. 1976.

[5-5] J.F. Abramatic, and L.M. Silverman, "Nonlinear restoration of noisy images," IEEE Trans. Pattern Anal. Machine Intell., vol. PAMI-4, pp. 141-149, March 1982.

[5-6] J.S. Lee, "Digital image enhancement and noise filtering by use of local statistics," IEEE Trans. Pattern Anal. and Machine Intell., vol. PAMI-2, pp. 165-168, March 1980.

[5-7] A.P. Sage, and J.L. Melsa, Estimation Theory with Applications to Communications and Control. New York, McGraw-Hill, 1971.

[5-8] T.S. Ferguson, Mathematical Statistics. New York, Academic Press, 1967.

[5-9] J.S. Lee, "Refined noise filtering using local statistics," Computer Graphics and Image Processing, vol. 15, pp. 380-389, 1981.

[6-1] J.W. Woods, and C.H. Radewan, "Kalman filtering in two dimensions," IEEE Trans. Information Theory, vol. IT-23, pp. 473-482, July 1977.

[6-2] J.W. Woods, and V.K. Ingle, "Kalman filtering in two dimensions: further results," IEEE Trans. Acoustics, Speech, and Signal Processing, vol. ASSP-29, pp. 188-196, April 1981.

[6-3] S.A. Rajala, and R.J.P. de Figueirido, "Adaptive nonlinear image restoration by a modified Kalman filtering approach," IEEE Trans. Acoustics, Speech, and Image Processing, vol. ASSP-29, pp. 1033-1042, Oct. 1981.

[6-4] V.K. Ingle, and J.W. Woods, "Multiple model recursive estimation of images," Proc. IEEE, ICASSP 79, pp. 642-645, Washington, D.C., April 1979.

[6-5] J.S. Meditch, Stochastic Optimal Linear Estimation and Control, McGraw-Hill, New York, 1969.

[7-1] T.S. McKechnie, "Speckle reduction" in Laser Speckle and Related Phenomena, edited by J.C. Dainty. Springer-Verley, Heidelberg, 1975. vol. 9, Topics in Applied Physics.

[7-2] L.J. Porcello, N.G. Massey, R.B. Innes, and J.M. Marks, "Speckle reduction in synthetic aperture radars," J. Opt. Soc. Am., vol.66, pp. 1306-1311, Nov. 1976.

[7-3] J.S. Zelenka, "Comparison of continuous and discrete mixed-integrator processors," J. Opt. Soc. Am., vol.66, pp. 1295-1304, Nov. 1976.

[7-4] J.S. Lim, and H. Nawab, "Techniques for speckle noise removal," Optical Engineering, vol.20, pp. 472-480, May/June 1981.

[7-5] J.S. Lee, "Speckle analysis and smoothing of synthetic aperture radar images," Computer Graphics and Image Processing, vol. 17, pp. 24-32, 1981.

[7-6] V.S. Frost, J.A. Stiles, K.S. Shanmugan, and J.C. Holtzman, "A model for radar images and its application to adaptive digital filtering for multiplicative noise," IEEE Trans. Pattern Analysis and Machine Intelligence, vol.PAMI-4, pp. 157-166, March 1982.

[7-7] J.W. Goodman, "Some fundamental properties of speckle," J. Opt. Soc. Am., vol. 66, pp. 1145-1149, Nov. 1976.

[7-8] H.H. Arsenault, and G. April, "Properties of speckle integrated with a finite aperture and logarithmically transformed," J. Opt. Soc. Am., vol. 66, pp. 1160-1163, Nov. 1976.

[7-9] K.S. Miller, Multivariate Distributions, Robert E. Krieger Publishing company, Huntington, New York, 1975.